Asymptotic-Preserving Schemes

Porto-Ercole summer school 2012

MMKT "Methods and Models of Kinetic Theory"

Modeling, Simulation and Mathematical Analysis of Magnetically Confined Plasmas

Claudia NEGULESCU

UNIVERSITÉ Paul Sabatier, Toulouse III

Institut de Mathématiques de Toulouse

Mathématiques pour l'Industrie et la Physique

Unité Mixte de Recherches CNRS - Université Paul Sabatier Toulouse 3 - INSA Toulouse - Université Toulouse 1

UMR 5640

UFR MIG, Université Paul Sabatier Toulouse 3, 118 route de Narbonne, 31062 TOULOUSE cédex 4, France

Foreword

These lecture notes summarize a succession of works dealing with the construction as well as the mathematical and numerical study of Asymptotic-Preserving schemes in the kinetic and fluid framework. The lectures are based on articles, which were chosen to illustrate different techniques in the design of AP-schemes and to treat different singular perturbation problems, occuring in kinetic and fluid theory.
The goal of this notes is to familiarize the reader with the general features of AP-schemes, which can be further applied for singular perturbation problems arising in several other domains, as for example in the quatum mechanical framework.

The author would like to acknowledge here her collegues for their support and is especially thankful to Nicolas Crouseilles and Fabrice Deluzet for helpful discussions and suggestions, for having performed some of the simulations as well as having corrected parts of this work.
Moreover, this work has been supported by the ANR project BOOST (Building the future Of numerical methOdS for iTer, 2010-2014), the ANR project ESPOIR (Edge Simulation of the Physics Of Iter Relevant turbulent transport, 2009-2013) and the ANR project IODISSEE (IOnospheric DIsturbanceS and SatEllite-to-Earth communications, 2009-2013).

Table des matières

Introduction

The central theme of this course is the introduction and study of Asymptotic-Preserving schemes for the numerical simulation of singularly perturbed problems, arising in the description of systems composed of N charged particles, evolving in an electromagnetic field. The schemes presented here can be applied in various (other) physical contexts, as for example for neutral gases, quantum mechanical systems or other multiscale problems, however we shall focus in the present course on plasma physics.

The word "plasma" has been introduced for the first time by the Czech medical scientist Johannes Parkinje (1787-1869), to describe the blood, when cleared by its various corpuscles. It comes from the grec word $\pi\,\lambda\,\alpha\,\sigma\,\mu\,\alpha$, which signifies "modulable substance". In 1927 the physicist I. Langmuir used this term firstly to describe ionized gases. A plasma gas is, at first glance, a gas of charged particles (ions, electrons). 99% of the universe is constituted of plasmas, as for example the stars, the solar wind, the intergalactic gas, the ionosphere, the lightnings, the aurora borealis, the tails of comets, *etc*. One may say that the earth is completely surrounded by a plasma gas, which is trapped within its magnetic field. In contrast to this, in our close environment plasmas are rather rare (1%) and occur (very often under artificial form) for example in plasma screens, fluorescent lamps, electric discharges, particle accelerators, nuclear fusion, *etc*. The rest of our nearby environment occurs under solid, liquid or gaseous form. But, even if the plasmas are fairly rare in our close environment, we are, without knowing it, in permanent contact with them. Indeed, all the electromagnetic fields around us come from some object constituted of plasmas, as for example the stars or the fluorescent lamps, and even for communication on earth and with the space (satellites), plasmas (and their interaction with the magnetic fields) are of crucial importance. Thus the study of this fourth state of matter, which is the site of quiet a large variety of physical phenomena, is interesting not only for its own, but also for lots of important applications, like semiconductor technologies, plasma lasers, controlled nuclear fusion, ion propulsion rockets, gas discharges, *etc*.

The fact that the plasma is constituted of charged particles changes completely its physical behaviour as compared to the dynamics of neutral gases.
Firstly, in a neutral gas binary collisions between the particles determine entirely the global behaviour of the gas, leading to a thermodynamical equilibrium via diffusion and convective transport. These collisions are of short range, called also "hard sphere collisions". In contrast to this, in a completely ionized plasma, the collisions are of electromagnetic type, hence of long range (Coulombian force decreases as $1/r^2$). These are

FIGURE 1: Natural plasmas : sun, lightening, aurora borealis

collectives interactions, fundamentally different from hard sphere collisions. One particle is interacting with its close neighbour but also with all other particles by means of the (mean) electromagnetic fields, created by them. If the plasma is partially ionized, then also short range collisions may occur between the charged particles and the neutrals.
Other physical phenomena, such as the electromagnetic screening, instabilities, turbulence, waves, chaos *etc* contribute to the fact that the plasma constitutes a remarkable domain of study. Indeed, a sufficiently high energy is needed in order to create a plasma (from neutral atoms) or to maintain it. This energy can be furnished by heating, radiation (absorption of energetic photons) or ionization by impact with energetic electrons. Without this energy, the plasma will recombine and become a neutral gas. Hence, being so energetic, plasmas are far from a thermodynamical equilibrium and are the site of high instabilities and turbulence. This turbulence concerns, apart from the density and velocity fluctuations, also the electromagnetic fluctuations.
Moreover, while in neutral gases only one type of wave occurs, the acoustic wave, in plasmas several types of waves develop, thanks to the collective behaviour of the plasma. These waves can be divided into two categories : the transverse electromagnetic waves, as for example the Alfén waves, and the longitudinal electrostatic waves, as the Langmuir or ion acoustic waves. All these phenomena lead to very intricate plasma dynamics and it is not surprising that much of the research is devoted to the description and understanding of wave propagation in plasmas.
Finally, another complexity of plasmas consists in the fact that they are highly anisotropic, the particle dynamics as well as the propagation of the fluctuations are very different if considered in the parallel respectively perpendicular direction to the magnetic field lines.

To briefly summarize this discussion, plasmas are much more than a gas constituted of charged particles. Collective effects play an important role and the underlying physics is very different from that of neutral gases. The behaviour of a plasma is very complex, the main reason being the nonlinear and self-consistent nature of the coupled system charged-particles $\leftrightarrow$ fields.

Let us now come to the particular field of magnetically confined fusion plasmas, which are studied today in order to try to find solutions for longer-term, clean energy production. The concept of nuclear transformations, like fusion and also fission, is to

create high binding energy nuclei, from lower ones, such that the energy difference is released. The thermonuclear fusion is a process which joints together two (or several) light atomic nuclei to build a heavier nucleus, the rearrangement resulting in a reduction of the total mass, which is transformed in energy via $E = mc^2$. In contrast to this, the nuclear fission is a process which splits a heavy nucleus in lighter ones, releasing again energy according to the mass-energy equivalence. Fission reactors are the common type of today's nuclear reactors. Fusion reactors, which try to mimic the physical phenomenon occurring in the centre of the sun and other stars, are in intensive study today, with the hope to develop a reliable, illimitable, clean power production system. The ambition is to construct a reactor which does not produce greenhouse gases, whose waste products are non-radioactive (ideally) and which comprises/possesses no explosion risk (no runaway reactions).

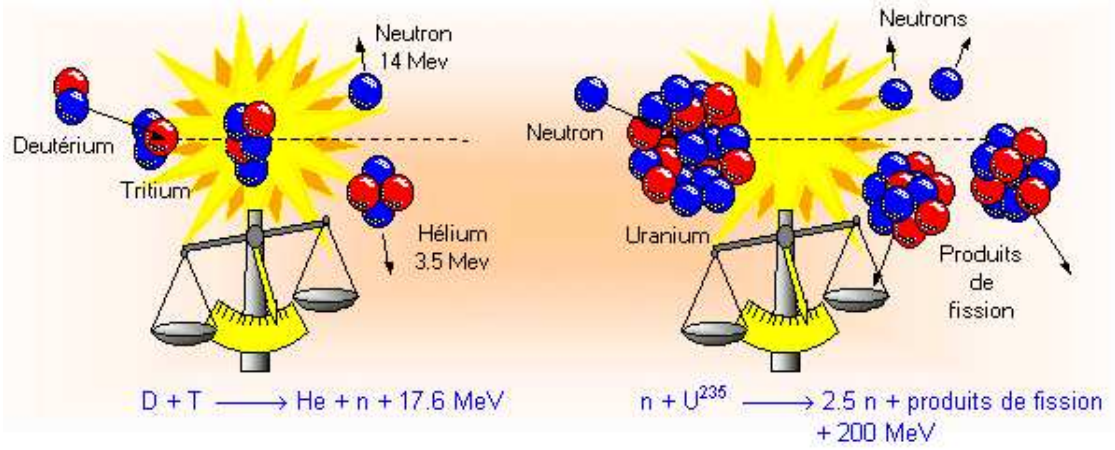

FIGURE 2: Fusion (left) and fission (right) reactions
(http ://www-fusion-magnetique.cea.fr)

The following Deuterium ($D = H^2$)-Tritium ($T = H^3$) reaction

$$D + T \rightarrow He^4 + n + 17,6\, MeV\,,$$

is retained at the moment for the fusion reaction, as it has the highest probability of fusion if compared to other fusion reactions, and as it reacts at lower temperatures also. As a result of this reaction, an α-particle is produced and a neutron released. The energy of the α-particle is used to sustain the necessary reaction temperature of the plasma, while the energy of the neutron is captured to produce energy.

The main difficulties in this fusion process are the following :
- the energy has to be high enough, in order to overcome the Coulomb repulsive force between the atomic particles, such that the attractive nuclear force can bind them into the new nucleus ($\sim$ hundred million kelvin, $\sim 15\, keV$)
- the confinement has to be strong enough, in order to avoid the dispersion of the energetic plasma and thus to permit the fusion process to occur

– more energy has to be produced than it is furnished to the system and moreover the process has to be self-sustained.

In summary, the essential physical challenges with fusion consist in finding the manner to sustain through time a far from equilibrium, unstable plasma gas. Confinement is determined by the balance between the magnetic and pressure forces, however the occurrence of instabilities can generate a plasma transport across the magnetic field lines, leading to a loss of energy as well as high surface temperatures. Thus, one has firstly to understand and control the high turbulent transport processes, in order to avoid the deconfinement of the plasma gas, and secondly to control the plasma edge (understand the complex plasma-wall interactions), in order to prevent the introduction of impurities in the core of the plasma and besides to avoid the deterioration of the wall materials. The most promising fusion reactor in study at present is the ITER tokamak (International Tokamak Experimental Reactor) in Cadarache, France.

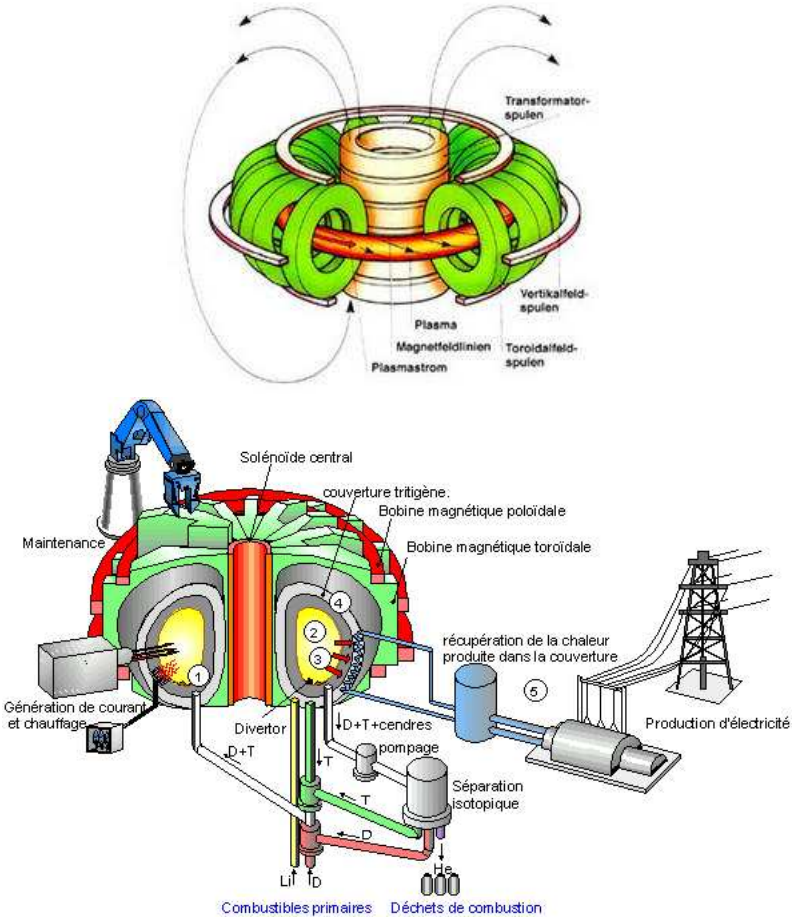

FIGURE 3: Fusion reactors, tokamaks. (http ://www-fusion-magnetique.cea.fr/)

The just described thermonuclear fusion process occurs naturally in stars, in particular in our own Sun. The Sun is a "dwarf" star of average size, temperature and brightness, held together by its own gravity, in other words it is a self-gravitating sphere

of plasma. The interior of the Sun is divided into three regions, defined by the different processes that occur there (see Fig. 4). First, there is the core, where the nuclear fusion reactions take place, turning hydrogen nuclei into helium nuclei. These reactions release the energy that escapes from the sun surface as visible light. On its way towards the Sun's surface, this energy is firstly transported by radiation (photons) through the radiative zone, a phenomenon which takes about a million years, due to the high density of the Sun's interior. As the temperature gets lower, the radiation becomes less significant and another process is set into motion in order to transport the energy, the convection. It is thought that most of the magnetic activity of the sun is driven by turbulent flows, rotation and shear in this convective zone and the origin of the magnetic field is believed to be in the tachocline, which is the thin interface layer between the radiative zone and the convective one. Anyhow, the dynamics of the Sun's interior is up to now still poorly understood. Given the wide range of temporal and spacial scales coexisting in the physical processes in the Sun, it is a great challenge to model self-consistently the solar interior and the dynamo effects. All these phenomena require state-of-the art numerical schemes supported by rigorous mathematical results.

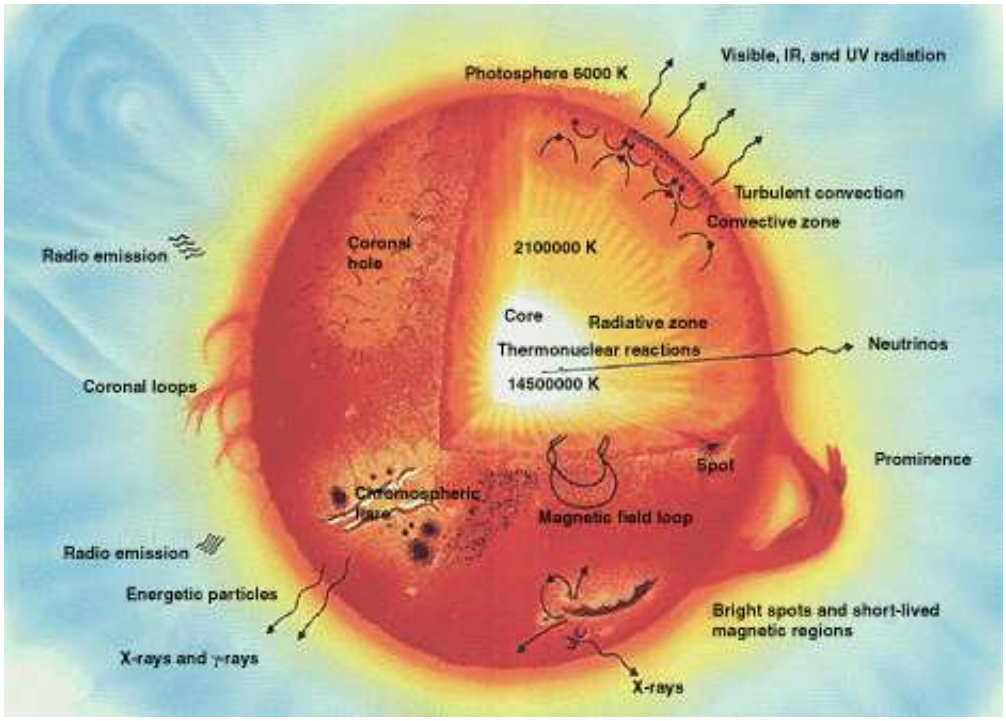

FIGURE 4: Schematic representation of the Sun's interior (http ://www.futuretimeline.net)

0.1 Different mathematical descriptions

Different approaches can be used in order to describe the evolution of charged particles in an electromagnetic field, as for example :

- the particle description, based on the motion of individual particles in an electromagnetic field
- the kinetic description, based on a collective plasma description via the particle distribution function $f_{e,i}(t, x, v)$
- the fluid description, describing the plasma in terms of averaged macroscopic quantities, depending only on t and x.

These successive models differ in complexity and precision. They are increasingly simplified, in the sense that they can be obtained from one another by decreasing the number of degrees of freedom, hereby becoming less accurate. Depending on the physical phenomenon one wants to investigate, one has to choose within all these models the one which is the most accurate with respect to the particular physical situation, paying attention at the same time to the numerical costs.

The first model, the particle dynamic model, is the most intuitive one and the physically most accurate one, but also the most inadequate/heavy from a numerical point of view. The evolution of each particle is described by means of Newton's law, $F = m\,a$, coupled to Maxwell's equations for the electromagnetic fields (E, B). A complete dynamical description of the whole system is however out of reach, as the system contains $6N$ degrees of freedom, where N is the number of particles, which is of the order of Avogadro's number, *i.e.* 10^{23}. No computer today can deal with such high dimensionalities, such that this approach remains purely theoretical.

But one is usually not interested in all the microscopic information, such that it can be averaged out and we can consider a second approach, based on a statistical picture of the gas of electrons/ions. The plasma dynamics is described via a distribution function $f(t, x, v)$, with $f(t, x, v)\,dv\,dx$ representing the number of particles occurring at the moment t in the phase-space volume $dv\,dx$ around (v, x). The equation governing the particle distribution evolution is a kinetic equation, like the Vlasov, Boltzmann or Fokker-Planck equation, coupled self-consistently with Maxwell's equations for the electro-magnetic fields (E, B). Although the precise locations of the individual particles are lost in the kinetic theory, detailed knowledge of the particle motion is still incorporated. However, even if the kinetic models are simpler than the particle models, they are used at the moment mainly at a theoretic level, as the numerical costs are still rather high, the system being 6 dimensional. They are generally the starting point for the derivation of more tractable macroscopic models, via asymptotic limits or moments methods.

A rather new and powerful approach consists in simplifying further the kinetic model, in order to obtain a 5-dimensional gyro-kinetic model. Indeed, the Vlasov equation is still too difficult to solve numerically, as it includes the very rapid gyro-motion of the particles around the magnetic field lines (see Fig. 5). One idea is now to average over the rapid gyro-phase motion, in order to get a guiding centre motion, which signifies nothing else than that the particles follow the field lines, at lowest order in the gyro-radius. The turbulent fluctuations, which one wants to describe accurately, are at much lower frequencies than the cyclotron motion, such that this approach provides today the deepest insight in plasma dynamics. However, high performance computing techniques are still necessary to solve the $5D$ gyro-kinetic equations, the employed numerical schemes being

either the Lagrangian, the semi-Lagrangian or the Eulerian methods.

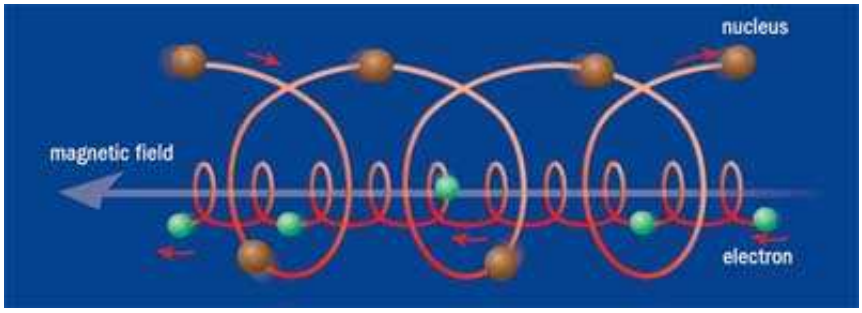

FIGURE 5: Gyration of the electrons/ions about a magnetic field line
(http ://www.scidacreview.org/0601/html/fusion.html)

The third approach is the macroscopic or fluid approach. The fluid models constitute a further simplification of the above kinetic models, and are hence numerically more attractive, but poor from a physical point of view. They deal with averaged quantities, like the particle density $n(t,x)$, the current density $j(t,x)$, the velocity $v(t,x)$, the temperature $T(t,x)$, which only depend on the position and the time variable. Even if physically not accurate, fluid models are still of wide use at the moment in plasma simulations, as they permit more easily to make use of the physical intuition one has and are numerically less demanding. Moreover, they permit to use the knowledge and the numerical codes from the fluid domain, adapting them however to the new "gas", as the plasma lacks the high collisionality of the fluids as well as their isotropy. However, one has to keep in mind that the extraordinary varied plasma behaviour (as for example plasma waves and oscillations) can only be fully captured in a kinetic framework.

0.2 Multiscale problems

Plasma dynamics is characterized by a multiscale nature. Magnetism creates anisotropy, which means that the properties of the plasma are rather different when considered in the parallel or in the transverse direction with respect to the magnetic field lines. This anisotropy contributes, jointly with other phenomena, to the multi-scale dynamics of the plasma, in particular a very large variety of time and space scales occurs (see Fig. 6). As an example, concerning the temporary scales, one can pass from the fast electron plasma frequency ω_p, to the fast Larmor gyromotion ω_c, further to the collisional frequencies $\nu_{i,e}$ and finally to the confinement time τ_E . Concerning the spatial scales, it ranges from the small Debye length λ_D, to the electron Larmor radius ρ_e, further to the mean free path of the particles and finally to the spacial extent of the tokamak L.

Many other problems in nature exhibit multiscale behaviours, which can be rather different in character. One can divide these problems in two categories. On one hand we have problems which exhibit local singularities, like for example boundary or internal

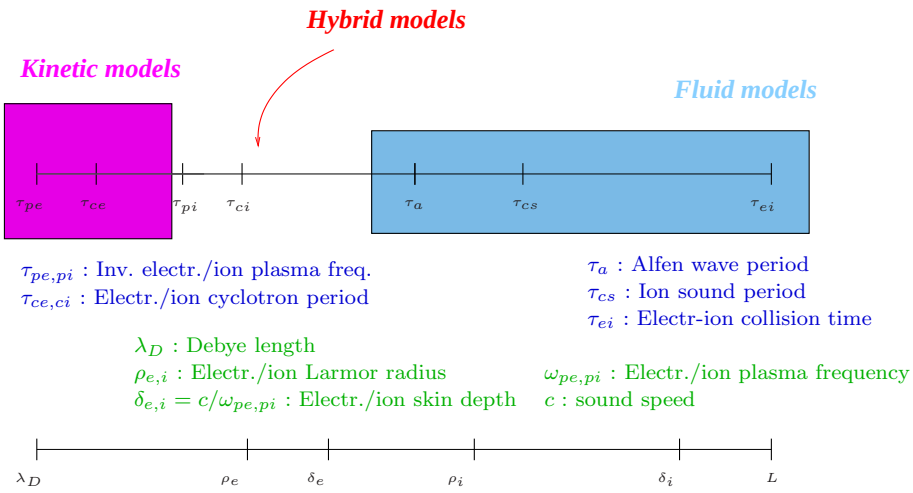

FIGURE 6: Different time and space scales occurring in a fusion plasma

layers, shocks, dislocations and so on. On the other hand we have problems, where microscopic and macroscopic scales coexist in the whole domain, as for example porous media flows, turbulent flows, highly oscillating problems *etc.* A general, unified treatment of all these problems is impossible, such that a lot of techniques have been developed in literature, each one being adapted to a particular situation.
When several scales occur in a physical problem, it is no more adequate to use an approach which describes the phenomenon on a single scale. Describing the problem on a microscopic level is physically very accurate, however from a computational point of view unfeasible. Using a macroscopic description, which means a model which uses explicit equations for the macroscopic scale, eliminating the other scales, is also inappropriate. Indeed, this procedure uses often empirical closures for the elimination/description of the microscopic scales, that are not justified nor well understood, as for example the viscosity tensor terms in turbulent flows. In all these cases, one has to go to multi-scale modelling, for example using different models, which describe the phenomena on the different scales, and taking care to achieve a balance between accuracy of the numerical results and efficiency of the numerical method. Briefly, the main goal of multiscale techniques is to design microscopic-macroscopic numerical schemes, which are more efficient than solving the full microscopic model and at the same time furnish the desired accuracy.

In more details, suppose we are interested in the evolution of a macroscopic quantity, say U, but we do not have an explicit macroscopic model for the description of U, which is valid everywhere. This can be either because we lack the constitutive relation or because the macroscopic model is invalid due to the presence of localized singularities for example. However, we dispose of a microscopic model, describing the dynamics of a microscopic quantity u, which is related to U by a relation $F(u) = U$. Our goal is to accurately approximate the variable U, using a macroscopic grid, in order to be efficient from a computational point of view. A standard method would require to use a fine grid, in order to resolve the small scales of the problem, obtaining thus u, and

computing then the correct macroscopic solution. However, this is usually a computationally phenomenal and unfeasible work. And moreover, for most engineering purposes, it is even unnecessary to know all the details of u. Engineers are often contented with accurate time-averaged properties of the flow, as the averaged velocities, pressures *etc.* Multi-scale methods were thus introduced in literature, based on different ideas, however with the same aim, which is to capture the macroscopic evolution, using the necessary/required microscopic information, without however having to resolve in detail the microscopic behaviour. Some analytical techniques to cope with multiscale problems are for example the "matched asymptotics method", used for problems which undergo rapid variations in localized regions, or the "homogenization methods", employed in the case of problems with oscillating coefficients and based on asymptotic expansions. Among the numerical approaches can be counted the multigrid methods and the adaptive mesh refinements, which are efficient techniques for the resolution of the small-scale behaviour of the solution. Furthermore, domain decomposition methods aim to couple different mathematical descriptions, corresponding to different regions of the domain, where the physics is distinct. And finally, multiscale finite element methods employ basis functions, which incorporate the small-scale information, permitting thus the use of coarse grids. For a detailed description of all these methods, we refer to the book of C. le Bris and M. H. Holmes [28, 34] as well as all the references therein.

0.3 Asymptotic-Preserving methods

The solutions of singularly perturbed problems reveal also a multiscale character, and their numerical resolution presents some major difficulties. Singular perturbation problems are characterized by the occurrence of one or several small parameters, denoted in this section by $0 < \varepsilon \ll 1$, and the mathematical as well as numerical difficulties arise due to a change in type of the equation as $\varepsilon \to 0$. The solutions of the singularly perturbed problem show a non-uniform behaviour as the parameter tends to zero, for instance the character of the limiting solution is different in nature from that of the solutions for finite values of $\varepsilon > 0$. Examples of such singularly perturbed problems are viscous flows with large Reynolds numbers, convective heat transport with large Peclet numbers, low Mach number flows, diffusive relaxation in kinetic models and so on.
The Asymptotic-Preserving schemes are efficient procedures for solving singularly perturbed problems P^ε. The solution of P^ε is supposed to converge, as the perturbation parameter tends to zero, towards the solution of a limit problem P^0, which is a well-posed problem. However, the fact that the singular limit $P^\varepsilon \to_{\varepsilon\to 0} P^0$ leads to a change in the type of the equation, explains somehow the difficulties encountered when trying to solve P^ε for too small ε-values. The use of standard numerical schemes for the resolution of singularly perturbed problems requires very restrictive time and space dicretization step conditions, of the type $\Delta t, \Delta x \sim \mathcal{O}(\varepsilon)$ or $\Delta t, \Delta x \sim \mathcal{O}(\varepsilon^2)$, due to stability reasons. This becomes rapidly too costly from a numerical point of view and consequently a numerical asymptotic study and even numerical simulations for small ε-values, are out of reach. Moreover, standard implicit schemes (even if computationally heavy) may be uniformly stable for $0 < \varepsilon < 1$, but yet provide a wrong solution in the limit $\varepsilon \to 0$, which means the scheme is not consistent with the limit problem P^0. Thus the design of

robust numerical methods for singularly perturbed problems, whose accuracy does not depend on the parameter ε (hence on the local scales of the singularity), allowing even to capture the limit $\varepsilon \to 0$, becomes an important task.

In order to tackle such problems, several methods were introduced in literature. One approach can be to solve directly the limit problem P^0 instead of P^ε, if ε is small. However, in some situations, the parameter ε can vary within the simulation domain, making thus this approach unusable. Indeed, ε is the ratio of two characteristic lengths, which can vary in space as well as in time. In this case, hybrid techniques can be employed, solving P^ε there where $\varepsilon \sim \mathcal{O}(1)$ and P^0 where ε is rather small. Several difficulties can be encountered with this approach, for example how to locate the interface between P^ε and P^0 and what type of interface conditions to use. Thus, this approach can be difficult to implement in practice.

Asymptotic-Preserving schemes were introduced the first time by S. Jin [30] with the aim to cope with such singularly perturbed problems, in particular in the framework of kinetic models in a diffusive regime. The construction of these AP-schemes necessitates the existence of a well-posed limit problem P^0, which has to be identified beforehand. The main feature of these schemes is that they permit a precise, ε-independent, resolution of the problem P^ε as well as of its limit problem P^0, with no huge computational effort. The main idea for the construction of AP-schemes is based on asymptotic arguments and consists in a mathematical reformulation of the singularly perturbed problem P^ε into an equivalent problem $(AP)^\varepsilon$, which is a regular perturbation of the limit problem P^0. The equivalent reformulation of P^ε into $(AP)^\varepsilon$ is a sort of "reorganization" of the problem into a form which is better suited for the numerical discretization, in particular which is a regular perturbation of P^0. The same numerical scheme is then used for the discretization of P^ε as well as for P^0, which means that they allow for an automatic numerical transition from P^ε to P^0. Remark that the AP-reformulation is by no means unique, and several AP-schemes can be conceived/designed for the same problem. It is necessary to underline here that the asymptotic preserving techniques are not used to derive a simplified "macroscopic" model, which is then solved numerically. Rather the objective is to construct a numerical scheme, using asymptotic techniques, whose solution does not deteriorate as the singular limit is approached.

To summarise, the essential properties of AP-schemes are (see diagram 7) :
- for fixed $\varepsilon > 0$, the AP-scheme, denoted in this diagram $P^{\varepsilon,h}$, is a consistent discretization of the continuous problem P^ε, where $h = (\Delta t, \Delta x)$
- the stability condition is independent of ε
- for fixed discretization parameters $h = (\Delta t, \Delta x)$, the AP-scheme $P^{\varepsilon,h}$ provides in the limit $\varepsilon \to 0$ a consistent discretization of the limit problem P^0

Thus, the asymptotic-preserving approach consists somehow in trying to mimic on the discrete level the asymptotic behaviour of the singularly perturbed problem solutions. It is thus very important to have a full understanding of the solutions behaviour. Remark that the AP-techniques have to be distinguished from the multiscale techniques, as the former solve the micro-scales when the (spacial or/and temporal) mesh-sizes

resolve these scales and automatically switch to the macroscopic behaviour when the mesh-sizes do not resolve the micro-scales. In other words, the AP-schemes catch the numerical transition from microscopic to macroscopic scales, in some difficult situations as singularly perturbed problems, however their primary focus is not to reduce the computational costs, as the multiscale methods do.

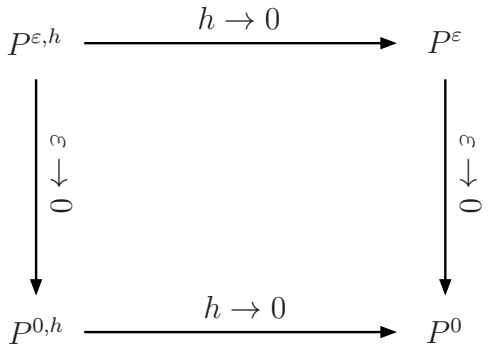

FIGURE 7: Properties of AP-schemes

0.4 Outline

The present work is a review of several Asymptotic-Preserving schemes, constructed in the kinetic and fluid framework. Inevitably, the choice of the model problems is related with the author's knowledge and with the concept of providing the reader with the most important features of AP-schemes. These schemes can be designed for several other singularly perturbed problems, that admit asymptotic behaviours/regimes.

An overview of the subject of this manuscript is :

- Chapter 1 deals with the Boltzmann equation in the drift-diffusion limit
- Chapter 2 discusses the Vlasov-Poisson system in the quasi-neutral limit
- Chapter 3 treats the subject of the Vlasov equation in the high-field limit and considering variable Larmor radii
- Chapter 4 introduces an Asymptotic-Preserving scheme for a highly elliptic potential equation
- Chapter 5 deals finally with a highly anisotropic, nonlinear, degenerate parabolic temperature equation.

PART I

Kinetic models

This part addresses the plasma modelling and simulation based on a kinetic approach. The phase-space particle distribution function $f_\alpha(t,x,v)$ (where α stands either for the electrons $\alpha = e$ or for the ions $\alpha = i$) evolves accordingly to the Boltzmann equation

$$\partial_t f_\alpha + v \cdot \nabla_x f_\alpha + \frac{e_\alpha}{m_\alpha}(E + v \times B) \cdot \nabla_v f_\alpha = Q(f_\alpha)\,, \tag{0.1}$$

where $e_\alpha = \pm e$ resp. m_α are the particle elementary charge resp. mass and $E(t,x)$ resp. $B(t,x)$ are the electric respectively magnetic fields, determined self-consistently from Maxwell's equations

$$\begin{cases} \nabla \cdot E = \dfrac{1}{\varepsilon_0}\rho \\ -\dfrac{1}{c^2}\partial_t E + \nabla \times B = \mu_0 j \\ \partial_t B + \nabla \times E = 0 \\ \nabla \cdot B = 0\,, \end{cases} \tag{0.2}$$

where ε_0, μ_0 and $c := (\varepsilon_0\,\mu_0)^{-1/2}$ are the free-space permittivity, permeability resp. speed of light and where the charge and current densities are computed via

$$\rho(t,x) = \sum_\alpha e_\alpha \int_{\mathbb{R}^3} f_\alpha(t,x,v)\,dv = e(n_i - n_e)\,, \quad j(t,x) := \sum_\alpha e_\alpha \int_{\mathbb{R}^3} v\, f_\alpha(t,x,v)\,dv\,.$$

The right hand side of (0.1) describes the collisions between the particles and its form is given by the particular physical phenomena one wants to investigate. Some examples of collision operators are the Boltzmann, the Fokker-Planck, the BGK collision operators and so on. In the electrostatic case ($B = 0$), Maxwell's equations (0.2) have to be replaced by Poisson's equation

$$-\varepsilon_0 \Delta \Phi = \rho\,, \tag{0.3}$$

where Φ is the electrostatic potential, related to the electric field E by $E = -\nabla\Phi$, where the sign comes from the convention that the electric field points in the direction of the ion motion.

As mentioned in the introduction, fusion plasmas exhibit a large amount of temporal and spacial scales, which make the numerical treatment of the plasma dynamics very challenging. Some of the main parameters characterizing the plasma are the Debye length, the particle Larmor radius, the mean free path, the plasma frequency, the cyclotron frequency, the relaxation time and so on. Depending on the physical phenomena one wants to study, different of these parameters can be considered as small in comparison to others, and various asymptotic regimes can be considered. Some of these different scalings are briefly sketched here :

– Hydrodynamic limit [15, 20, 21, 23, 24] :

$$\partial_t f + v \cdot \nabla_x f = \frac{1}{\varepsilon} Q(f)\,,$$

where $\varepsilon \ll 1$ stands here for the particle mean free path or Knudsen number. This kinetic equation is a diffusive (or collisional) equation and in the limit $\varepsilon \to 0$, one gets the compressible Euler equations.

– Drift-Diffusion scaling [14, 31–33, 36] :

$$\partial_t f + \frac{1}{\varepsilon}(v \cdot \nabla_x f + \nabla_x \Phi \cdot \nabla_v f) = \frac{1}{\varepsilon^2} Q(f)\,,$$

where again $\varepsilon \ll 1$ stands for the Knudsen number. In the diffusive limit $\varepsilon \to 0$, one obtains the Drift-Diffusion model.

– Vlasov-Poisson system in the quasi-neutral limit [4, 16] :

$$\begin{cases} \partial_t f + v \cdot \nabla_x f + \nabla_x \Phi \cdot \nabla_v f = 0 \\ -\lambda^2 \Delta \Phi = 1 - n_e\,, \end{cases}$$

with $\lambda \ll 1$ the rescaled Debye length. The $\lambda \to 0$ limit of this system, is still poorly understood from a mathematical point of view.

– High magnetic field limit [7–9, 25, 26] :

$$\partial_t f + \frac{1}{\varepsilon} v(p) \cdot \nabla_x f - \frac{1}{\varepsilon}(E + v(p) \times \frac{B}{\varepsilon}) \cdot \nabla_v f = 0\,,$$

where this time $\varepsilon \ll 1$ corresponds to the cyclotronic period. This particular non-collisional kinetic equation is no more diffusive, and the asymptotic behaviour of the solutions f_ε is rather different from the above ones (highly oscillating).

In this part of the review we will be concerned with some of these asymptotic regimes, in particular we are interested in constructing Asymptotic-Preserving schemes for some of these singular limits.

Chapitre 1

Boltzmann equation in the drift-diffusion limit

Chapter based on the articles of :
N. Crouseilles, M. Lemou [1]
M. Lemou and L. Mieussens [2]

In this chapter we shall consider the linear Boltzmann equation in a diffusive scaling $((t,x) \to (t/\varepsilon^2, x/\varepsilon))$, i.e.

$$(P_\varepsilon) \quad \partial_t f + \frac{1}{\varepsilon}\left(v \cdot \nabla_x f + E \cdot \nabla_v f\right) = \frac{1}{\varepsilon^2} Q(f)\,, \quad (x,v) \in \mathbb{R}^3 \times \mathbb{R}^3\,, \ \ t \in \mathbb{R}^+\,. \tag{1.1}$$

This equation describes the state of a gas constituted of ions, evolving in a given electric field E. The distribution function $f(t,x,v)$ stands for the density of the particles located at the position $x \in \mathbb{R}^3$ with velocity $v \in \mathbb{R}^3$ at time $t \geq 0$. The low-density collision operator Q is defined as follows

$$Q(g)(v) := \int \sigma(v,v')\left[M(v)g(v') - M(v')g(v)\right] dv'\,, \tag{1.2}$$

where g belongs to a suitable functional space and M is the Maxwellian distribution function, given by

$$M(v) := \frac{1}{(\pi)^{3/2}} e^{-v^2}\,. \tag{1.3}$$

The cross section σ satisfies the following positivity, boundedness and symmetry (micro-reversibility principle) property

$$0 < \sigma_1 \leq \sigma(v,v') = \sigma(v',v) \leq \sigma_2\,. \tag{1.4}$$

1. "An asymptotic preserving scheme based on a micro-macro decomposition for collisional Vlasov equations : diffusion and high-field scaling limits" , KRM 4 (2011), 441-477.

2. "A new asymptotic preserving scheme based on micro-macro formulation for linear kinetic equations in the diffusion limit", SIAM J. Sci. Comput. 31 (2008), no. 1, 334-368.

The small parameter $0 < \varepsilon \ll 1$ measures the distance of the system to the thermodynamical equilibrium defined by M, and is related to the particle mean free path. In other words, this Boltzmann equation models the dynamics of charged particles, evolving in a given electric field E and a highly collisional framework. It is obtained from a many-body problem under the mean-field approximation. The special linear form of the collision operator is widely used, for example in semiconductor or plasma applications, the model considered here being associated with a linear, low density approximation of the electron-phonon collisions. However, the Asymptotic-Preserving procedure presented in this chapter can be adapted also for other collision operators, as for example the Landau, Fokker-Planck or Boltzmann collision operators.
In the limit $\varepsilon \to 0$, the dominant operator in (1.1) relaxes the system towards an equilibrium state, described by a function belonging to the kernel of Q, the Maxwellian (1.3). The numerical resolution of the Boltzmann equation (1.1) is however rather arduous from a computational point of view, firstly due to its high dimensionality and secondary due to the supplementary difficulty coming from the smallness of ε. Indeed, (1.1) is a singularly perturbed problem and letting formally ε go to zero in (1.1) leads to an ill-posed problem, *i.e.* $Q(f) = 0$. A direct resolution of the Boltzmann equation, via standard schemes, will hence have to cope with this ill-posedness of the problem if ε becomes too small. Refined temporal and spatial grids (dependent on the ε-parameter) are consequently required to allow for an accurate resolution, a procedure which becomes rapidly too costly from a numerical point of view.
Hence, in order to study numerically the asymptotic behaviour of (1.1), one has to try to mimic the asymptotics of the continuous solutions. For this, we will thus firstly investigate the dominant operator and identify the Limit model, when $\varepsilon \to 0$.

1.1 Mathematical framework

Let us keep all over this section the variables (t, x) as fixed (parameters) and consider the Hilbert space

$$\mathcal{H} := L^2(\mathbb{R}^3; M^{-1}(v)\,dv) = \left\{ f \in L^2(\mathbb{R}^3) \ / \ \int_{\mathbb{R}^3} |f(v)|^2 M^{-1}(v)\,dv < \infty \right\} ,$$

associated with the following scalar product

$$(f, g)_{\mathcal{H}} := \int_{\mathbb{R}^3} f(v)\, g(v)\, M^{-1}(v)\, dv\,.$$

Then one can show the following properties of the collision operator Q :

Proposition 1.1.1 *[5,43] Under the assumption (1.4), the collision operator Q, defined by (1.2), satisfies the following properties :*
(i) The linear operator $Q : \mathcal{H} \to \mathcal{H}$ is bounded, symmetric and non-positive.
(ii) The kernel of Q is given by

$$\mathrm{Ker}(Q) := \{\rho M(v) \ / \ \rho \in \mathbb{R}\} \ .$$

(iii) The orthogonal to the kernel of Q is

$$(\mathrm{Ker}(Q))^{\perp} := \left\{ f \in \mathcal{H} \ / \ \int_{\mathbb{R}^3} f(v)\, dv = 0 \right\} .$$

(iv) $-Q$ is coercive on $(\mathrm{Ker}(Q))^{\perp}$, i.e.

$$-\langle Q(f), f \rangle \geq C ||f||^2_{\mathcal{H}} , \quad \forall f \in (\mathrm{Ker}(Q))^{\perp} .$$

(v) The range $\mathcal{I}m(Q)$ of Q is closed and coincides with $(\mathrm{Ker}(Q))^{\perp}$. We have moreover the one-to-one mapping

$$Q : (\mathrm{Ker}(Q))^{\perp} \to (\mathrm{Ker}(Q))^{\perp} .$$

Proposition 1.1.2 *Let Π be the mapping defined by*

$$\Pi : \mathcal{H} \to \mathrm{Ker}(Q) , \quad \Pi(f)(v) := \int_{\mathbb{R}^3} f(v')\, dv'\, M(v) = \langle f \rangle\, M(v) , \quad \forall f \in \mathcal{H} . \tag{1.5}$$

Then, we have

$$(f - \Pi(f), g)_{\mathcal{H}} = 0 , \quad \forall f \in \mathcal{H} , \forall g \in \mathrm{Ker}(Q) ,$$

which means that Π is an orthogonal projection on $\mathrm{Ker}(Q)$.

All these properties permit now to identify the limit problem of the Boltzmann equation (1.1) when the perturbation parameter ε tends to zero, which means for vanishing particle mean free path. This limit leads necessary to a macroscopic description of the particle gas. Indeed, inserting the Hilbert-Ansatz

$$f = f_0 + \varepsilon f_1 + \varepsilon^2 f_2 + \cdots$$

in the Boltzmann equation (1.1) and equating the terms of the same order in ε, yields first that $f_0(t, x, \cdot) \in \mathrm{Ker}(Q)$. This means that there exists a density function $\rho_0(t, x)$ such that $f_0 = \rho_0 M$. Moreover, the second equation permits to compute the unique $f_1(t, x, \cdot) \in (\mathrm{Ker}(Q))^{\perp}$ via

$$v \cdot \nabla_x f_0 + E \cdot \nabla_v f_0 = Q(f_1) \quad \Rightarrow f_1 = Q^{-1}(vM) \cdot (\nabla_x \rho_0 - 2\rho_0 E) .$$

The third equation finally yields the limit model (L-model)

$$(L) \ \ \partial_t \rho_0 - \nabla_x \cdot [D(\nabla_x \rho_0 - 2\rho_0 E)] = 0 , \tag{1.6}$$

with the diffusion-matrix given by $D := -\langle v \otimes Q^{-1}(vM) \rangle$. This is the so-called Drift-Diffusion model, describing the evolution of the macroscopic density function ρ_0 in the limit of vanishing mean free path. Remark that the microscale information is contained in this equation in a homogenized way, via the diffusion matrix D.

When the parameter ε is very small, one prefers to solve the macroscopic Drift-Diffusion equation (1.6) instead of (1.1) due to the inherent numerical difficulties detailed in the introduction. However, the DD-model describes well the physics close to the

equilibrium and is thus not suited to describe non equilibrium phenomena. If the mean-free path of the particles ($\sim \varepsilon$) varies within the computational domain, one has to adopt a hybrid strategy in order to get accurate results, solving the Boltzmann equation in regimes where $\varepsilon \sim \mathcal{O}(1)$ and the Drift-Diffusion equation when $\varepsilon \ll 1$. Hybrid strategies are however very laborious from a practical point of view, due to the difficulty to obtain coupling conditions and also to locate the interface between the two regions. The aim of the present chapter is to avoid such a hybrid strategy and to propose a numerical scheme which switches automatically between the Boltzmann and the Drift-Diffusion equations.

1.2 Micro-Macro decomposition

We have seen above that the solution of the kinetic model (1.1) tends, in the limit of vanishing mean free path $\varepsilon \to 0$, towards the solution of a macroscopic model (1.6). Trying to capture this asymptotic behaviour numerically is a very challenging problem. The idea of the construction of such Asymptotic-Preserving schemes is to reformulate the Boltzmann equation in such a manner that it becomes a regular perturbation of the limit problem (1.6).
In more details, the AP-scheme we propose in this chapter is based on a decomposition of the unknown f into a macroscopic part belonging to $\mathrm{Ker}(Q)$ and a microscopic part belonging to $(\mathrm{Ker}(Q))^\perp$. This decomposition is inspired from the fact that in the limit $\varepsilon \to 0$, the solutions f_ε tend towards a function belonging to the kernel of the collision operator, hence inspired from the Hilbert-expansion done above and the obtained Limit-model. A coupled system of equations is then obtained for the micro- respectively macro-components, which degenerates in the limit $\varepsilon \to 0$ towards the Drift-Diffusion limit model.

Let us thus decompose f as follows

$$f = \rho M + \varepsilon G\,, \quad \rho(t,x)M = \Pi(f) \in \mathrm{Ker}(Q)\,, \quad G := \frac{1}{\varepsilon}(f - \Pi(f)) \in (\mathrm{Ker}(Q))^\perp\,.$$

This unique decomposition into an equilibrium and a non-equilibrium part is illustrated in Figure 1.1. Inserting this Ansatz in the kinetic equation (1.1), yields

$$(\partial_t \rho)M + \varepsilon \partial_t G + \frac{1}{\varepsilon}\left(\nabla_x \rho \cdot v M + \varepsilon v \cdot \nabla_x G - 2\rho E \cdot v M + \varepsilon E \cdot \nabla_v G\right) = \frac{1}{\varepsilon} Q(G)\,.$$

Applying now the projection Π on this equation, and performing the subtraction $I - \Pi$ permits to get a micro-macro system for $(\rho M, G)$ (called in the sequel MM-model)

$$(MM) \quad \begin{cases} \partial_t \rho + \nabla_x \cdot \langle vG \rangle = 0 \\ \\ \varepsilon \partial_t G + (I - \Pi)(v \cdot \nabla_x G) + E \cdot \nabla_v G = \dfrac{1}{\varepsilon} Q(G) - \dfrac{1}{\varepsilon}(\nabla_x \rho) \cdot v M + \dfrac{2}{\varepsilon} \rho E \cdot v M\,. \end{cases} \tag{1.7}$$

This formulation is by construction equivalent to the initial equation (1.1). Moreover, in the limit $\varepsilon \to 0$ it permits to get immediately the macroscopic diffusion model, allowing

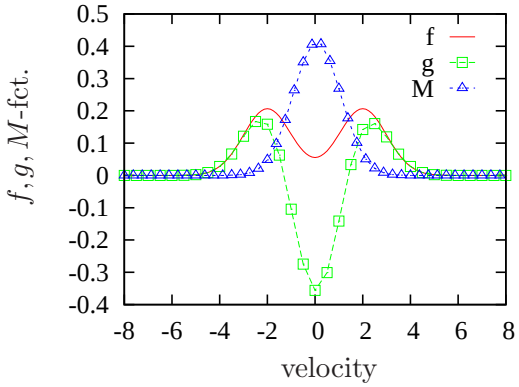

FIGURE 1.1: Micro-macro decomposition of f.

thus for a uniform transition between the kinetic and the macroscopic models. Indeed, one obtains from the second equation, as $\varepsilon \to 0$, that

$$Q(G) = (\nabla_x \rho - 2\rho E) \cdot vM \,,$$

which admits a unique solution $G \in (\mathrm{Ker}(Q))^\perp$, as the right hand side belongs to $\mathcal{I}m(Q)$. This solution has the form

$$G = -(\nabla_x \rho - 2\rho E) \cdot \theta \,, \quad \text{where } Q(\theta) = -vM \,, \ \theta \in \left((\mathrm{Ker}(Q))^\perp\right)^3 \,.$$

Thus, defining the diffusion coefficient-matrix $D := \langle v \otimes \theta \rangle$, and inserting this G in the first equation of (1.7), yields the $\varepsilon \to 0$ limit model

$$(L) \quad \partial_t \rho - \nabla_x \cdot [D\,(\nabla_x \rho - 2\rho E)] = 0 \,, \tag{1.8}$$

which is exactly the Drift-Diffusion model, we obtained in section 1.1.

To summarize, the micro-macro decomposition of the unknown f, permits to reformulate the singularly perturbed Boltzmann equation (1.1) into an equivalent system (1.7), which is a regular perturbation of the limit problem (1.8). Thus solving numerically (1.7) instead of (1.1) will permit to shift automatically to the limit problem, if the perturbation parameter ε is too small. No temporal or spatial ε-grid-restrictions are any more required to get accurate results, as it would be the case for standard schemes.
This just introduced micro-macro procedure is rather general, and can be simply adapted for a large class of collision operators.

1.3 AP-scheme

To construct an efficient numerical scheme for the resolution of the Boltzmann equation (1.1), we will discretize the equivalent reformulation (1.7) and search for the unknowns $\rho(t,x)$ respectively $G(t,x,v)$. One has to pay attention not to loose, during this discretization-procedure, the AP-property we have established in the continuous case. For simplicity reasons, we will restrict in this chapter the presentation of the AP-scheme to the $1D$ case, the generalisation to multi-D cases being straightforward, but computationally more resource demanding.

1.3.1 Semi-discretization in time

For simplicity, let us introduce a homogeneous discretization of the time-interval $[0,T]$

$$0 = t_0 < \cdots < t_k < \cdots < t_K = T\,; \quad t_k := k\Delta t\,,\ \ k = 0, \cdots, K\,;\ \ K \in \mathbb{N}\,,$$

with the time-step $\Delta t := T/K$. We will denote by $\rho^k(x)$ resp. $G^k(x,v)$ the approximations of $\rho(t_k,x)$ resp. $G(t_k,x,v)$. Then a semi-discretization of (1.7) writes

$$\left\{\begin{array}{l} \dfrac{\rho^{k+1}-\rho^k}{\Delta t} + \nabla_x \cdot \langle v G^{k+1}\rangle = 0\,, \\ \varepsilon\dfrac{G^{k+1}-G^k}{\Delta t} + (I-\Pi)(v\cdot\nabla_x G^k) + E^k\cdot\nabla_v G^k = \dfrac{1}{\varepsilon}Q(G^{k+1}) - \dfrac{1}{\varepsilon}(\nabla_x\rho^k)\cdot vM + \dfrac{2}{\varepsilon}\rho^k E^k\cdot vM\,, \end{array}\right. \tag{1.9}$$

with ρ^0 and G^0 given by the initial conditions. Remark that only the flux in the first equation and the collision term in the second one are taken implicitly. The time-discretization is a hard part in the construction of AP-schemes, in particular the determination of the terms which have to be taken implicitly is arduous and not unique. The important point is that one has to try to implicit only those necessary terms, in order to guarantee the AP-property of the scheme, in particular to recover the correct diffusion limit for $\varepsilon \to 0$. However, the level of implicitness has to be kept low, in order to minimise the computational costs.

Let us now investigate, at least formally, if the just proposed discretization (1.9) tends for $\varepsilon \to 0$ towards a time semi-discretization of the limit model (1.8). Letting thus ε tend to zero in the last equation of (1.9) leads indeed to

$$Q(G^{k+1}) = (\nabla_x\rho^k)\cdot vM - 2\rho^k E^k\cdot vM \quad \Rightarrow \quad G^{k+1} = (\nabla_x\rho^k - 2\rho^k E^k)\cdot Q^{-1}(vM)\,,$$

which, inserted in the first equation, yields indeed a discretization of the limit problem

$$\frac{\rho^{k+1}-\rho^k}{\Delta t} - \nabla_x\cdot\left[D\,(\nabla_x\rho^k - 2\rho^k E^k)\right] = 0\,,$$

with the diffusion matrix again given by $D := -\langle v\otimes Q^{-1}(vM)\rangle$.

1.3.2 Fully discrete system

Let us now introduce a homogeneous discretization of the phase-space interval $[0,L]\times[v_{min},v_{max}]$. Remark that we will consider the macroscopic equation of (1.9) at $x_i := i\Delta x$ for $i = 0,\cdots,N_x$ where $N_x \in \mathbb{N}$ and $\Delta x := L/N_x$ is the space-step. In contrast to this, the microscopic equation of (1.9) will be considered at $x_{i-1/2} := (i-1/2)\Delta x$ for $i = 1,\cdots,N_x$ and at $v_j := v_{min} + j\Delta v$ for $j = 0,\cdots,N_v$ where $N_v \in \mathbb{N}$ and $\Delta v := (v_{max}-v_{min})/N_v$ is the velocity-step. We denote in the sequel by ρ_i^k resp. $G_{i-1/2,j}^k$ the approximations of $\rho(t_k,x_i)$ resp. $G(t_k,x_{i-1/2},v_j)$. Moreover we shall denote by $\rho_{i-1/2}^k := (\rho_i^k+\rho_{i-1}^k)/2$ and evaluate the electric field E at $x_{i-1/2}$, denoting $E_{i-1/2}^k := E(t_k,x_{i-1/2})$. As we are dealing with transport equations, we will use the upwind scheme for the

transport terms and the centred difference scheme for the rest of the terms. Then a phase-space discretization of (1.9) writes : Find $(\rho_i^{k+1}, G_{i-1/2,j}^{k+1})$ solution of

$$\left\{\begin{array}{l} \dfrac{\rho_i^{k+1}-\rho_i^k}{\Delta t} + \left\langle v_j \dfrac{G_{i+1/2,j}^{k+1}-G_{i-1/2,j}^{k+1}}{\Delta x}\right\rangle = 0\,, \quad i=0,\cdots,N_x\,, \\ \varepsilon\dfrac{G_{i-1/2,j}^{k+1}-G_{i-1/2,j}^{k}}{\Delta t} + (I-\Pi)\Phi_{i-1/2,j}^k + \Psi_{i-1/2,j}^k \\ \qquad = \dfrac{1}{\varepsilon}Q_j(G_{i-1/2,\cdot}^{k+1}) - \dfrac{1}{\varepsilon}\left(\dfrac{\rho_i^k-\rho_{i-1}^k}{\Delta x}\right) v_j M_j + \dfrac{2}{\varepsilon}\rho_{i-1/2}^k E_{i-1/2}^k\, v_j M_j\,, \quad i=1,\cdots,N_x\,, \\ \qquad\qquad\qquad\qquad\qquad\qquad\qquad\qquad\qquad\qquad\qquad\qquad j=0,\cdots,N_v\,, \end{array}\right. \tag{1.10}$$

where the fluxes are defined by

$$\Phi_{i-1/2,j}^k := \frac{1}{\Delta x}\left(v_j^+(G_{i-1/2,j}^k - G_{i-3/2,j}^k) + v_j^-(G_{i+1/2,j}^k - G_{i-1/2,j}^k)\right)\,,$$

$$\Psi_{i-1/2,j}^k := \frac{1}{\Delta v}\left(E_{i-1/2}^{k,+}(G_{i-1/2,j}^k - G_{i-1/2,j-1}^k) + E_{i-1/2}^{k,-}(G_{i-1/2,j+1}^k - G_{i-1/2,j}^k)\right)\,,$$

and where we used the notations $v_j^\pm := \frac{v_j \pm |v_j|}{2}$ as well as $E_{i-1/2}^{k,\pm} := \frac{E_{i-1/2}^k \pm |E_{i-1/2}^k|}{2}$. In the discrete case, the bracket $\langle\cdot\rangle$ and the collision operator Q_j are defined by

$$\langle\Theta_j\rangle := \Delta v \sum_{j=0}^{N_v-1}\Theta_j\,, \quad Q_j(g) := \Delta v \sum_{l=0}^{N_v-1}\sigma(v_j,v_l)\left[M(v_j)g_l - M(v_l)g_j\right]\,.$$

Again, let us formally verify that in the limit $\varepsilon\to 0$, we get a discretization of the limit problem (1.8). Putting formally in the microscopic equation $\varepsilon = 0$ yields

$$Q_j(G_{i-1/2,\cdot}^{k+1}) = \left(\frac{\rho_i^k-\rho_{i-1}^k}{\Delta x}\right) v_j M_j - 2\rho_{i-1/2}^k E_{i-1/2}^k\, v_j M_j\,, \ \ \forall j=0,\cdots,N_v$$

which gives

$$G_{i-1/2,j}^{k+1} = \left(\frac{\rho_i^k-\rho_{i-1}^k}{\Delta x} - 2\rho_{i-1/2}^k E_{i-1/2}^k\right) Q_j^{-1}(vM)\,, \ \ \forall j=0,\cdots,N_v\,.$$

Inserting this in the macroscopic equation yields a discretization of (1.8).

1.3.3 Boundary conditions

To solve numerically the Boltzmann equation (1.1), we need a bounded domain and hence realistic boundary conditions. Usually inflow boundary conditions are prescribed for the distribution function f, *i.e.*

$$f(t,0,v) = f_L(v)\,, \quad v>0\,; \qquad f(t,L,v) = f_R(v)\,, \quad v<0\,, \tag{1.11}$$

and $f(t,x,v) = 0$ for all $v \notin (v_{min}, v_{max})$. The problem now is that it is rather hard (or even impossible) to translate the boundary conditions for f in boundary conditions

for the micro-macro unknowns $(\rho(t,x), G(t,x,v))$, which are indispensable for our computations via the developed AP-scheme (1.10). This problem was treated in [14], by introducing artificial boundary conditions, which lead to some unsatisfactory boundary layers, but are more simple to present in the current framework. We will thus expose here this strategy, however, a more realistic approach is proposed in [35], based on a more appropriate micro-macro decomposition, which takes from the beginning better into account for the boundary conditions.

The inflow boundary conditions (1.11) can be rewritten for the micro-macro unknowns as follows

$$\begin{aligned} \rho(t,x_0)M_j + \frac{\varepsilon}{2}\big(G(t,x_{1/2},v_j) + G(t,x_{-1/2},v_j)\big) &= f_L(v_j)\,, \quad \text{if } v_j > 0 \\ \rho(t,x_{N_x})M_j + \frac{\varepsilon}{2}\big(G(t,x_{N_x+1/2},v_j) + G(t,x_{N_x-1/2},v_j)\big) &= f_R(v_j)\,, \quad \text{if } v_j < 0\,. \end{aligned} \tag{1.12}$$

For the other velocities, artificial Neumann boundary conditions are imposed, *i.e.*

$$G(t,x_{-1/2},v_j) = G(t,x_{1/2},v_j)\,, \quad \text{if } v_j < 0\,; \quad G(t,x_{N_x+1/2},v_j) = G(t,x_{N_x-1/2},v_j)\,, \quad \text{if } v_j > 0\,, \tag{1.13}$$

as well as $G(t,x,v) = 0$ for $v \notin (v_{min}, v_{max})$. This altogether shall permit to get sufficient information from the boundary, in order to solve the system (1.10). Indeed, these formulae permit to compute the remaining "ghost"-points, via

$$\begin{aligned} G^{k+1}_{-1/2,j} &= \tfrac{2}{\varepsilon}(f_{L,j} - \rho_0^{k+1}M_j) - G^{k+1}_{1/2,j} \quad \text{if } v_j > 0\,; \quad G^{k+1}_{-1/2,j} = G^{k+1}_{1/2,j} \quad \text{if } v_j < 0; \\ G^{k+1}_{N_x+1/2,j} &= \tfrac{2}{\varepsilon}(f_{R,j} - \rho_{N_x}^{k+1}M_j) - G^{k+1}_{N_x-1/2,j} \quad \text{if } v_j < 0\,; \quad G^{k+1}_{N_x+1/2,j} = G^{k+1}_{N_x-1/2,j} \quad \text{if } v_j > 0\,. \end{aligned} \tag{1.14}$$

1.4 Numerical results

For a numerical analysis of the Asymptotic-Preserving scheme introduced so far, in particular for a detailed stability and consistency study, with a special regard on the ε-independent error estimates, we refer to [38]. In the present section, we shall only compare, for validation, the numerical results obtained via the AP-scheme in the one-dimensional case ($d = 1$), with those obtained via :

– a time explicit upwind scheme for the original Boltzmann equation (1.1), referred to as the "Vlasov-scheme", and where the discretization step sizes are chosen so that the standard transport CFL condition is satisfied, *i.e.*

$$\Delta t = C\min(\varepsilon\beta_x, \varepsilon\beta_v, \varepsilon^2)\,, \quad \beta_x := \frac{\Delta x}{v_{max}}\,, \quad \beta_v := \frac{\Delta v}{E_{max}}\,.$$

– a standard explicit discretization of the diffusion equation (1.8), referred to as the "LIM-scheme", and where the discretization step sizes are chosen so that the standard diffusion stability condition is satisfied, *i.e.*

$$\Delta t = C\min(\Delta x/E_{max}, \Delta x^2)\,.$$

Remark that the time-step size for the Asymptotic-Preserving MM-scheme is linked to the space-step size as follows [14] :

$$\begin{aligned}\Delta t &= C \min_{\varepsilon} \left(\min[C\varepsilon\beta_x/\max(0;1-C\beta_x/\varepsilon), C\varepsilon\beta_v/\max(0;1-C\beta_v/\varepsilon)]\right)\\ &\leq C\min\left(4(C\beta_x)^2, 4(C\beta_v)^2\right)\,.\end{aligned}$$

This stability condition is a combination between a transport CFL-condition and a diffusion stability condition, and has the essential advantage of being ε-independent. The aim is to present some numerical tests in order to validate the asymptotic-preserving property of the micro-macro scheme. For comparisons in the kinetic regime $\varepsilon \sim \mathcal{O}(1)$ we use the Vlasov-solver described above. As this scheme is no more AP in the diffusion limit $\varepsilon \to 0$, we shall compare for $\varepsilon \ll 1$ the MM-scheme results with those obtained by the DD-model.

We coupled our AP-system with the Poisson equation, to be physically more realistic. The initial conditions for the three models are set to

$$\begin{aligned}&(Vlasov) \quad f_0(x,v) := \frac{1}{\sqrt{2\pi}}\exp^{-v^2/2}(1+\alpha\cos(\kappa x))\,, \quad (x,v)\in[0,2\pi/\kappa]\times[v_{min},v_{max}]\,,\\ &(MM) \quad \rho_0(x) := (1+\alpha\cos(\kappa x))\,, \quad g_0(x,v)=0\,, \quad (x,v)\in[0,2\pi/\kappa]\times[v_{min},v_{max}]\,,\\ &(LIM) \quad \rho_0(x) := (1+\alpha\cos(\kappa x))\,, \quad x\in[0,2\pi/\kappa]\,.\end{aligned}$$

α	0.05	$N_x = N_v$	128
κ	0.5	$-v_{min} = v_{max}$	6
ε	$1, \cdots, 0.01$	σ	1

TABLE 1.1: Parameters used in the numerical simulations.

This test case, corresponds to the Landau damping problem and consists in a small perturbation of a Maxwellian equilibrium distribution function and the re-establishment of this equilibrium (for more details see next chapter).

We are plotting in Figure 1.2 the density $\rho(t,x)$, computed via the Vlasov and the MM-scheme, for a large ε-value. As one can observe, the MM-scheme gives results which are very close to those obtained with the "reference" Vlasov-solver. As ε becomes smaller, the computational time for the Vlasov solver becomes prohibitive, such that we can no more compare the MM-solutions with this reference solution. However, we compared in Figure 1.3 the density-function $\rho(t,x)$, computed via the MM-scheme with the results of the limit diffusion model. As one can see, for small ε-values, the MM-results are in good agreement with the Limit-model results.
To compare we also plot in Figure 1.4 the damping (in time) of the electric field $||E(t)||_{L^2}$, obtained with the three different schemes, i.e. Vlasov, MM and LIM-scheme. As one can observe, for $\varepsilon \ll 1$ the details are no more captured with the MM-scheme, as the plasma oscillations are no more resolved. However, the macroscopic behaviour is well recovered. In other words, the MM-scheme is uniformly stable and accurate along the transition from the kinetic to the macroscopic regimes, in particular it is consistent with the Drift-Diffusion model as $\varepsilon \to 0$.

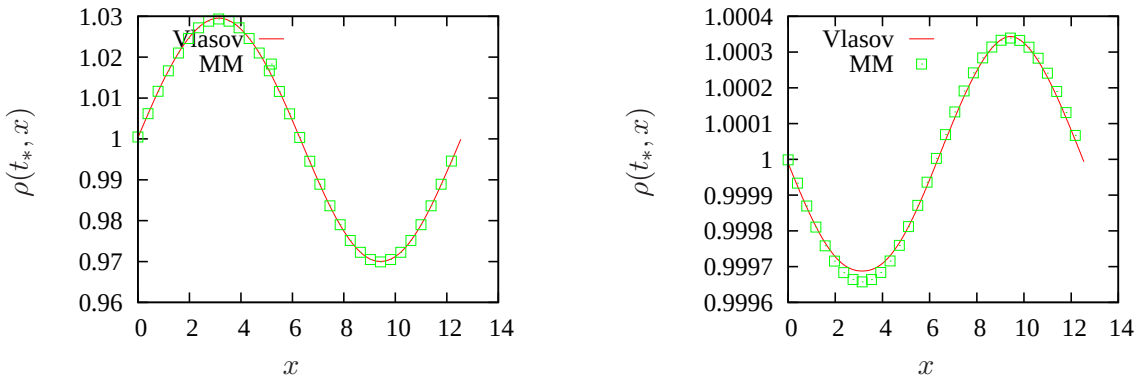

FIGURE 1.2: Density function $\rho(t, x)$ for $t = 1$ and $t = 5$. Perturb. parameter $\varepsilon = 1$

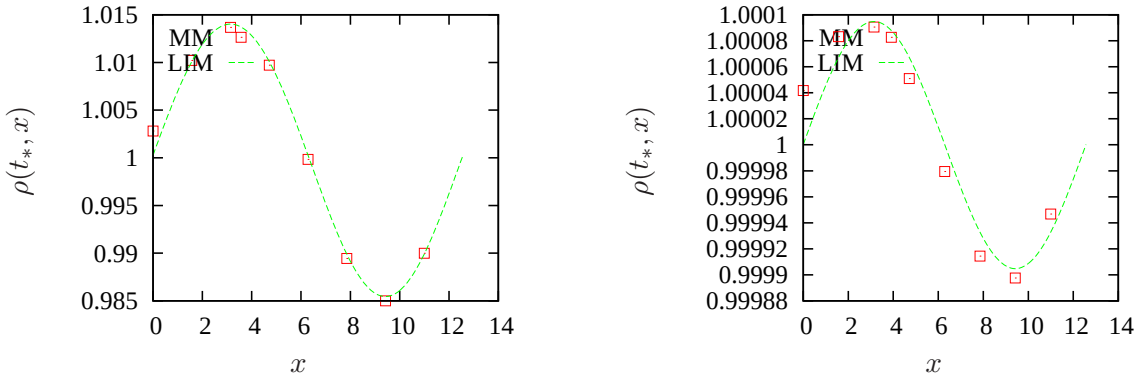

FIGURE 1.3: Density function $\rho(t, x)$ for $t = 1$ and $t = 5$. Perturb. parameter $\varepsilon = 0.01$

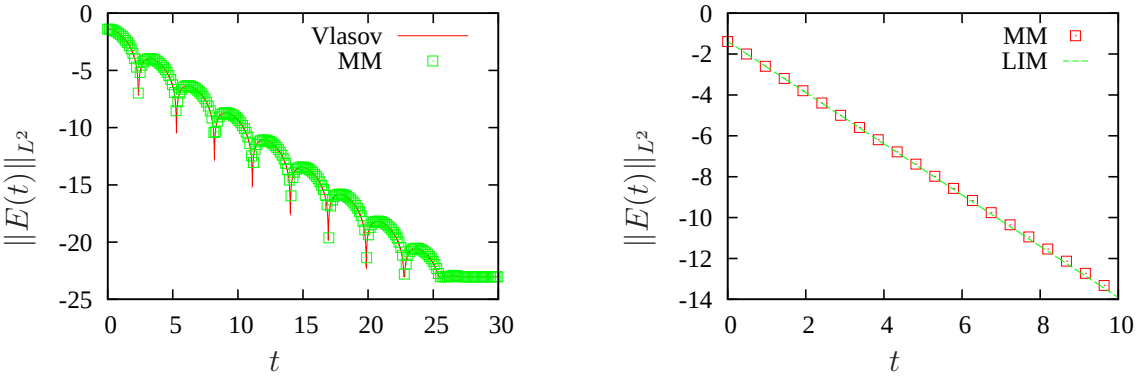

FIGURE 1.4: Linear Landau damping. Electric field evolution $||E(t)||_{L^2}$ (in log scale) for $\varepsilon = 1$ (left) and $\varepsilon = 0.01$ (right).

Chapitre 2

Vlasov-Poisson system in the quasi-neutral limit

Chapter based on the articles of :
P. Degond, F. Deluzet, L. Navoret, A-B. Sun, M-H.Vignal [1]
R. Belaouar, N. Crouseilles, P. Degond, E. Sonnendrücker [2]

The objective of this chapter shall be to investigate the following Vlasov-Poisson system

$$(P_\lambda) \quad \begin{cases} \partial_t f + v \cdot \nabla_x f + \nabla_x \Phi \cdot \nabla_v f = 0\,, \quad (x,v) \in \mathbb{T}^3 \times \mathbb{R}^3\,, \ t \in \mathbb{R}^+\,, \\ -\lambda^2 \Delta_x \Phi = 1 - \rho\,, \quad x \in \mathbb{T}^3\,, \ t \in \mathbb{R}^+ \end{cases} \tag{2.1}$$

in the quasi-neutral regime $0 < \lambda \ll 1$. Here $\mathbb{T}^3$ denotes the torus (periodic boundary conditions in x-space) and $\lambda := \lambda_D/L$ is the rescaled Debye length, which measures the typical length of charge unbalances and is of particular importance in plasma modelling. It can be seen as the typical length below which charge separation occurs. The asymptotics we are interested in, $0 < \lambda \ll 1$, means that we are considering large scales as compared to the Debye length, such that the plasma appears to be electrically neutral. A second parameter is important in this context, the plasma frequency ω_P, which characterizes the plasma oscillations which occur, when a perturbation of the quasi-neutrality is introduced.
The electron density ρ is given in terms of the electron distribution function $f(t,x,v)$ as follows

$$\rho(t,x) := \int_{\mathbb{R}^3} f(t,x,v)\, dv\,, \quad x \in \mathbb{T}^3\,, \ t \in \mathbb{R}^+\,.$$

The ratio of the electron's to the ion's mass is very large, such that one can assume that the ions are at rest and distributed uniformly on a regular grid, with density $\rho_{ion} \equiv 1$.

1. "Asymptotic-Preserving Particle-In-Cell method for the Vlasov-Poisson system near quasineutrality", J. Comput. Phys., 229 (2010), pp. 5630–5652
2. "An asymptotically stable semi-lagrangian scheme in the quasi-neutral limit", Journal of Scientific Computing, 41 (2009), pp. 341-365

The numerical resolution of equation (2.1) can be challenging for example when describing plasmas evolving in the edge region of a tokamak, where the Debye length λ may vary by several orders of magnitude and where one has to match quasi-neutral regions (where a macroscopic model is adequate) with non-neutral regions (where a microscopic model is necessary). The aim of this chapter shall be to introduce a numerical scheme which should be able to describe accurately situations where both quasi-neutral as well as non-neutral regimes coexist in the simulation domain, and this on a grid independent on the small perturbation parameter λ.

The problem (2.1) is singularly perturbed, and is hence not well-suited for numerical simulations in the limit $\lambda \to 0$. Indeed, the limit model obtained formally for $\lambda \to 0$ is

$$(P_0) \quad \begin{cases} \partial_t f + v \cdot \nabla_x f + \nabla_x \Phi \cdot \nabla_v f = 0\,, \quad (x,v) \in \mathbb{T}^3 \times \mathbb{R}^3\,,\ t \in \mathbb{R}^+\,, \\ \rho = 1\,, \quad x \in \mathbb{T}^3\,,\ t \in \mathbb{R}^+\,. \end{cases} \tag{2.2}$$

The Poisson equation degenerates into the quasi-neutrality constraint $\rho = 1$, such that the possibility to compute the electrostatic potential Φ via this Poisson equation is lost. The electrostatic potential gradient $\nabla_x \Phi$ becomes the Lagrange multiplier corresponding to the quasi-neutrality constraint. Mainly due to this difficulty of a constraint Lagrangian multiplier structure of the Limit problem, it is not adequate to use the P_λ-problem to study numerically the quasi-neutral limit regime $\lambda \to 0$.

The aim of the present chapter is to present an AP-scheme which is consistent with the P_λ-problem when the discretization parameters Δt, Δx resolve the scales associated to the parameter λ ($\Delta t \ll \omega^{-1}, \Delta x \ll \lambda$), and which allows stable simulations even if the time and space scales do not resolve the plasma period and the Debye length. Moreover, if the limit $P_\lambda \to_{\lambda \to 0} P_0$ is justified mathematically, the AP-scheme shall be at the same time consistent with the asymptotic problem P_0 when $\lambda \to 0$ and for fixed Δt, Δx. In other words, this AP-scheme shall permit to handle situations with strongly varying parameter λ in a uniform framework, without the severe requirements of standard schemes, consisting in reducing the space and/or time steps with vanishing λ.

2.1 Instabilities of the Vlasov-Poisson system

With reference to the mathematical study of the Vlasov-Poisson system P_λ (well-posedness, stability of equilibria, *etc*) rigorous results are still incomplete. The existence/uniqueness of global weak solutions $(f_\lambda, \Phi_\lambda)_{\lambda>0}$ is for example firstly due to Arsenev [2] and several other works deal with these problems, a non-exhaustive list being [3, 22, 29, 37, 42, 44]. Furthermore, the asymptotic limit $\lambda \to 0$ is also rather difficult to investigate and only partial results are obtained till now, for example [10,27]. The reason for these mathematical difficulties lies in the (linear or non-linear) instabilities of some equilibrium distribution functions.

Briefly, the Vlasov equation has infinitely many equilibria, such as spatially homogeneous ones $f(v)$ or functions of the total energy $f(E)$ with $E(x,v) := \frac{|v|^2}{2} + \Phi(x)$.

These equilibria are so important as they are the only physical situations we encounter in reality. Important questions arise now, as for example : Are these equilibria stable ? Which of them are attractive and so on. A stability criterion due to Penrose mentions that if the initial condition f_0 is a small perturbation of an increasing/decreasing distribution function, for example a Maxwellian with a small secondary bump, then linear stability follows. However, if the bump gets larger, there will be a linear instability which will develop, like the bump-on-tail instability or the two-stream instability. All this is valid in a space domain with periodic boundary conditions $\Omega_x := \mathbb{T}^3$. The situation is completely different when considered on the whole space $\Omega_x := \mathbb{R}^3$.

Accordingly, the formal limit $P_\lambda \to P_0$ we performed above is not justified in general cases, but only valid for well-prepared initial conditions, like for example small perturbations of Maxwellian distribution functions, or mono-kinetic distribution functions as

$$f_0(x,v) := \rho_0(x)\delta_{v=u_0(x)}\,.$$

For this special initial conditions, one can get a rigorous asymptotic study, and it is this case which shall be investigated in the present study. We would like to underline here that the construction of AP-schemes requires a well-posed mathematical framework, in particular the solutions f_λ of the singularly perturbed problem have to converge towards the solution f_0 of a limit problem, which has to be identified and also be well-posed. In the opposite situation no AP-scheme can be constructed and the problem remains unsolved.

The above quasi-neutral limit can be seen as the kinetic counterpart of the incompressible limit in fluid dynamics. Indeed, integrating the Vlasov equation with respect to v and taking furthermore the velocity moment, leads to a non-closed system of two macroscopic equations, corresponding to the conservation of the mass ρ respectively momentum $\rho\, u$

$$\left\{\begin{array}{l} \partial_t\rho + \nabla_x\cdot(\rho u) = 0\,,\\ \partial_t(\rho u) + \nabla_x\cdot S - \rho\nabla_x\Phi = 0\\ -\lambda^2\Delta_x\Phi = 1-\rho\,, \end{array}\right. \tag{2.3}$$

where the momentum ρu and the specific (momentum) flux S are given by

$$\rho\, u := \int_{\mathbb{R}^3} v f\, dv\,, \quad S := \int_{\mathbb{R}^3} f v\otimes v\, dv\,,$$

and $\otimes$ is the tensor product. Letting now formally λ tend to zero, yields

$$\left\{\begin{array}{l} \rho = 1\\ \partial_t u + \nabla_x\cdot\displaystyle\int_{\mathbb{R}^3} v\otimes v\, f\, dv - \nabla_x\Phi = 0\\ \nabla_x\cdot u = 0\,. \end{array}\right. \tag{2.4}$$

For mono-kinetic distribution functions $f(t,x,v) := \rho(t,x)\delta_{v=u(t,x)}$, one passes in the fluid framework and obtains for $\lambda\to 0$ immediately the limit from the compressible to

the incompressible Euler equations

$$\begin{cases} \partial_t u + (u \cdot \nabla_x) u - \nabla_x \Phi = 0 \\ \nabla_x \cdot u = 0 \,. \end{cases}$$

For this reason, the limit problem (2.2) can be seen as the kinetic counterpart of the incompressible Euler equations. Thus, the AP-scheme constructed in the subsequent section, can be equally applied for the Euler-Poisson system in the quasi-neutral regime.

2.2 AP-Reformulation of the Vlasov-Poisson system

In order to construct a numerical scheme, which shall permit to solve (2.1) uniformly accurate in λ, hence being better suited for the quasi-neutral limit $\lambda \to 0$ simulations, we will reformulate in this section the problem (2.1) such that it does no more degenerate in the limit $\lambda \to 0$. The idea is to try to replace the constraint $\rho = 1$ in the limit with an equation allowing for the computation of Φ.

For this, let us make the same manipulations as above, in order to obtain the macroscopic system (2.3). Differentiating now the first equation of (2.3) in time and the second one in space, yields after subtraction of the two resulting equations

$$\partial_t^2 \rho - \nabla_x \cdot (\nabla_x \cdot S) + \nabla_x \cdot (\rho \nabla_x \Phi) = 0 \,.$$

Denoting now by : the contracted product of two tensors, in this case $\nabla_x^2 : S := \sum_{i,j} \partial_j \, \partial_i \, S_{ij} = \nabla_x \cdot (\nabla_x \cdot S)$ and substituting in this last equation the Poisson equation, yields the reformulated Poisson equation

$$-\nabla_x \cdot \left[(\lambda^2 \partial_t^2 + \rho) \, \nabla_x \Phi \right] = -\nabla_x^2 : S \,.$$

To summarize, the reformulated Vlasov-Poisson system writes now

$$(RP)_\lambda \quad \begin{cases} \partial_t f + v \cdot \nabla_x f + \nabla_x \Phi \cdot \nabla_v f = 0 \,, \quad \forall (x,v) \in \mathbb{T}^3 \times \mathbb{R}^3 \,, \ \forall t \in \mathbb{R}^+ \\ -\nabla_x \cdot \left[(\lambda^2 \partial_t^2 + \rho) \, \nabla_x \Phi \right] = -\nabla_x^2 : S \,, \quad \forall x \in \mathbb{T}^3 \,, \ \forall t \in \mathbb{R}^+ \,. \end{cases} \tag{2.5}$$

The original Vlasov-Poisson system (P_λ) is equivalent to the reformulated system $(RP)_\lambda$, if and only if the initial data $\Phi(t=0,x) =: \Phi_0$ as well as $\partial_t \Phi(t=0,x) =: \Phi_0'$ satisfy the two Poisson equations

$$\begin{aligned} -\lambda^2 \Delta_x \Phi_0 &= (1-\rho)_0 \,, \\ -\lambda^2 \Delta_x \Phi_0' &= (1-\rho)_0' = \nabla_x \cdot (\rho_0 u_0) \,. \end{aligned} \tag{2.6}$$

This comes from the fact that differentiating in time and space (2.3), we lost some information, which has to be recovered by fixing some initial conditions.
Letting now λ tend to zero in the reformulated system, one obtains the system

$$(RP)_0 \quad \begin{cases} \partial_t f + v \cdot \nabla_x f + \nabla_x \Phi \cdot \nabla_v f = 0 \,, \quad \forall (x,v) \in \mathbb{T}^3 \times \mathbb{R}^3 \,, \ \forall t \in \mathbb{R}^+ \\ -\nabla_x \cdot (\rho \, \nabla_x \Phi) = -\nabla_x^2 : S \,, \quad \forall x \in \mathbb{T}^3 \,, \ \forall t \in \mathbb{R}^+ \,, \end{cases} \tag{2.7}$$

associated with the initial constraints (2.6).
This system is equivalent to the limit problem $(P)_0$ introduced above, as one can immediately verify. The main difference of the reformulated limit problem $(RP)_0$ as compared to (P_0) is however, that the constraint $\rho = 1$ has been replaced by an elliptic equation for the computation of the electrostatic potential Φ, which is an essential advantage, as it allows to investigate numerically the quasi-neutral limit $\lambda \to 0$ in a straightforward way. It also permits to treat, in a unified framework, problems where λ varies from $\mathcal{O}(1)$-values to $\lambda \ll 1$ within the computational domain.
The construction of an AP-scheme will hence be based on the discretization of the reformulated Vlasov-Poisson system (2.5) and will be the aim of the next section.

2.3 Discretization of Vlasov-Poisson systems

The development of precise, fast and not memory demanding numerical schemes for the resolution of Vlasov-Poisson systems is a very hard task, due to several aspects. Some of the problems one has to face are the high dimensionality of the problem (3 space +3 velocity +1 time variable), the restrictive small time steps to be chosen and the preservation of the positivity and other conservation quantities.
Several approaches have thus been introduced in literature to approximate numerically Vlasov-Poisson systems, each of them having their advantages and disadvantages. Three of them are the PIC (Particle-in-Cell) methods, the semi-Lagrangian methods and the Eulerian methods.

The first two methods rely on the characteristics method. The characteristic flow, associated to the Vlasov equation is given by the solution of the following ODE

$$\begin{cases} \dfrac{dX}{ds}(s;x,v,t) = V(s;x,v,t)\,, \\ \dfrac{dV}{ds}(s;x,v,t) = \nabla_x \Phi(s, X(s;x,v,t))\,, \end{cases} \tag{2.8}$$

associated with the following initial conditions

$$X(t;x,v,t) = x\,, \quad V(t;x,v,t) = v\,.$$

Knowing these characteristic curves, the solution of the Vlasov equation is simply constant along them, such that one has

$$f(t,x,v) = f_0(X(0;x,v,t), V(0;x,v,t))\,, \quad \forall (t,x,v) \in \mathbb{R}^+ \times \mathbb{R}^3 \times \mathbb{R}^3\,,$$

where f_0 is the initial condition for the Vlasov equation.

The PIC method consists in approaching the initial particle distribution function by N macro-particles, as follows

$$f_0(x,v) \sim \sum_{j=1}^{N} f_j\, \delta(x - X_j^0)\, \delta(v - V_j^0)\,,$$

where (X_j^0, V_j^0) are the initial positions respectively velocities of the macro-particles. Then, it can be shown rigorously that the solution of the Vlasov equation has the form

$$f(t,x,v) \sim \sum_{j=1}^{N} f_j \, \delta(x - X_j(t)) \, \delta(v - V_j(t)) \, ,$$

where the trajectories $(X_j(t), V_j(t))$ follow the characteristic curves of the Vlasov equation, starting in (X_j^0, V_j^0). The Poisson equation (original or reformulated) is then solved on a grid of the x-space via standard finite difference or finite element methods, and by assembling the charge density as

$$\rho(t,x) = \int_{\mathbb{R}^3} f(t,x,v) \, dv = \sum_{j=1}^{N} f_j \, \delta(x - X_j(t)) \, .$$

Remark that for this trajectory-mesh coupling-procedure one needs to interpolate the values of the density ρ on the x-mesh and inversely the value of the electric potential Φ on the characteristic curves.
The PIC-method is well-suited for large $3D$ computations, since only the space variable x has to be discretized, and it has also the advantage of conserving the mass of the distribution function f. Moreover, as the particles evolve along the characteristic curves, no CFL-condition has to be imposed (more precisely, the stability conditions can be largely relaxed), such that the restrictive choice of small time-steps is avoided. Unfortunately the PIC-methods produce large numerical noise, which makes the method of rather low precision, insufficient to capture detailed structures. The introduction of a finite number of macro-particles is responsible for this noise creation. To reduce the noise, the number of macro-particles has to be increased, however the reduction is rather low, $\sim 1/\sqrt{N}$, and leads to higher computational costs.

For lower-dimensional problems ($2D$ or $1D$), the semi-Lagrangian methods are preferred. The backward semi-Lagrangian method consists in advecting the conserved quantities, like f, along the characteristic paths (updating thus f at t_{n+1} from the value at t_n) and solving then the Poisson equation with a standard discretization scheme on the x-grid. Given the value of f at time level n and at each phase-grid point, the first part of the semi-Lagrangian procedure for updating f at t_{n+1}, consists in two steps :

- determine for each grid point (x_k, v_l) the origin of the characteristic curve ending at this point, *i.e.* $(X(t_n; x_k, v_l, t_{n+1}), V(t_n; x_k, v_l, t_{n+1}))$ and set $f(t_{n+1}, x_k, v_l) = f(t_n, X(t_n; x_k, v_l, t_{n+1}), V(t_n; x_k, v_l, t_{n+1}))$
- compute an approximation of the distribution function at this origin point by interpolation (B-splines) from the known neighbouring mesh-point values at time level n

Figure 2.1 illustrates one step of the backward semi-Lagrangian procedure in order to get the new value $f(t_{n+1}, x_k, v_l)$.
An essential feature of the semi-Lagrangian method is that it releases the time step restrictions (analogous to the PIC method), and it can be rendered conservative. However, as the method is grid-based (phase-grid), it is very memory demanding and time consuming, hence being used for the moment only in low dimensions. The great advantage

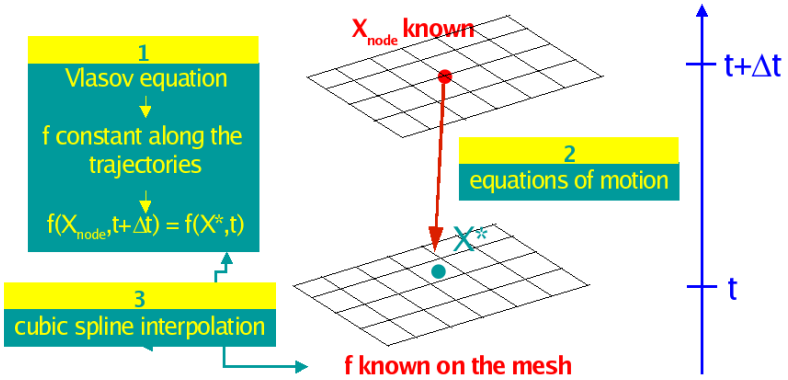

FIGURE 2.1: Backward semi-Lagrangian method

anyhow is that no numerical noise is generated, such that the method is largely more precise than the PIC method.

The Eulerian methods are classical time-space discretizations of the Vlasov-Poisson system (2.5) in the phase-space (x, v), like for example finite difference, finite element or finite volume methods. As these method are not using the characteristic curves to evolve the distribution function f, a sever CFL-condition has to be imposed, which makes these methods very costly, even if they are rather accurate.

2.4 Numerical results

In order to validate the AP-methodology introduced in section 2.2, let us present here some numerical results performed in the $1D$ framework and extracted from the works [4,16]. Two approaches are considered for the discretization of the Vlasov equation, the PIC- and the semi-Lagrangian methods, in their classical or asymptotic-preserving version when regarding the coupling with the Poisson equation. Remark that as no explicit solutions are known for the Vlasov-Poisson system, we shall compare the obtained AP-results with standard simulations, and this on very fine grids (resolved case). In the unresolved case however, when the standard schemes are no more accurate, the accuracy of our AP-method shall be checked, by comparing the numerically obtained damping of some small perturbations or growth of some instabilities, with the analytically computed decay/growth rates. The test cases we shall consider here are rather standard :

- slight perturbation of a Maxwellian, with particular consideration of the Landau damping phenomena
- bump-on-tail instability .

The intention behind all these tests is the understanding of the long-time behaviour of the solutions, when the initial data corresponds to a small perturbation of a spatially homogeneous equilibrium.

2.4.1 Slight perturbation of a Maxwellian/Landau damping

The first test case deals with the simulation of the Vlasov-Poisson system, with an initial condition of the form

$$f_0(x,v) := \pi^{-1/2}(1+\delta\sin(\kappa\pi x))\, e^{-v^2}\,,$$

which corresponds to a small perturbation of a Maxwellian, with amplitude $\delta = 10^{-2}$ and frequency $\kappa = 2220$. This is a slight perturbation of a stable equilibrium. What is expected is that the electric field converges in times towards zero, and the equilibrium is recovered in the long-time asymptotic.

Two different tests are performed with the PIC approach, in the standard and AP-approach. The space-simulation domain is $(0,1)$, with $N_x := 1/\Delta x + 1$ and 100 particles per cell. Periodic boundary conditions are imposed in space for the Vlasov equation, whereas homogeneous Dirichlet boundary conditions for the Poisson equation. The re-scaled Debye length is $\lambda := 10^{-4}$, such that the plasma frequency is $\omega := 1/\lambda = 10^4$.

In the first test, both time and space scales are resolved, as we are taking $\Delta x := \lambda = 10^{-4}$ and Δt satisfying the CFL condition of the Vlasov equation as well as resolving the plasma period, *i.e.*

$$\Delta x = \lambda\,, \quad \omega\Delta t \leq 1\,, \quad v_{max}\,\Delta t \leq \Delta x\,,$$

where v_{max} is the maximal electron velocity at each time step. In Fig. 2.2, we present results obtained with the classical PIC, and two different PICAP-schemes. These two PICAP-schemes correspond to two slightly different time-discretization strategies of the reformulated Vlasov-Poisson system (2.5), which conserve both the asymptotic-preserving property, but which shall not be detailed here (see [16] for more details). Fig. 2.2 (left) gives the electric potential as a function of the position at an instant $t = 10\,\omega^{-1}$. The electric potential is almost identical with the three schemes. In Fig. 2.2 (right) we plot the electric potential after a large number of plasma periods ($t = 2000\,\omega^{-1}$). We can see that the amplitude of the plasma waves is of the same order of magnitude as previously when using the classical PIC scheme, while it has been strongly damped out with the PICAP-1 and PICAP-2 methods. This shows that the AP strategy damps out the energy of the plasma waves and allows to capture phenomena which occur on longer time scales.

The second test case corresponds to the case, where both time and space scales are under-resolved, which means

$$\Delta x > \lambda\,, \quad \Delta t > \omega^{-1}\,, \quad v_{max}\,\Delta t \leq \Delta x\,.$$

We choose $\Delta x = 10^{-2}$ while $\lambda = 10^{-4}$ and the total number of particles is kept unchanged. For both PICAP-1 and PICAP-2 schemes, we use a time step determined by the CFL condition : $v_{\max}\Delta t \leq \Delta x$. This constraint still allows Δt of the order of 30 times the plasma period ω^{-1}. Simultaneously, we use a uniform time step for the Classical PIC scheme, with $\Delta t = 30\omega^{-1}$. Remark that the CFL condition is not satisfied for the

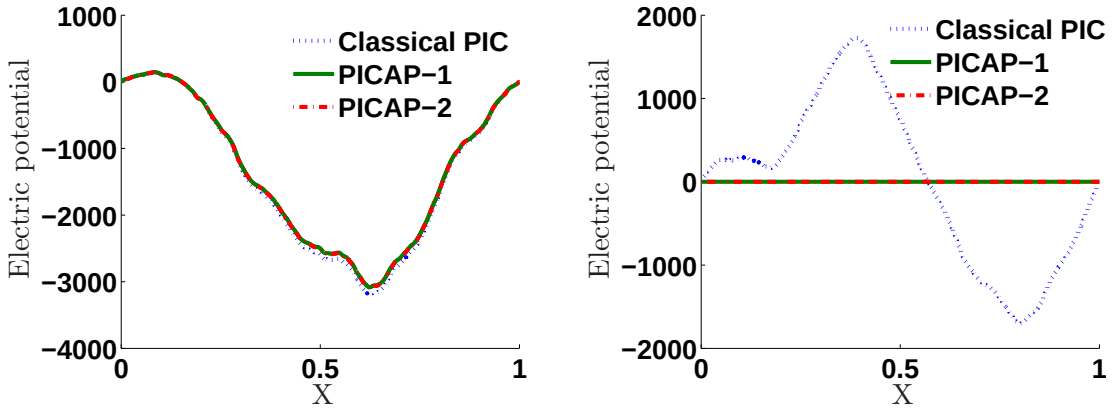

FIGURE 2.2: Perturbation of a quasi-neutral Maxwellian plasma. Resolved case : $\Delta x = \lambda = 10^{-4}$ and $\Delta t < \omega^{-1} = 10^{-4}$. Electric potential with Classical PIC, PICAP-1 and PICAP-2. Left : at time $t = 10\omega^{-1} = 10^{-3}$; Right : at time $t = 0.2 = 2000\omega^{-1}$.

classical PIC scheme, because the instability generates very large particle velocities and enforcing this CFL condition would generate very small time steps, which is unfeasible.

Fig. 2.3 depicts the electric potential at time $t = 2000\,\omega^{-1}$. The left picture shows a result using the classical PIC scheme. The instability of the scheme is clearly visible since the amplitude of the potential oscillations are now of the order of ten times those of the initial potential (see Fig. 2.2 for instance). With the PICAP-1 or PICAP-2 schemes, these amplitudes are now very small, showing that the schemes are stable and have damped out plasma waves, as in the resolved case.

Let us now come to the Landau damping, which is a relaxation property near stable equilibria, driven by conservative phenomena. The idea is to investigate how, starting from an initial perturbation of a Maxwellian, the electric field converges to zero at a rate, which is exponential. This phenomena occurs due to the interaction between plasma waves and particles. Particles gain energy from the wave or lose it to the wave, such that in the Maxwellian case, energy is finally transferred from the electric field to the particles, resulting in an "exponential" collisionless damping of the electric field.

The initial condition of the Vlasov-Poisson equation is now given by

$$f_0(x,v) = (2\pi)^{-\frac{1}{2}}(1 + \delta\sin(\kappa x))\exp^{-v^2/2}, \tag{2.9}$$

on the space-interval $(0, 2\pi/\kappa)$. The perturbation amplitude is taken equal to $\delta = 10^{-2}$ and $\kappa = 1$. The target of such a test case is to measure the accuracy of the numerical schemes for capturing nonlinear Landau damping, which is a phenomenon occurring on the time scales of the plasma oscillations.

In the first test case, the PICAP-1 and PICAP-2 schemes are compared to the classical PIC scheme in the resolved case. We take $\Delta x = 2 \times 10^{-2}$ and we consider 10^4 particles per cell (in average). Thus, the total number of particles is of the same order

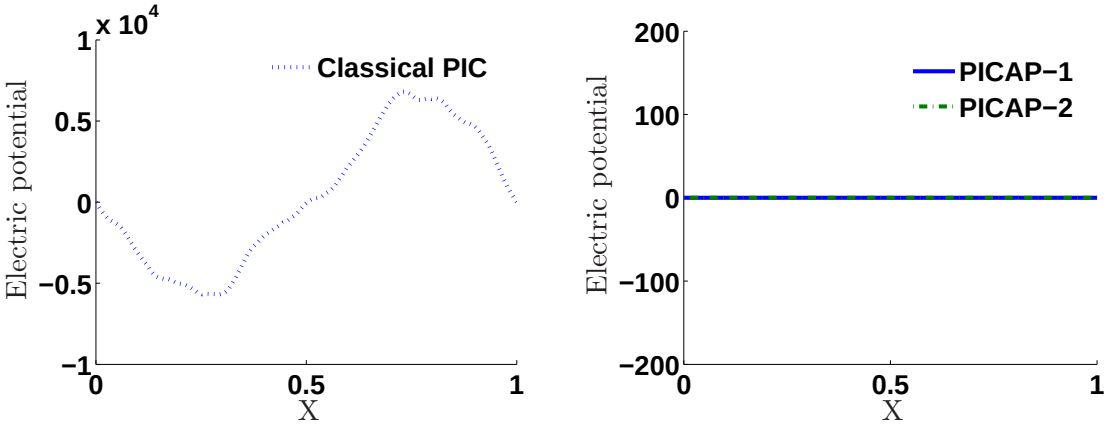

FIGURE 2.3: Perturbation of a quasi-neutral Maxwellian plasma. Under-resolved case : $\Delta x = 10^{-2} > \lambda = 10^{-4}$ and $\Delta t > \omega^{-1} = 10^{-4}$. Electric potential with Classical PIC scheme (left), and PICAP-1, PICAP-2 schemes (right), at time $t = 0.2 = 2000\omega^{-1}$.

as in the previous test case. Fig. 2.4 (left) shows the results corresponding to case, when time and space scales are resolved, *i.e.*

$$\Delta x = 2 \times 10^{-2} < \lambda = 1\,, \quad \omega \Delta t \leq 1\,, \quad v_{\max} \Delta t = 0.9 \Delta x\,.$$

The L^2-norm of the electric field evolution (in log scale), obtained with the classical PIC, PICAP-1, PICAP-2, is plotted on the left. The three schemes give identical results. The measured slope is about 0.64, which has the same order as the theoretical estimates. However, due to the noise which is inherent to particle simulations, this value is not as precise as for semi-Lagrangian simulations (see below). For the same reason, the damping is stopped at $t \simeq 4\omega^{-1}$ instead of going on. The oscillations observed in Figure 2.4 (left) and in the following Figures, come from the fact that the electrons bounce back and forth several times in the potential well, before the wave is damped.

The second test case is devoted to the results for an under-resolved case, *i.e.*

$$\Delta x = 2 \times 10^{-2} > \lambda = 10^{-4}\,, \quad \Delta t > \omega^{-1} = 10^{-4}\,, \quad v_{\max} \Delta t = 0.9 \Delta x\,.$$

For the classical PIC we use a uniform time step $\Delta t = 30\omega^{-1}$. For the other schemes, the time step is determined by the CFL conditions : $v_{\max}\Delta t = 0.9\Delta x$. Fig. 2.4 (right) shows the L^2-norm of the electric field (in log scale) as a function of time for the different schemes. As in the previous study, the classical PIC is unstable. This is because plasma oscillations are not resolved at all in this situation. Moreover none of the tested schemes is able to provide a reliable estimate of the damping rate, the fine scale details being ignored. What can be also remarked is that both PICAP methods provide an over-damping of the plasma waves.

In order to compare the PIC and semi-Lagrangian approach, we illustrate in Fig. 2.5-2.9 some similar results concerning the Landau damping effect and the electric field, obtained via the semi-Lagrangian AP-scheme. The semi-Lagrangian AP-scheme is compared here (in the resolved case) with a classical semi-Lagrangian discretization scheme,

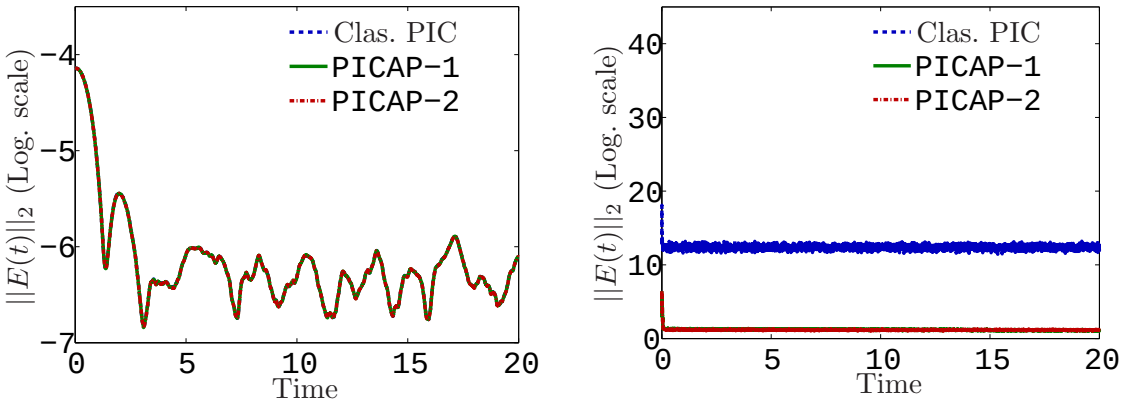

FIGURE 2.4: Linear Landau damping. Time evolution of $\log(||E(t)||_{L^2})$ via classical PIC, PICAP-1, PICAP-2. Left : Resolved case : $\Delta x = 2 \times 10^{-2} < \lambda = 1$ and $\Delta t < \omega^{-1} = 1$. Right : Under-resolved case : $\Delta x = 2 \times 10^{-2} > \lambda = 10^{-4}$ and $\Delta t > \omega^{-1} = 10^{-4}$.

called Ampère-method. As for the PIC-method, the rescaled case permits to validate the AP-scheme, called here RPE, with respect to classical schemes. In the under-resolved case, the classical schemes give rise to unstable results and are thus not plotted here. The numerical damping coefficients obtained via the AP-scheme, are in a good agreement with the analytical ones, fact which validates somehow the AP-schemes in the under-resolved cases.
What can be observed in all the following semi-Lagrangian figures, in comparison with the PIC-approach, is the lack of numerical noise. This permits to see more clearly some details/phenomena, as for example the oscillations.
For the following semi-Lagrangian tests, the same initial condition was chosen, however with some slightly modified parameters : $\delta = 10^{-3}, \Delta t = 0.5\Delta x/v_{max}, N_v = 128, v_{max} = 6$, with velocity domain $(-v_{max}, v_{max})$.

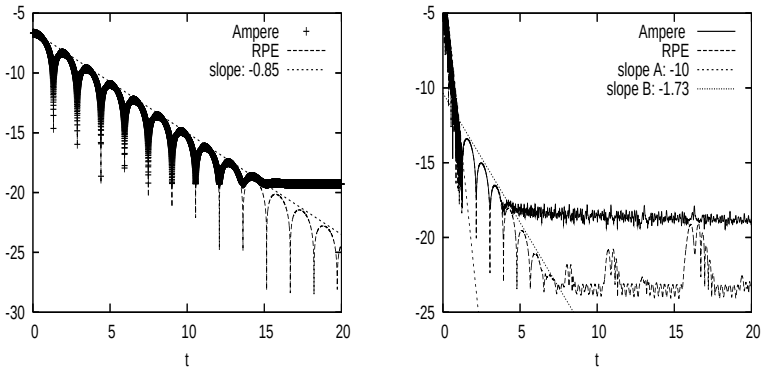

(a) (b)

FIGURE 2.5: Resolved cases, comparison of the two methods : time evolution of $\log(\|E(t)\|_2)$ with $\Delta x = 2 \cdot 10^{-2}$ for (a) $\lambda = 1$ and (b) $\lambda = 10^{-2}$. The slopes correspond to the numerical Landau damping rates (roots of the dispersion relation).

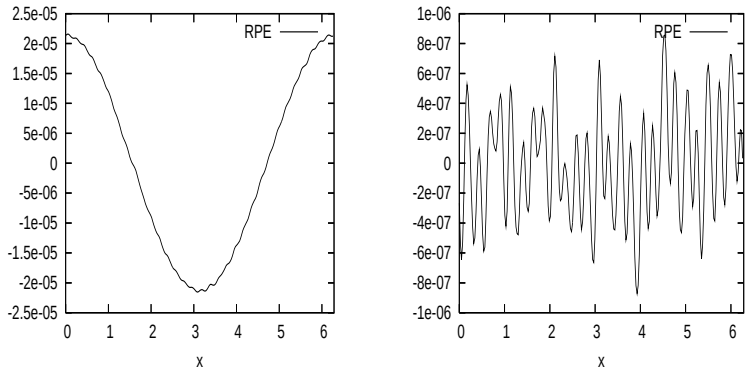

(a) (b)

FIGURE 2.6: Under-resolved case, numerical results for the RPE approach : electric field at $t = 2\,\omega_p^{-1}$ (a), and at $t = 10\,\omega_p^{-1}$ (b). $\Delta x = 2 \cdot 10^{-2}$, $\lambda = 10^{-3}$.

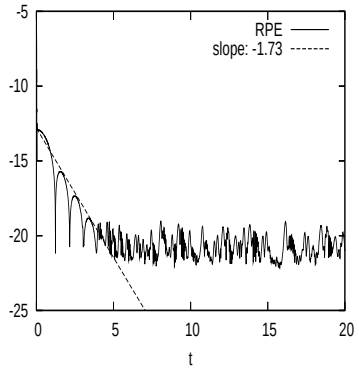

FIGURE 2.7: Under-resolved case, numerical results for the RPE approach : time evolution of $\log(\|E(t)\|_2)$. $\Delta x = 2 \cdot 10^{-2}$, $\lambda = 10^{-3}$. The slope -1.73 corresponds to the numerical Landau damping rate (root of the dispersion relation).

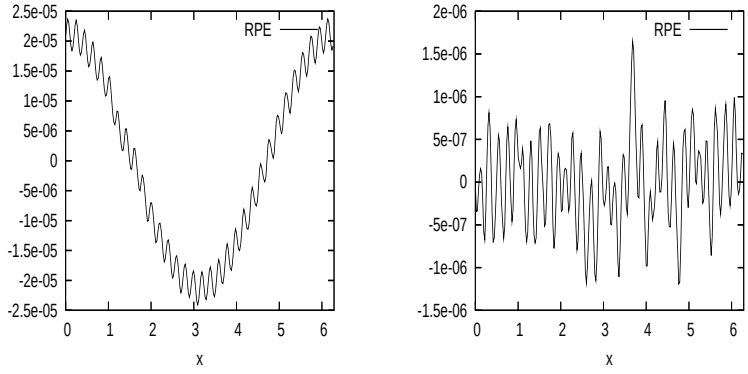

(a) (b)

FIGURE 2.8: Under-resolved case, numerical results for the RPE approach : electric field at $t = 2\,\omega_p^{-1}$ (a), and at $t = 10\,\omega_p^{-1}$ (b). $\Delta x = 2 \cdot 10^{-2}$, $\lambda = 10^{-4}$.

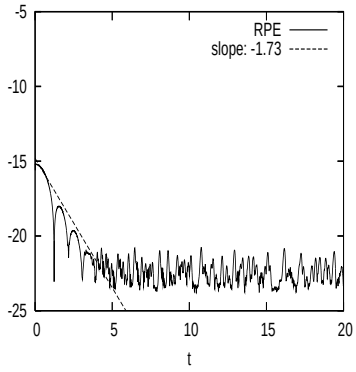

FIGURE 2.9: Under-resolved case, numerical results for the RPE approach : time evolution of $\log(\|E(t)\|_2)$. $\Delta x = 2 \cdot 10^{-2}$, $\lambda = 10^{-4}$. The slope -1.73 corresponds to the numerical Landau damping rate (root of the dispersion relation).

2.4.2 Bump-on-tail test-case

In this section, we compare the AP-methods with classical schemes (PIC respectively semi-Lagrangian versions) in the case of a bump-on-tail instability, which is a form of the two-stream instabilities. We initialize the Vlasov-Poisson equation with

$$f_0(x,v) = f_1(v)(1+\delta\cos(\kappa x)), \quad f_1(v) = C\left(\exp^{-v^2/2} + \alpha \exp^{-(v-v_d)^2/2v_t^2}\right), \qquad (2.10)$$

with C a renormalization constant. Periodic boundary conditions for the Vlasov system and homogeneous Dirichlet boundary conditions for the Poisson equations are considered. The numerical parameters are $\delta = 0.04$, $\kappa = 0.3$, $v_d = 4.5$, $v_t = 0.5$ and $\alpha = 2/9$. The space domain is $(0, 20\pi)$.

The evolution of the solutions, corresponding to the bump-on-tail test-case, is very different from the evolution of the Landau damping solutions investigated above. A small spatial perturbation of the equilibrium distribution function leads to a growth of the electric field strength, in other words we are in the case of an unstable equilibrium.

Fig. 2.10 (left) shows results corresponding to the resolved case, where $\lambda = 1$ and $\Delta x = 2 * 10^{-3}$. We consider 10 particles per cell (in average). We consider also the CFL condition $v_{\max}\Delta t = 0.9\Delta x$, which consequently ensures the resolution of time scales. The electric field is plotted in Fig. 2.10 (left) for Classical PIC, PICAP-1, PICAP-2 schemes. The various schemes are in very good agreement one with each other, up to time $100\omega^{-1}$. After the instant $50\omega^{-1}$, the results are altered by the damping due to the numerical noise of the PIC methods. However, all the schemes capture the dynamics well, despite the small number of particles per cell.

We consider now the following under-resolved case : $\Delta x = 3$ while $\lambda = 10^{-1}$. We consider $6 * 10^4$ particles per cell (in average). For the Classical PIC scheme, we enforce the condition $\Delta t = 4\omega^{-1}$ to be sure that time is under-resolved. For the PICAP-1, the PICAP-2 the time step is computed from the CFL conditions $v_{\max}\Delta t = 0.9\Delta x$. In Fig. 2.10 (right), the electric field is plotted for Classical PIC, PICAP-1, PICAP-2 schemes : while Classical PIC exhibits a large instability before damping, PICAP-1 and PICAP-2 rapidly damp the energy.

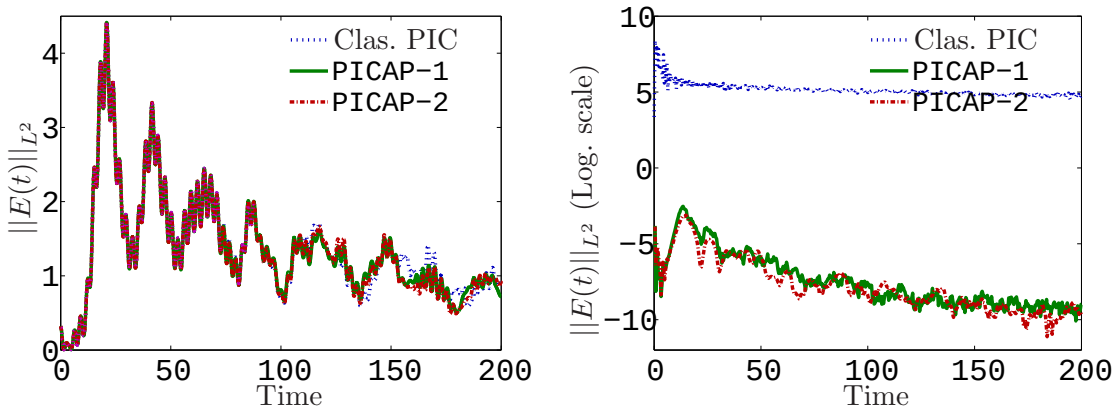

FIGURE 2.10: Bump on tail instability. Time evolution of $||E(t)||_{L^2}$ with Classical PIC, PICAP-1, PICAP-2. Left : Resolved case : $\Delta x = 2 \times 10^{-3} < \lambda = 1$ and $\Delta t > \omega^{-1} = 1$. Right : Under-resolved case : $\Delta x = 3 > \lambda = 10^{-1}$ and $\Delta t > \omega^{-1} = 10^{-1}$.

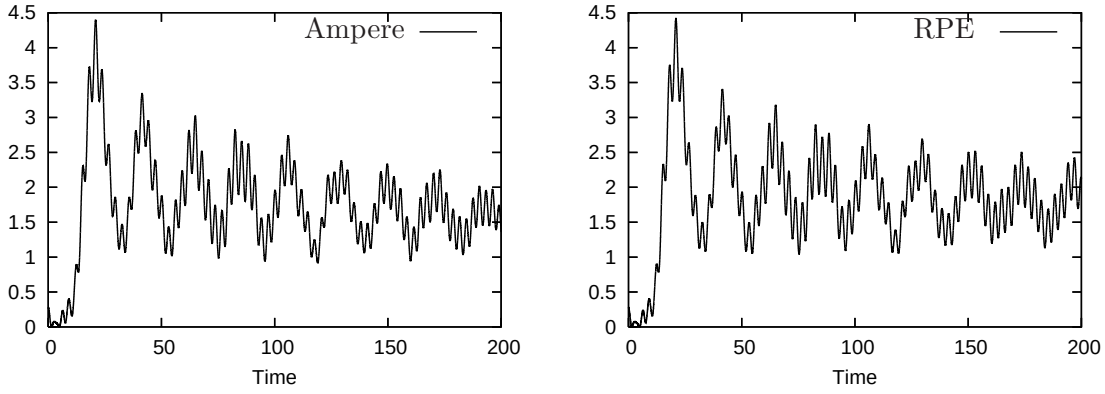

FIGURE 2.11: Resolved case : Time evolution of $||E(t)||_{L^2}$ for the Ampère approach (left) and the RPE approach (right).

All these results can be compared with the results obtained via a semi-Lagrangian AP-scheme, on a phase-space domain of $(0, 20\pi) \times (-v_{max}, v_{max})$ with $v_{max} := 9$ and $N_x = N_v = 1024$.

To summarize, all these numerical results permitted to show the efficiency of the AP-scheme (as compared to standard schemes) for the resolution of the Vlasov-Poisson system (2.1) in the quasi-neutral regime $0 < \lambda \ll 1$, on a grid which does not resolve the small space and time scales, *i.e.* $\Delta x > \lambda$ and $\Delta t > \omega^{-1}$. The use of larger time and space steps for the same precision is an essential advantage, as it permits a considerable gain in computational time. The limit $\lambda \to 0$ was not investigated in the present chapter, however the developed AP-scheme is consistent also with the limit model P^0 when λ tends to zero and for fixed discretization parameters Δt, Δx, as long as this limit is mathematically justified.

Chapitre 3

Vlasov equation in the high-field limit regime and with variable Larmor radii

Chapter based on the article of :
N. Crouseilles, M. Lemou, C. Negulescu [1]

The presence of large magnetic fields B in a plasma introduces additional small space- and time-scales, related to the gyromotion of the charged particles around the magnetic field lines, hence to the Larmor radius ρ_L and the cyclotron frequency ω_c. When charged particles are submitted to a large magnetic field, their movement in first approximation follows the magnetic field lines (the particles get trapped along the field lines). When observing the particles on larger time scales however, an additional drift movement perpendicular to the magnetic field lines is observed. Depending on the physical phenomena one wants to investigate, different scalings of the kinetic model have been introduced in literature, permitting to study various asymptotic regimes when the magnetic field gets larger, for example the guiding-centre, drift-kinetic, gyro-kinetic models.

The subject of the present chapter is the study of a Vlasov equation in a two small-scale situation, in other words the investigation of the following finite Larmor radius equation

$$(P)^{\tau,\varepsilon} \quad \partial_t f + v_{||} \cdot \nabla_{\mathbf{x}} f + E \cdot \nabla_v f + \frac{1}{\tau} v_\perp \cdot \nabla_{\mathbf{x}} f + \frac{1}{\varepsilon} (v \times B) \cdot \nabla_v f = 0, \tag{3.1}$$

where ε stands for the particle cyclotronic period, which is small due to the large magnetic field B, and the parameter $\tau \in [\varepsilon, 1]$ comes from the rescaling of the perpendicular space-variable. This scaling comes from the fact that the characteristic length in the parallel direction to B is taken as $L_{||} \sim \tau$ whereas the characteristic length perpendicular

1. "Multiscale numerical study of the Vlasov equation in the high-field limit regime and with variable Larmor radii" , in preparation.

to B is $L_\perp \sim \varepsilon$, which means that the spatial observation scale in the plane perpendicular to the magnetic field is chosen smaller than the one in the parallel direction. This allows the electric field to vary across the Larmor radius, and to recover different phenomena in the asymptotic limit.

The aim of this chapter is to find a numerical procedure, being able to describe in a homogeneous manner the evolution of charged particles in the high B-field limit, each of them possessing different Larmor radii. As an example one can mention ions composed of many various components, owning each of them a different Larmor radius, or electrons in the zero Larmor radius limit. Again we have to cope with a singularly perturbed problem, the solutions becoming highly oscillating in the limit $\varepsilon \to 0$, requiring thus some averaging procedures.

Let us consider a homogeneous magnetic field $B = |B|b$, with the direction $b := e_z$ and where for simplification we take $|B| \equiv 1$. Given this vector field b, one can decompose now vectors $v \in \mathbb{R}^3$, gradients $\nabla\phi$, with $\phi(x)$ a scalar function, and divergences $\nabla\cdot v$, with $v(x)$ a vector field, into a part parallel to the magnetic field and a part perpendicular to it. These parts are defined as follows :

$$\begin{aligned}
&v_{||} := (v\cdot b)b\,, && v_\perp := (Id - b\otimes b)v\,, && \text{such that} \quad v = v_{||} + v_\perp\,,\\
&\nabla_{||}\phi := (b\cdot\nabla\phi)b\,, && \nabla_\perp\phi := (Id - b\otimes b)\nabla\phi\,, && \text{such that} \quad \nabla\phi = \nabla_{||}\phi + \nabla_\perp\phi\,,\\
&\nabla_{||}\cdot v := \nabla\cdot v_{||}\,, && \nabla_\perp\cdot v := \nabla\cdot v_\perp\,, && \text{such that} \quad \nabla\cdot v = \nabla_{||}\cdot v + \nabla_\perp\cdot v\,,
\end{aligned} \tag{3.2}$$

where we denoted by $\otimes$ the vector tensor product. Thus, the velocity is decomposed in $v_{||} = (0,0,v_z)^t$ and $v_\perp = (v_x, v_y, 0)^t$, so that $v_{||} + v_\perp = v$.

The Vlasov equation (3.1) describes in particular two different asymptotic regimes, which can be frequently encountered in literature [6, 7] :

1. $\varepsilon = \tau \ll 1$: Gyrokinetic, finite-Larmor radius equation (for ions)

$$\partial_t f + v_{||}\cdot\nabla_{\mathbf{x}} f + E\cdot\nabla_v f + \frac{1}{\varepsilon}\, v_\perp\cdot\nabla_{\mathbf{x}} f + \frac{1}{\varepsilon}\,(v\times B)\cdot\nabla_v f = 0\,, \tag{3.3}$$

with the dominant operator denoted by $\mathcal{T}_1 := v_\perp\cdot\nabla_{\mathbf{x}} + (v\times B)\cdot\nabla_v$.

2. $\tau = 1$, $0 < \varepsilon \ll 1$: Guiding-center, zero-Larmor radius equation (for electrons)

$$\partial_t f + v_{||}\cdot\nabla_{\mathbf{x}} f + E\cdot\nabla_v f + v_\perp\cdot\nabla_{\mathbf{x}} f + \frac{1}{\varepsilon}\,(v\times B)\cdot\nabla_v f = 0\,, \tag{3.4}$$

where the dominant operator is $\mathcal{T}_2 := (v\times B)\cdot\nabla_v$.

New difficulties arise in the numerical treatment of the kinetic equation (3.1), due to the occurrence of two different small scales and hence the appearance of several asymptotic behaviours in the limit. Many other physical, biological, chemical phenomena have

a similarly complicated behaviour, involving in particular several small-scale parameters. Much effort has been done on the development of numerical schemes for singularly perturbed problems containing only one small parameter, however efficient schemes for singularly perturbed multi-parameter problems still lack. It is thus very important to design and study numerical schemes for such multi-parameter problems, especially to be able to investigate the interaction or organisation of two (or several) distinct phenomena. The objective of this chapter is thus to introduce an AP-scheme, capable to capture all these asymptotics in a unified framework.

3.1 Study of the two limit regimes

First, let us study separately the two limit regimes and identify the corresponding limit problems. In order to simplify the computations, we will shift sometimes from the Cartesian to the polar coordinates for the velocity, *i.e.*

$$v = (v_x, v_y, v_z) \Leftrightarrow (r, \theta, v_z)\,, \quad \left\{ \begin{array}{ll} v_x := r\cos(\theta) & \theta \in [0, 2\pi) \\ v_y := r\sin(\theta) & r \geq 0 \end{array} \right. ,$$

and use the notations (where $B := e_z$)

$$v_{||} := (0, 0, v_z)^t\,, \quad v_\perp = (v_x, v_y, 0)^t\,, \quad {}^\perp v := (v_y, -v_x, 0)^t = v \times B\,.$$

The Vlasov equation writes then in polar coordinates

$$\begin{aligned} \partial_t F + v_z\partial_z F + E_z\partial_{v_z} F + (E_x\cos\theta + E_y\sin\theta)\,\partial_r F - \tfrac{1}{r}\,(E_x\sin\theta - E_y\cos\theta)\,\partial_\theta F \\ + \frac{1}{\tau} r\,(\cos\theta\partial_x F + \sin\theta\partial_y F) - \frac{1}{\varepsilon}\partial_\theta F = 0\,, \end{aligned} \tag{3.5}$$

where the unknown now is $F(t, x, y, z, r, \theta, v_z)$. To simplify the notations, let us introduce the following operators

$$\mathcal{A}F := \left(v_z\partial_z + E_z\partial_{v_z} + (E_x\cos\theta + E_y\sin\theta)\,\partial_r - \frac{1}{r}\,(E_x\sin\theta - E_y\cos\theta)\,\partial_\theta \right) F,$$

and

$$\mathcal{T}_3 F := (r\cos\theta\partial_x + r\sin\theta\partial_y)F = (v_x\partial_x + v_y\partial_y)F\,, \quad \mathcal{T}_2 F := -\partial_\theta F\,,$$

such that we can simply rewrite the Vlasov equation (3.5) as

$$\partial_t F + \mathcal{A}F + \frac{1}{\tau}\mathcal{T}_3 F + \frac{1}{\varepsilon}\mathcal{T}_2 F = 0. \tag{3.6}$$

Introducing now the new parameter $\alpha := \frac{\varepsilon}{\tau}$, which designs somehow the Larmor radius, and defining the operator

$$\mathcal{T}_1^\alpha F := \mathcal{T}_3 F + \frac{1}{\alpha}\mathcal{T}_2 F,$$

the Vlasov equation (3.5) rewrites as

$$\partial_t F + \mathcal{A}F + \frac{1}{\tau}\left(\mathcal{T}_3 + \frac{1}{\alpha}\mathcal{T}_2\right) F = \partial_t F + \mathcal{A}F + \frac{1}{\tau}\mathcal{T}_1^\alpha F = 0. \tag{3.7}$$

In the following we will study the asymptotic behaviour of the solution $F^{\alpha,\tau}$ to this equation in the the two regimes :

– $\alpha = \alpha_0 > 0$ fixed and $\tau \to 0$ (automatically one has then $\varepsilon = \alpha_0 \tau \to 0$) ,

– $\tau = \tau_0$ fixed and $\alpha \to 0$ (automatically one has then $\varepsilon = \alpha \tau_0 \to 0$) .

The first limit corresponds to a finite-Larmor radius regime, whereas the second one to the zero-Larmor radius regime.

3.1.1 Study of $\mathcal{T}_1^\alpha$ and $\mathcal{T}_2$

As a first step, let us investigate separately the two dominant operators $\mathcal{T}_1^\alpha$ and $\mathcal{T}_2$. For this, we shall work in the Hilbert-space $\mathcal{V} := L^2(\mathbb{R}^3 \times \mathbb{R}^3)$.

Study of $\mathcal{T}_1^\alpha$: The operator

$$\mathcal{T}_1^\alpha : D(\mathcal{T}_1^\alpha) \subset \mathcal{V} \to \mathcal{V} , \quad \mathcal{T}_1^\alpha f := \left(v_\perp \cdot \nabla_{\mathbf{x}} + \frac{1}{\alpha} \, {}^\perp v \cdot \nabla_v \right) f,$$

is defined on

$$D(\mathcal{T}_1^\alpha) := \{ f \in \mathcal{V} \ / \ \left(v_\perp \cdot \nabla_{\mathbf{x}} + \frac{1}{\alpha} \, {}^\perp v \cdot \nabla_v \right) f \in \mathcal{V} \} .$$

Its kernel is given by

$$\ker(\mathcal{T}_1^\alpha) := \{ M_1^\alpha(t, x + \alpha r \sin\theta, y - \alpha r \cos\theta, z, r, v_z) \} . \tag{3.8}$$

To determine the orthogonal projection Π_1^α on this kernel, we will investigate the characteristics associated to the operator $\mathcal{T}_1^\alpha$, which satisfy

$$\dot{X} = V_\perp = (V_x, V_y, 0)^t ; \quad \dot{V} = \frac{1}{\alpha} \, {}^\perp V = \frac{1}{\alpha} (V_y, -V_x, 0)^t .$$

Defining the rotation matrices $\mathcal{R}^\alpha(s)$ and $\mathcal{P}^\alpha(s)$

$$\mathcal{R}^\alpha(s) := \begin{pmatrix} \cos(\frac{s}{\alpha}) & \sin(\frac{s}{\alpha}) & 0 \\ -\sin(\frac{s}{\alpha}) & \cos(\frac{s}{\alpha}) & 0 \\ 0 & 0 & 1 \end{pmatrix} , \quad \mathcal{P}^\alpha(s) = \begin{pmatrix} \sin(\frac{s}{\alpha}) & 1 - \cos(\frac{s}{\alpha}) & 0 \\ \cos(\frac{s}{\alpha}) - 1 & \sin(\frac{s}{\alpha}) & 0 \\ 0 & 0 & 0 \end{pmatrix}$$

the characteristics corresponding to the dominant operator $\mathcal{T}_1^\alpha$ write

$$X(s; x, v, t) = x + \alpha \mathcal{P}^\alpha(s - t) v , \quad V(s; x, v, t) = \mathcal{R}^\alpha(s - t) v .$$

These characteristics are $2\pi\alpha$-periodic, such that one can introduce the average of a function f along one of these periods. It can be shown then, that this gives exactly the

expression of the projection operator Π_1^α. Indeed,

$$\begin{aligned}
\Pi_1^\alpha(f) &:= \frac{1}{2\pi\alpha}\int_t^{t+2\pi\alpha} f(t, x+\alpha\mathcal{P}^\alpha(s-t)v, \mathcal{R}^\alpha(s-t)v)\,ds \\
&= \frac{1}{2\pi\alpha}\int_t^{t+2\pi\alpha} F\left(t, x+\alpha\sin\left(\frac{s-t}{\alpha}\right)r\cos\theta+\alpha\left(1-\cos\left(\frac{s-t}{\alpha}\right)\right)r\sin\theta,\right. \\
&\qquad \left. y+\alpha\left(\cos\left(\frac{s-t}{\alpha}\right)-1\right)r\cos\theta+\alpha\sin\left(\frac{s-t}{\alpha}\right)r\sin\theta, z, r, \theta-\frac{s-t}{\alpha}, v_z\right)ds \\
&= \frac{1}{2\pi\alpha}\int_t^{t+2\pi\alpha} F\left(t, x+\alpha r\sin\theta+\alpha r\sin\left(\frac{s-t}{\alpha}-\theta\right),\right. \\
&\qquad \left. y-\alpha r\cos\theta+\alpha r\cos\left(\frac{s-t}{\alpha}-\theta\right), z, r, \theta-\frac{s-t}{\alpha}, v_z\right)ds \\
&= \frac{1}{2\pi}\int_0^{2\pi} F\left(t, x+\alpha r\sin\theta-\alpha r\sin\xi, y-\alpha r\cos\theta+\alpha r\cos\xi, z, r, \xi, v_z\right)d\xi \\
&= M_1^\alpha(t, x+\alpha r\sin\theta, y-\alpha r\cos\theta, z, r, v_z)
\end{aligned} \tag{3.9}$$

We have the following properties :

Proposition 3.1.1 *The average operator Π_1^α defined in (3.9) is linear and continuous. Moreover, it coincides with the orthogonal projection on the kernel of $\mathcal{T}_1^\alpha$. Indeed, one has*

$$\Pi_1^\alpha : \mathcal{V} \to \ker\mathcal{T}_1^\alpha\,, \quad \mathcal{T}_1^\alpha : D(\mathcal{T}_1^\alpha)\subset\mathcal{V}\to\mathcal{I}m(\mathcal{T}_1^\alpha) = (\ker(\mathcal{T}_1^\alpha))^\perp\,,$$

$$\int_{\mathbb{R}^3}\int_{\mathbb{R}^3}(f-\Pi_1^\alpha(f))\,\Phi\,dvdx = 0\,, \quad \forall\Phi\in\ker(\mathcal{T}_1^\alpha)\,.$$

Study of $\mathcal{T}_2$: The operator

$$\mathcal{T}_2 : D(\mathcal{T}_2)\subset\mathcal{V}\to\mathcal{V}\,, \quad \mathcal{T}_2F := (v\times B)\cdot\nabla_v f = -\partial_\theta F\,,$$

is defined on

$$D(\mathcal{T}_2) := \{f\in\mathcal{V}\ /\ -\partial_\theta F\in\mathcal{V}\}\,.$$

Its kernel is given by

$$\ker(\mathcal{T}_2) := \{M_2(t, x, y, z, r, v_z)\}\,, \tag{3.10}$$

and the orthogonal projection on this kernel writes

$$\Pi_2(F) := \frac{1}{2\pi}\int_0^{2\pi} F(t, x, y, z, r, \theta, v_z)\,d\theta\,.$$

One can prove that

Proposition 3.1.2 *The orthogonal projection operator Π_2 is linear and continuous. Moreover, one has*

$$\Pi_2 : \mathcal{V} \to \ker\mathcal{T}_2\,, \quad \mathcal{T}_2 : D(\mathcal{T}_2)\subset\mathcal{V}\to\mathcal{I}m(\mathcal{T}_2) = (\ker(\mathcal{T}_2))^\perp\,,$$

$$\int_{\mathbb{R}^3}\int_{\mathbb{R}^3}(f-\Pi_2(f))\,\Phi\,dvdx = 0\,, \quad \forall\Phi\in\ker(\mathcal{T}_2)\,.$$

Remark, that one has also the important properties

$$\Pi_2 \mathcal{T}_3 M = 0\,, \quad \Pi_2 \mathcal{T}_1^{\alpha} M = 0\,, \quad \forall M \in \ker(\mathcal{T}_2)\,.$$

Indeed,

$$\int_0^{2\pi} (r\cos(\theta)\partial_x M + r\sin(\theta)\partial_y M)\; d\theta - \int_0^{2\pi} \partial_\theta M\, d\theta$$
$$= r\partial_x M \int_0^{2\pi} \cos(\theta)\, d\theta + r\partial_y M \int_0^{2\pi} \sin(\theta)\, d\theta = 0\,, \quad \forall M \in \ker(\mathcal{T}_2)\,.$$

3.1.2 Identification of the limit models

In this subsection, we will identify the two Limit models corresponding to the two asymptotic regimes $0 < \tau \ll 1$, $\alpha = \alpha_0$ (finite Larmor radius) or $\tau = \tau_0$, $0 < \alpha \ll 1$ (zero Larmor radius). We will moreover introduce the two different Asymptotic-Preserving reformulations of the P-problem (3.1), corresponding to these two limit regimes, and will prove their convergence towards the associated Limit models.

Finite-Larmor radius regime : $\alpha = \alpha_0$, $\tau \to 0$

To identify the Limit problem, we will start with a standard Chapman-Enskog expansion $F = M + \tau g$, which leads after insertion in the Vlasov equation (3.7) to

$$\partial_t(M + \tau g) + \mathcal{A}(M + \tau g) + \frac{1}{\tau}\left[\mathcal{T}_3(M + \tau g) + \frac{1}{\alpha_0}\mathcal{T}_2(M + \tau g)\right] = 0.$$

Comparing now the terms of the same order in τ, one gets that $M \in \ker \mathcal{T}_1^{\alpha_0} = \ker(\mathcal{T}_3 + \frac{1}{\alpha_0}\mathcal{T}_2)$. At next order, we get an evolution equation for M

$$\partial_t M + \mathcal{A}M + \mathcal{T}_1^{\alpha_0} g = 0.$$

To eliminate the unknown g, we apply the projection operator $\Pi_1^{\alpha_0}$, which leads to the limit model

$$(L)_1^{\alpha_0} \quad \partial_t M + \Pi_1^{\alpha_0} \mathcal{A} M = 0. \tag{3.11}$$

This procedure permits to get some information about the behaviour of F in the limit $\tau \to 0$, in particular that F tends towards an element of the kernel of $\mathcal{T}_1^{\alpha_0}$. This shall permit to reformulate the initial singular perturbation problem (3.7) in such a manner to capture automatically the Limit model $(L)_1^{\alpha_0}$ as τ tends to zero.

Indeed, decomposing F as $F = M_1^{\alpha_0} + G_1^{\alpha_0}$ where $M_1^{\alpha_0} \in \ker \mathcal{T}_1^{\alpha_0}$ and $G_1^{\alpha_0} \in \mathcal{I}m\mathcal{T}_1^{\alpha_0}$, one can reformulate the singularly perturbed problem (P) as follows

$$(AP)_1^{\alpha_0} \quad \begin{cases} \partial_t M_1^{\alpha_0} + \Pi_1^{\alpha_0} \mathcal{A} F = 0 \\ \partial_t G_1^{\alpha_0} + (I - \Pi_1^{\alpha_0})\mathcal{A} F + \frac{1}{\tau}\mathcal{T}_1^{\alpha_0} G_1^{\alpha_0} = 0\,. \end{cases} \tag{3.12}$$

This system is equivalent to (3.7) and moreover a regular perturbation of the Limit problem $(L)_1^{\alpha_0}$. Indeed, letting τ tend to zero in the second equation, permits to show that

$$\mathcal{T}_1^{\alpha_0} F = 0 \quad \Rightarrow F \in \ker(\mathcal{T}_1^{\alpha_0}) \quad \Rightarrow F = M_1^{\alpha_0}\,,\; G_1^{\alpha_0} \equiv 0\,.$$

Inserting $G_1^{\alpha_0} = 0$ in the first equation of (3.12) yields the Limit model (3.11).
Hence, passing to the limit $\tau \to 0$ in $(AP)_1^{\alpha_0}$ will lead to no numerical problems, which was not the case for (3.7), being singularly perturbed.

Zero-Larmor radius regime : $\tau = \tau_0$ and $\alpha \to 0$

In the same spirit as previously, a Chapman-Enskog expansion $F = M + \alpha g$ leads to

$$\partial_t(M+\alpha g) + \mathcal{A}(M+\alpha g) + \frac{1}{\tau_0}\mathcal{T}_3(M+\alpha g) + \frac{1}{\tau_0\alpha}\mathcal{T}_2(M+\alpha g) = 0.$$

At leading order in α, we get $M \in \ker \mathcal{T}_2$, which means M does not depend on θ. At next order, we get the evolution equation

$$\partial_t M + \mathcal{A}M + \frac{1}{\tau_0}\mathcal{T}_3 M + \frac{1}{\tau_0}\mathcal{T}_2 g = 0.$$

Integrating with respect to θ (or applying Π_2), permits to eliminate the unknown g and to get the Limit model

$$(L)_2 \quad \partial_t M + \Pi_2 \mathcal{A} M = 0\,, \tag{3.13}$$

where we have used the property $\Pi_2 \mathcal{T}_3 M = 0$.

To get a reformulation, which preserves the asymptotic behaviour of the solution F, we decompose again F as $F = M_2 + G_2$ with $M_2 \in \ker \mathcal{T}_2$ and $G_2 \in \mathcal{I}m\mathcal{T}_2$. Inserting this decomposition in (3.7) one can reformulate the singularly perturbed problem (P) as follows

$$(AP)_2 \quad \left\{ \begin{array}{l} \partial_t M_2 + \Pi_2 \left(\mathcal{A} + \frac{1}{\tau_0}\mathcal{T}_3\right) F = 0 \\ \partial_t G_2 + (I-\Pi_2)\left(\mathcal{A} + \frac{1}{\tau_0}\mathcal{T}_3\right) F + \frac{1}{\tau_0\alpha}\mathcal{T}_2 G_2 = 0\,. \end{array} \right. \tag{3.14}$$

This system is equivalent to (3.7) and moreover a regular perturbation of the Limit problem $(L)_2$.

3.2 Micro-macro decomposition

The concern of this section is to extend the methodology presented so far, in order to develop a numerical method able to treat accurately both limit regimes, and this in a unified framework. In other words, we would like to construct a scheme which is AP in both asymptotics, *i.e.* stable uniformly with respect to α and τ and consistent with both Limit models, when the different limits are considered. Moreover we would like that the method shifts automatically from one regime to the other, such that one can treat easily problems where different regimes occur in different parts of the domain.

In order to treat both limit regimes together, we shall first fix the parameters τ and α and start from the singularly perturbed kinetic equation (3.7) and the decomposition

$$f = M_1^{\tau,\alpha} + G_1^{\tau,\alpha}\,, \quad M_1^{\tau,\alpha} = \Pi_1^\alpha(F) \in \ker \mathcal{T}_1^\alpha\,, \quad G_1^{\tau,\alpha} \in \mathcal{I}m\mathcal{T}_1^\alpha\,. \tag{3.15}$$

Plugging this decomposition in the initial Vlasov equation, projecting on the kernel of $\mathcal{T}_1^\alpha$ and subtracting the obtained equation from (3.7), leads to the micro-macro system

$$(MM)^{\tau,\alpha} \quad \left\{ \begin{array}{l} \partial_t M_1^{\tau,\alpha} + \Pi_1^\alpha \mathcal{A} F = 0 \\ \partial_t G_1^{\tau,\alpha} + (I-\Pi_1^\alpha)\mathcal{A}F + \frac{1}{\tau}\mathcal{T}_1^\alpha F = 0\,. \end{array} \right. \tag{3.16}$$

Remark that for fixed (α, τ) this is an equivalent reformulation of the kinetic equation (3.7), due to the uniqueness of the decomposition (3.15).

In the next section we will show that this system is able to capture the different asymptotic regimes. This property comes essentially from the fact that for $\tau = \tau_0$ and $\alpha \ll 1$, one has $\Pi_1^\alpha = \Pi_2 + O(\alpha)$, such that $M_1^{\tau=\tau_0,\alpha} = \Pi_1^\alpha(F) = M_2 + O(\alpha)$ and $G_1^{\tau=\tau_0,\alpha} = G_2 + O(\alpha)$. Indeed, recalling the definition of Π_1^α

$$\Pi_1^\alpha(f) = \frac{1}{2\pi}\int_0^{2\pi} F\left(t, x + \alpha r\sin\theta - \alpha r\sin\xi, y - \alpha r\cos\theta + \alpha r\cos\xi, z, r, \xi, v_z\right)\, d\xi$$

and using Taylor's formula, *i.e.*

$$F\left(t, x + \alpha r\sin\theta - \alpha r\sin\xi, y - \alpha r\cos\theta + \alpha r\cos\xi, z, r, \xi, v_z\right) =$$
$$F(t, x, y, z, r, \xi, v_z) + \alpha\left\{(r\sin\theta - r\sin\xi)\partial_x F - (r\cos\theta - r\cos\xi)\partial_y F\right\} + \mathcal{O}(\alpha^2)\,,$$

permits by integration over ξ to show that $\Pi_1^\alpha = \Pi_2 + O(\alpha)$. This ingredient shall permit to get the right limits in the different asymptotic regimes.

3.2.1 Asymptotic limits

The main goal of this section, is to investigate the asymptotics illustrated in diagram 5.1. In particular we are interested in the behaviour of the $(MM)^{\tau,\alpha}$-reformulation as one of the two different limit regimes is considered. We shall show that the $(MM)^{\tau,\alpha}$-problem is a small perturbation of the (AP)-reformulations considered so far, allowing thus to recover the micro-macro model for (M_1^α, G_1^α) on the one hand and for (M_2, G_2) on the other hand (for the corresponding limits). These micro-macro models recover then the good asymptotics in the limit, as we have seen previously.

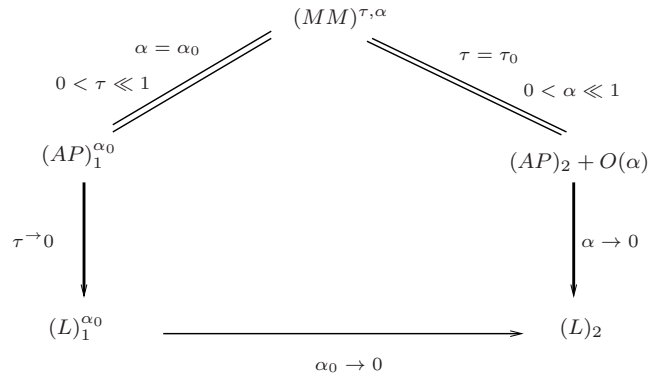

FIGURE 3.1: Diagram of the different asymptotic limits we are investigating.

Finite-Larmor radius regime : $\alpha = \alpha_0$, $\tau \to 0$

In this case, the $(MM)^{\tau,\alpha}$-reformulation is nothing but the $(AP)_1^{\alpha_0}$-reformulation, such that everything works very well.

Zero-Larmor radius regime : $\tau = \tau_0$ and $\alpha \to 0$

Inserting now formally the expansions

$$\Pi_1^\alpha = \Pi_2 + O(\alpha)\,, \quad M_1^{\tau=\tau_0,\alpha} = \Pi_1^\alpha(F) = M_2 + O(\alpha)\,, \quad G_1^{\tau=\tau_0,\alpha} = G_2 + O(\alpha)\,, \quad (3.17)$$

in (3.16), yields

$$\begin{cases} \partial_t M_2 + \Pi_2 \mathcal{A} F = \mathcal{O}(\alpha) \\ \partial_t G_2 + (I - \Pi_2)\mathcal{A} F + \frac{1}{\tau_0}\mathcal{T}_3 F + \frac{1}{\tau_0 \alpha}\mathcal{T}_2 F = \mathcal{O}(\alpha)\,. \end{cases}$$

Remarking also that $G_2 = \mathcal{O}(\alpha)$, one can see immediately, that the $(MM)^{\tau,\alpha}$-reformulation is in this case a small perturbation of the $(AP)_2$-reformulation.

Both asymptotics

What can be remarked is that both limits commute, *i.e.* the $(MM)^{\tau,\alpha}$-reformulation leads towards the limit model $(L)_2$ no matter which of both asymptotics is taken in priority. Indeed, this can seen by observing that the $(L)_1^{\alpha_0}$-model is recovering the $(L)_2$-problem, as α_0 tends to zero. Plugging indeed the above expansions (3.17) in (3.11) yields formally for $\alpha_0 \to 0$ the desired limit model $(L)_2$.

In summary, all these formal asymptotics permit to understand that reformulating the initial singularly perturbed problem (3.1) under the form (3.16) will allow to recover the right asymptotic regimes if one of the two limits is considered, as well as if both are considered independently. Naturally, one has now to discretize in time and space the new reformulation (3.16) in such a manner, that the obtained asymptotic preserving properties are not destroyed on the discrete level. This work is in progress at the moment.

$\mathcal{PART}$ II

Fluid models

Let us consider in this part a fluid description of the plasma dynamics, obtained via the moment method from the kinetic approach (Boltzmann equation). Let α denote the particle species ($\alpha = e$ for electrons and $\alpha = i$ for ions) and n_α be the particle density, u_α the velocity field, T_α the particle temperature. The bi-fluid model describing the plasma evolution reads now

$$\left\{\begin{array}{l} \partial_t n_\alpha + \nabla\cdot(n_\alpha u_\alpha) = S_{n\alpha}\,, \\ m_\alpha n_\alpha\left[\partial_t u_\alpha + (u_\alpha\cdot\nabla)u_\alpha\right] = -\nabla p_\alpha + n_\alpha e_\alpha(E + u_\alpha\times B) - \nabla\cdot\Pi_\alpha + R_\alpha\,, \\ \dfrac{3}{2}n_\alpha k_B\left[\partial_t T_\alpha + (u_\alpha\cdot\nabla)T_\alpha\right] + p_\alpha\nabla\cdot u_\alpha = -\nabla\cdot q_\alpha - \Pi_\alpha : \nabla u_\alpha + Q_\alpha\,, \end{array}\right. \tag{3.18}$$

where some constitutive laws are needed for the pressure p_α, the stress viscosity tensor Π_α and the heat flux term q_α, in order to close this system. In the Braginskii closure, the pressure is specified as $p_\alpha := n_\alpha\, T_\alpha$ (perfect gas assumption), the plasma viscosity is assumed negligible, such that $\nabla\cdot\Pi_\alpha = 0$ and $\Pi_\alpha : \nabla u_\alpha = 0$ and the energy flux q_α is supposed to have a diffusive form, given in terms of the temperature gradient as follows $q_\alpha := -\kappa_\alpha\nabla T_\alpha$ (Fourier law) with κ_α the thermal conductivity coefficient. The terms $S_{n\alpha}$, R_α resp. Q_α represent a particle source term, a friction force due to collisions resp. a particle exchange energy term due also to collisions and taken under the form $Q_\alpha := \pm 3\frac{m_e}{m_i}\frac{n_\alpha}{\tau_e}(T_e - T_i)$, where τ_e is the electron-ion collision time. Again the system has to be coupled with Maxwell's equations for the computation of the electromagnetic fields (E, B).

Similarly to the kinetic framework, a dimensional analysis gives rise to dimensionless parameters as for example the Mach number, the Reynolds number, the Prandtl number, the Peclet number *etc*, and one has to deal again with singular limits as one of these parameters vanishes or goes to infinity. Here are some of these asymptotic regimes, in the one-fluid (electrons) framework :

– Euler-Poisson system in the quasi-neutral limit [13, 18] :

$$\begin{cases} \partial_t n + \nabla \cdot (n\,u) = 0 \\ \partial_t (n\,u) + \nabla \cdot (n\,u \otimes u) + \nabla p(n) = n\,\nabla \Phi \\ -\lambda^2 \Delta \Phi = 1 - n\,, \end{cases}$$

where $\lambda \ll 1$ stands for the rescaled Debye length. In the limit $\lambda \to 0$ the Euler-Poisson system reduces to the incompressible Euler equations.

– High field limit (Euler-Lorentz) [11, 17] :

$$\begin{cases} \partial_t n + \nabla \cdot (n\,u) = 0 \\ \partial_t (n\,u) + \nabla \cdot (n\,u \otimes u) + \dfrac{1}{\tau} \nabla p(n) = -\dfrac{1}{\tau}\, n\,(E + u \times B)\,, \end{cases}$$

where $\tau \ll 1$ describes the gyro-period period as well as the Mach number. This equation describes a plasma gas submitted to a strong Lorentz force and possessing a low Mach number. In the $\tau \to 0$ limit, one switches to the Drift-fluid (or Gyro-fluid) regime.

– Low Mach number limit [12, 19] :

$$\begin{cases} \partial_t n + \nabla \cdot (n\,u) = 0 \\ \partial_t (n\,u) + \nabla \cdot (n\,u \otimes u) + \dfrac{1}{\varepsilon^2} \nabla p(n) = 0\,, \end{cases}$$

with $\varepsilon \ll 1$ the rescaled Mach number. This low Mach number limit describes the passage from the compressible Euler equations (or equivalently Navier-Stokes eq.) to the incompressible ones.

– Highly anisotropic temperature equation [39, 40] :

$$\partial_t T - \frac{1}{\varepsilon} \nabla_{||} \cdot (K_{||} \nabla_{||} T) - \nabla_{\perp} \cdot (K_{\perp} \nabla_{\perp} T) = 0\,,$$

where the subscripts $||$ (resp. $\perp$) refer to the direction parallel (resp. perpendicular) to the magnetic field lines and $\varepsilon \ll 1$ describes the large diffusivity of the temperature T along the magnetic field lines.

The goal of this part of the review will be to investigate from a numerical point of view two singular limits arising in the fluid framework. These two singular perturbation problems occur when one tries to solve the full system (3.18) in some particular situations.

Chapitre 4

Highly anisotropic elliptic equations

Chapter based on the articles of :
P. Degond, F. Deluzet, C. Negulescu [1]
P. Degond, F. Deluzet, A. Lozinski, J. Narski, C. Negulescu [2]
P. Degond, A. Lozinski, J. Narski, C. Negulescu [3]

The aim of this chapter is the construction of Asymptotic-Preserving schemes for an efficient numerical resolution of highly anisotropic elliptic equations, arising in several fields of application, such as flows in porous media, electrocardiogram simulations (biomathematics), semiconductor modelling and so on. In plasma modelling, the high anisotropy comes from the fact that the strong magnetic field B confines the charged particles in the direction perpendicular to the field lines, and permits them to evolve freely in the parallel direction. This property leads to rather different dynamics (in magnitude) in the perpendicular and parallel directions, yielding highly anisotropic equations, which are difficult to solve numerically.

Let us specify the mathematical context. We consider a regular, bounded domain $\Omega \subset \mathbb{R}^d$ with $d = 2, 3$ and boundary Γ. The anisotropy direction is given by a vector field $b \in (C^\infty(\Omega))^d$, satisfying $|b(x)| = 1$ for each $x \in \Omega$. Given this vector field b, one can decompose now each vector $v \in \mathbb{R}^d$, gradient $\nabla\phi$, with $\phi(x)$ a scalar function, and divergence $\nabla \cdot v$, with $v(x)$ a vector field, in a part parallel to the anisotropy and a perpendicular part. All these parts are defined as :

$$\begin{aligned}
&v_{||} := (v \cdot b)b\,, && v_\perp := (Id - b \otimes b)v\,, && \text{such that} \quad v = v_{||} + v_\perp\,,\\
&\nabla_{||}\phi := (b \cdot \nabla\phi)b\,, && \nabla_\perp\phi := (Id - b \otimes b)\nabla\phi\,, && \text{such that} \quad \nabla\phi = \nabla_{||}\phi + \nabla_\perp\phi\,,\\
&\nabla_{||} \cdot v := \nabla \cdot v_{||}\,, && \nabla_\perp \cdot v := \nabla \cdot v_\perp\,, && \text{such that} \quad \nabla \cdot v = \nabla_{||} \cdot v + \nabla_\perp \cdot v\,,
\end{aligned} \tag{4.1}$$

1. "An asymptotic preserving scheme for strongly anisotropic elliptic problems", SIAM-MMS.
2. "Duality based Asymptotic-Preserving Method for highly anisotropic diffusion equations", CMS.
3. "An Asymptotic-Preserving method for highly anisotropic elliptic equations based on a micro-macro decomposition", JCP.

where $\otimes$ denotes the tensor product. With all these notations, we can introduce now the singularly perturbed problem we are interested in, describing the evolution of the electric potential ϕ of a magnetically confined plasma :

$$(P)_\varepsilon \quad \begin{cases} -\frac{1}{\varepsilon}\nabla_\parallel \cdot \left(A_\parallel \nabla_\parallel \phi^\varepsilon\right) - \nabla_\perp \cdot (A_\perp \nabla_\perp \phi^\varepsilon) = f & \text{in } \Omega, \\ \frac{1}{\varepsilon} n_\parallel \cdot \left(A_\parallel \nabla_\parallel \phi^\varepsilon\right) + n_\perp \cdot (A_\perp \nabla_\perp \phi^\varepsilon) = 0 & \text{on } \Gamma_N, \\ \phi^\varepsilon = 0 & \text{on } \Gamma_D\,, \end{cases} \tag{4.2}$$

where n is the exterior normal to the boundary of Ω and where the different boundaries are defined by

$$\Gamma_D = \{x \in \Gamma \mid b(x)\cdot n = 0\}, \quad \Gamma_{in} = \{x \in \Gamma \mid b(x)\cdot n < 0\}, \quad \Gamma_{out} = \{x \in \Gamma \mid b(x)\cdot n > 0\}, \tag{4.3}$$

and $\Gamma_N := \Gamma_{in} \cup \Gamma_{out}$. We will suppose that $f \in L^2(\Omega)$, $\overset{\circ}{\Gamma}_D \neq \varnothing$ and that the diffusion coefficients $A_\parallel \in L^\infty(\Omega)$ and $A_\perp \in \mathbb{M}_{d\times d}(L^\infty(\Omega))$ satisfy

$$\begin{gathered} 0 < A_0 \leq A_\parallel(x) \leq A_1\,, \quad \text{f.a.a. } x \in \Omega, \\ A_0||v||^2 \leq v^t A_\perp(x) v \leq A_1||v||^2\,, \quad \forall v \in \mathbb{R}^d \text{ with } v\cdot b(x) = 0 \text{ and f.a.a. } x \in \Omega. \end{gathered} \tag{4.4}$$

The parameter $0 < \varepsilon \ll 1$ represents here the fraction between the perpendicular mobility of the particles and the parallel one, and can significantly vary in magnitude within the simulation domain. In the limit $\varepsilon \to 0$, the problem $(P)_\varepsilon$ degenerates to

$$(R) \quad \begin{cases} -\nabla_\parallel \cdot \left(A_\parallel \nabla_\parallel \phi\right) = 0 & \text{in } \Omega, \\ n_\parallel \cdot \left(A_\parallel \nabla_\parallel \phi\right) = 0 & \text{on } \Gamma_N, \\ \phi = 0 & \text{on } \Gamma_D. \end{cases} \tag{4.5}$$

This is an ill-posed problem as it has an infinite amount of solutions, especially those being constant along the field lines of b. That is the reason why solving $(P)_\varepsilon$ (for $\varepsilon \ll 1$) with standard schemes would lead to ill-conditioned linear systems, requiring more care, or leading (in the opposed case) to unacceptable numerical errors.

The aim of this chapter is hence to construct an AP-scheme, which shall be able to resolve the singularly perturbed problem $(P)_\varepsilon$ uniformly accurate in ε and with no huge computational costs. To do this, one has to change strategy and think about the following questions :

- are the solutions ϕ^ε of $(P)_\varepsilon$ convergent towards some function ϕ^0 when $\varepsilon \to 0$?
- if yes, does this limit solution ϕ^0 solve some limit problem $(P)_0$ (denoted also (L)) ?
- is this limit problem $(P)_0$ well-posed ?

The identification of this well-posed limit problem $(P)_0$ passes through the mathematical study of the dominant operator in the singularly perturbed problem $(P)_\varepsilon$. This identification will then permit to reformulate the singularly perturbed problem $(P)_\varepsilon$ in such a manner that it will recover automatically the limit problem $(P)_0$ if ε tends to zero.

The AP-scheme we introduce in the following can be applied also to other highly anisotropic elliptic situations, such as the following degenerate elliptic problem

$$\begin{cases} -\frac{1}{\varepsilon}\nabla_{||}(A_{||}\nabla_{||}\phi) + \phi = f\,, \quad \text{in} \quad \Omega\,, \\ n_{||}\cdot(A_{||}\nabla_{||}\phi) = 0 \quad \text{on} \quad \Gamma_N\,, \end{cases}$$

or the nonlinear, anisotropic, elliptic problem (for the electron density n)

$$\begin{cases} -\nabla_{||}\cdot(\nabla_{||}p(n)) + \varepsilon n = \varepsilon f\,, \quad \text{on} \quad \Omega\,, \\ \mathbf{n}_{||}\cdot\nabla_{||}p(n) = \varepsilon g \quad \text{on} \quad \Gamma_N\,. \end{cases}$$

4.1 Identification of the Limit problem

In order to construct an efficient numerical scheme for the resolution of the singularly perturbed problem (4.2), one has to begin with understanding the asymptotic behaviour of the solutions ϕ^ε. For this, let us firstly introduce an adequate mathematical framework. Let $\mathcal{V}$ be the Hilbert space

$$\mathcal{V} := \{\phi \in H^1(\Omega) \;/\; \phi_{|\Gamma_D} = 0\}\,, \quad (\phi,\psi)_{\mathcal{V}} := (\nabla_{||}\phi,\nabla_{||}\psi)_{L^2} + (\nabla_\perp\phi,\nabla_\perp\psi)_{L^2}\,.$$

We are thus seeking for solutions $\phi^\varepsilon \in \mathcal{V}$ of problem (4.2), written under weak form as

$$(P)_\varepsilon \qquad a_{||}(\phi^\varepsilon,\psi) + \varepsilon a_\perp(\phi^\varepsilon,\psi) = \varepsilon(f,\psi)\,, \quad \forall\psi\in\mathcal{V}\,, \tag{4.6}$$

where $(\cdot,\cdot)$ denotes the L^2 scalar-product and where the bilinear forms $a_{||}:\mathcal{V}\times\mathcal{V}\to\mathbb{R}$ and $a_\perp:\mathcal{V}\times\mathcal{V}\to\mathbb{R}$ are given by

$$a_{||}(\phi,\psi) \;:=\; \int_\Omega A_{||}\nabla_{||}\phi\cdot\nabla_{||}\psi\,dx\,, \quad a_\perp(\phi,\psi) := \int_\Omega (A_\perp\nabla_\perp\phi)\cdot\nabla_\perp\psi\,dx\,. \tag{4.7}$$

The Lax-Milgram theorem permits then to deduce immediately that the problem (4.6) admits a unique solution $\phi^\varepsilon\in\mathcal{V}$ for each fixed $\varepsilon>0$.

To discern the asymptotic behaviour of the sequence $\{\phi^\varepsilon\}_{\varepsilon>0}$ as $\varepsilon\to 0$, one necessitates to investigate the dominant operator in (4.2), in particular to identify its kernel and introduce a projection operator on this kernel. The kernel is immediately recognized as the Hilbert space of functions with zero gradient along the anisotropy field lines b, *i.e.*

$$\mathcal{G} = \{\phi\in\mathcal{V} \mid \nabla_\parallel\phi = 0\}\,, \quad (\phi,\psi)_{\mathcal{G}} := (\nabla_\perp\phi,\nabla_\perp\psi)_{L^2}\,, \quad \forall\phi,\psi\in\mathcal{G}\,. \tag{4.8}$$

In order to identify now the limit problem, let us suppose that $\phi^\varepsilon\to\phi^0$ in some sense when ε tends to zero and try to find out the problem solved by ϕ^0. The first remark is that ϕ^0 has to belong to the kernel of the dominant operator, $\phi^0\in\mathcal{G}$. Taking then in (4.6) test functions $\psi\in\mathcal{G}$ (which means nothing else than averaging the equation along the field lines or projecting on the kernel), one obtains

$$\int_\Omega A_\perp\nabla_\perp\phi^\varepsilon\cdot\nabla_\perp\psi\,dx = \int_\Omega f\psi\,dx\;\;, \quad \forall\psi\in\mathcal{G}\,. \tag{4.9}$$

Passing now to the limit $\varepsilon \to 0$ in this last equation yields finally the variational formulation of the limit problem, satisfied by ϕ^0 : Find $\phi^0 \in \mathcal{G}$, solution of

$$(L) \quad \int_\Omega A_\perp \nabla_\perp \phi^0 \cdot \nabla_\perp \psi \, dx = \int_\Omega f\psi \, dx \quad , \quad \forall \psi \in \mathcal{G} \, . \tag{4.10}$$

Again, the Lax-Milgram theorem permits to deduce the existence and uniqueness of a solution of this problem.

The goal now is to reformulate the singularly perturbed problem (4.6) in such a manner, in order to get automatically the Limit problem (4.10) when ε tends to zero. Two different reformulations will be presented in this chapter.

4.2 First AP-reformulation

The first Asymptotic-Preserving reformulation of (4.2) is based on the decomposition of the unknown ϕ^ε into :

- a macroscopic part p^ε belonging to the kernel of the dominant operator, and which is chosen in this case as the average of ϕ^ε along the anisotropy field lines
- a microscopic part q^ε, the fluctuating part, lying in the L^2-orthogonal complement $\mathcal{A}$ of $\mathcal{G}$, *i.e.*

$$\mathcal{A} := \{\phi \in \mathcal{V} \, | (\phi, \psi) = 0 \quad , \quad \forall \psi \in \mathcal{G}\} \, . \tag{4.11}$$

The Hilbert space $\mathcal{V}$ is decomposed in this case as follows

$$\mathcal{V} = \mathcal{G} \oplus^\perp \mathcal{A} \, , \tag{4.12}$$

with the L^2-orthogonal projection operator on the kernel $\mathcal{G}$ given by

$$P : \mathcal{V} \to \mathcal{G} \;\text{ such that }\; (P\phi, \psi) = (\phi, \psi) \;\; \forall \phi \in \mathcal{V}, \;\; \psi \in \mathcal{G} \, . \tag{4.13}$$

Applying this projection P to a function ϕ is nothing but averaging ϕ along the anisotropy field lines of b. Each function $\phi^\varepsilon \in \mathcal{V}$ can thus be decomposed uniquely as $\phi^\varepsilon = p^\varepsilon + q^\varepsilon$, where $p^\varepsilon = P\phi^\varepsilon \in \mathcal{G}$ and $q^\varepsilon = (I - P)\phi^\varepsilon \in \mathcal{A}$. Inserting this decomposition in the singularly perturbed problem (4.6) and taking test functions $\eta \in \mathcal{G}$ and $\xi \in \mathcal{A}$, permits to reformulate the original problem into an asymptotic preserving formulation : Find $(p^\varepsilon, q^\varepsilon) \in \mathcal{G} \times \mathcal{A}$ such that

$$(AP) \quad \begin{cases} a_\perp(p^\varepsilon, \eta) + a_\perp(q^\varepsilon, \eta) = (f, \eta), & \forall \eta \in \mathcal{G}, \\ a_{||}(q^\varepsilon, \xi) + \varepsilon a_\perp(q^\varepsilon, \xi) + \varepsilon a_\perp(p^\varepsilon, \xi) = \varepsilon(f, \xi), & \forall \xi \in \mathcal{A}. \end{cases} \tag{4.14}$$

Taking test functions $\eta \in \mathcal{G}$ resp. $\xi \in \mathcal{A}$ means nothing else but applying the projection P resp. $(I - P)$ to the original problem. Contrary to the Singular Perturbation problem (4.6), setting formally $\varepsilon = 0$ in (4.14) yields the system

$$(L') \quad \begin{cases} a_\perp(p^0, \eta) + a_\perp(q^0, \eta) &= (f, \eta) \, , & \forall \eta \in \mathcal{G} \\ a_{||}(q^0, \xi) &= 0 \, , & \forall \xi \in \mathcal{A} \, , \end{cases} \tag{4.15}$$

which has a unique solution $(p^0, q^0) \in \mathcal{G} \times \mathcal{A}$, where p^0 is the unique solution of the L-problem (4.10) and $q^0 \equiv 0$. Indeed, taking $\xi = q^0$ as test function in the second equation of (4.15) yields $\nabla_{||} q^0 = 0$, which means $q^0 \in \mathcal{G}$. But at the same time, $q^0 \in \mathcal{A}$, so that $q^0 \in \mathcal{G} \cap \mathcal{A} = \{0\}$. Setting then $q^0 \equiv 0$ in the first equation of (4.15), shows that p^0 is the unique solution of the L-problem.

4.3 Characterization of the spaces $\mathcal{G}$ and $\mathcal{A}$

In order to solve numerically the reformulated system (4.14) one has to think about the numerical discretization of the spaces $\mathcal{A}$ and $\mathcal{G}$, which is not a simple task for general anisotropy fields b. In the following we will apply Lagrange multiplier techniques to cope with this problem.

To avoid the use of the constrained space $\mathcal{A}$, we can remark that $\mathcal{A}$ can be characterized as being the orthogonal complement (in the L^2 sense) of the $\mathcal{G}$-space. Thus, instead of (4.14), a slightly changed system will be solved : Find $(p^\varepsilon, q^\varepsilon, l^\varepsilon) \in \mathcal{G} \times \mathcal{V} \times \mathcal{G}$ such that

$$\begin{cases} a_\perp(p^\varepsilon, \eta) + a_\perp(q^\varepsilon, \eta) = (f, \eta) & \forall \eta \in \mathcal{G}, \\ a_{||}(q^\varepsilon, \xi) + \varepsilon a_\perp(q^\varepsilon, \xi) + \varepsilon a_\perp(p^\varepsilon, \xi) + (l^\varepsilon, \xi) = \varepsilon(f, \xi) & \forall \xi \in \mathcal{V}, \\ (q^\varepsilon, \chi) = 0 & \forall \chi \in \mathcal{G}. \end{cases} \tag{4.16}$$

The constraint $(q^\varepsilon, \chi) = 0$, $\forall \chi \in \mathcal{G}$ forces the solution q^ε to belong to $\mathcal{A}$, and this property is carried over in the limit $\varepsilon \to 0$. We have thus circumvented the difficulty of discretizing $\mathcal{A}$ by introducing a new variable $l^\varepsilon \in \mathcal{G}$ (Lagrange multiplier) and enlarging the linear system.

In order to eliminate now the problems that arise when dealing with the discretization of $\mathcal{G}$, the Lagrange multiplier method will again be used. First note that

$$p \in \mathcal{G} \Leftrightarrow \begin{cases} \nabla_{||} p = 0 \\ p \in \mathcal{V} \end{cases} \Leftrightarrow \begin{cases} \displaystyle\int_\Omega A_{||} \nabla_{||} p \cdot \nabla_{||} \lambda \, dx = a_{||}(p, \lambda) = 0, \quad \forall \lambda \in \mathcal{L} \\ p \in \mathcal{V}, \end{cases} \tag{4.17}$$

where $\mathcal{L}$ is the functional space

$$\mathcal{L} := \{\lambda \in L^2(\Omega) \ / \ \nabla_{||} \lambda \in L^2(\Omega), \ \ \lambda_{|\Gamma_{in}} = 0\}. \tag{4.18}$$

The choice of this Lagrangian space has been done so that one could find for any $\zeta \in L^2(\Omega)$ a unique $\lambda \in \mathcal{L}$ satisfying $\nabla_{||} \lambda = \zeta$.

Using the characterization (4.17) of the constrained space $\mathcal{G}$, we will now reformulate

the system (4.16) as follows : Find $(p^\varepsilon,\ \lambda^\varepsilon,\ q^\varepsilon,\ l^\varepsilon,\ \mu^\varepsilon) \in \mathcal{V}\times\mathcal{L}\times\mathcal{V}\times\mathcal{V}\times\mathcal{L}$ such that

$$(DB)\quad \left\{\begin{array}{l} a_\perp(p^\varepsilon,\eta)+a_\perp(q^\varepsilon,\eta)+a_{||}(\eta,\lambda^\varepsilon)=(f,\eta)\ , \quad \forall\eta\in\mathcal{V}\,,\\ a_{||}(p^\varepsilon,\kappa)=0\,,\quad \forall\kappa\in\mathcal{L}\,,\\ a_{||}(q^\varepsilon,\xi)+\varepsilon a_\perp(q^\varepsilon,\xi)+\varepsilon a_\perp(p^\varepsilon,\xi)+(l^\varepsilon,\xi)=\varepsilon\,(f,\xi)\ , \quad \forall\xi\in\mathcal{V}\,,\\ (q^\varepsilon,\chi)+a_{||}(\chi,\mu^\varepsilon)=0\,,\quad \forall\chi\in\mathcal{V}\,,\\ a_{||}(l^\varepsilon,\tau)=0\,,\quad \forall\tau\in\mathcal{L}\,. \end{array}\right. \tag{4.19}$$

The advantage of this formulation, as compared to (4.14), is that we only have to discretize the spaces $\mathcal{V}$ and $\mathcal{L}$ (at the price of the introduction of three additional variables), which is much easier than the discretization of the constrained spaces $\mathcal{G}$ and $\mathcal{A}$. More importantly, the dual formulation (4.19) does not require any change of coordinates to express the fact that p^ε is constant along the b-field lines and that q^ε averages to zero along these lines. Therefore it is particularly well adapted to arbitrary, time-dependent b-fields and can be simply used on Cartesian grids. The system (4.19) will be called in the sequel Duality-Based Asymptotic-Preserving formulation (DB-scheme).

4.4 Second AP-reformulation

A second Asymptotic-Preserving reformulation of the singularly perturbed problem $(P)_\varepsilon$ can be designed by proposing a different micro-macro decomposition. Instead of decomposing each $\phi^\varepsilon = p^\varepsilon + q^\varepsilon$ into its mean part along the anisotropy field lines, $p^\varepsilon\in\mathcal{G}$, and the fluctuation part $q^\varepsilon\in\mathcal{A}$, one can mimic a "Hilbert-Ansatz" by posing

$$\phi^\varepsilon = p^\varepsilon + \varepsilon q^\varepsilon\,,\quad \nabla_{||}\phi^\varepsilon = \varepsilon\nabla_{||}q^\varepsilon\,,\quad q^\varepsilon_{|\Gamma_{in}}=0\,. \tag{4.20}$$

Fundamentally, the space $\mathcal{A}$ for the variable q^ε has been replaced by the space $\mathcal{L}$ of functions vanishing on the inflow boundary. With this new decomposition, the singularly perturbed problem (4.6) can be reformulated as : Find $(u^\varepsilon, q^\varepsilon)\in\mathcal{V}\times\mathcal{L}$, solution of

$$(MM)\quad \left\{\begin{array}{ll} \displaystyle\int_\Omega (A_\perp\nabla_\perp\phi^\varepsilon)\cdot\nabla_\perp v\,dx+\int_\Omega A_{||}\nabla_{||}q^\varepsilon\cdot\nabla_{||}v\,dx=\int_\Omega fv\,dx, & \forall v\in\mathcal{V}\\ \displaystyle\int_\Omega A_{||}\nabla_{||}\phi^\varepsilon\cdot\nabla_{||}w\,dx-\varepsilon\int_\Omega A_{||}\nabla_{||}q^\varepsilon\cdot\nabla_{||}w\,dx=0, & \forall w\in\mathcal{L}\,. \end{array}\right. \tag{4.21}$$

This AP-reformulation will be called in the sequel Asymptotic-Preserving problem based on a micro-macro decomposition (MM-problem). It is, for fixed $\varepsilon>0$, an equivalent reformulation of the original (P_ε)-problem. Moreover, in the limit $\varepsilon\to 0$ one obtains a well-posed saddle-point problem, which is equivalent to the Limit-problem (4.10).

The essential advantage of this MM-reformulation, as compared to the first one, is that no more constraint spaces appear, such that the MM-formulation can be solved immediately without the introduction of additional variables. Remark also that the basic difference between the two reformulations is simply the manner how to render the decomposition of $\mathcal{V}$ unique, on one hand by imposing zero average along the anisotropy field lines, *i.e.* $\bar{q}_\varepsilon\equiv 0$, on the other hand by fixing the boundary condition $q_{|\Gamma_{in}}\equiv 0$.

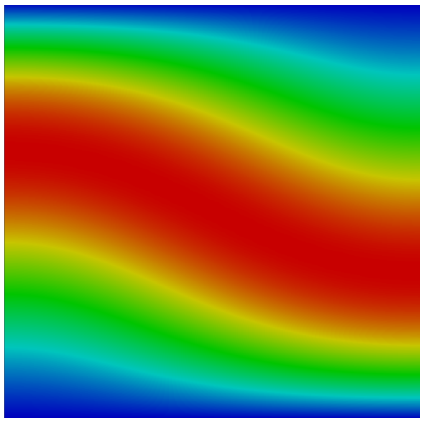

FIGURE 4.1: The limit solution ϕ^0 for the non-uniform anisotropy field b.

4.5 Numerical results

Let us present now some numerical simulations performed for a variable field b with both AP-schemes and compare for validation the obtained results with those of a standard discretization of the singularly perturbed problem $(P)_\varepsilon$. In particular, we are interested in the validation of the Asymptotic-Preserving property of the new schemes, in their ability to capture the Limit-model (L) as ε tends to zero, without refining the grids.

The non-uniform magnetic field b we choose, is given by

$$b = \frac{B}{|B|}, \quad B = \begin{pmatrix} 2(2y-1)\cos(\pi x) + \pi \\ 2\pi(y^2 - y)\sin(\pi x) \end{pmatrix}. \tag{4.22}$$

Note that the field B satisfies $\mathrm{div} B = 0$, which is an important property in the framework of plasma simulations. Furthermore, we have $B \neq 0$ in the computational domain.
Now, in order to test the space-convergence of the schemes, regardless of ε, we construct an exact solution ϕ^ε, given by

$$\phi^\varepsilon = \sin\big(\pi y + 2(y^2 - y)\cos(\pi x)\big) + \varepsilon \cos(2\pi x)\sin(\pi y)$$

and the associated force term is calculated using the equation, i.e.

$$f = -\nabla_\perp \cdot (A_\perp \nabla_\perp \phi^\varepsilon) - \frac{1}{\varepsilon}\nabla_\parallel \cdot (A_\parallel \nabla_\parallel \phi^\varepsilon).$$

In Figure 4.1 we plotted the limit solution of the sequence $\{\phi^\varepsilon\}_{\varepsilon>0}$, which permits to distinguish the anisotropy field lines.

The relative errors between the exact solution ϕ^ε and the numerical ones, obtained in this framework with the three methods, the standard FE-discretization of the P_ε-problem, the DB-scheme and the MM-scheme, are presented on Figure 4.2, as a function of the parameter ε and for several mesh-sizes. Both, the Micro-Macro and the Duality-Based AP-approaches, give the same accuracy, they converge with the optimal rate in both L^2- and H^1-norms, independently of ε. The singularly-perturbed model gives however reliable results only for ε-values larger than a critical value ε_P. Furthermore the

condition number of the DB- and MM-schemes is bounded independently on ε, whereas the one for the P_ε-problem is exploding with $1/\varepsilon$ (see Fig. 4.3).
As a concluding remark, the AP-methods presented here are shown to be very efficient schemes for the resolution of highly anisotropic elliptic problems, permitting an accurate resolution, independent on ε, and without having to adapt the grid to the anisotropy.

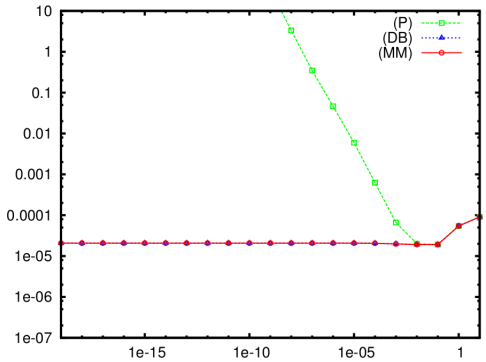

(a) L^2 error for a grid with 50×50 points.

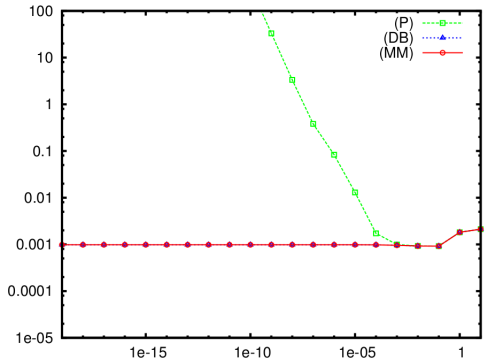

(b) H^1 error for a grid with 50×50 points.

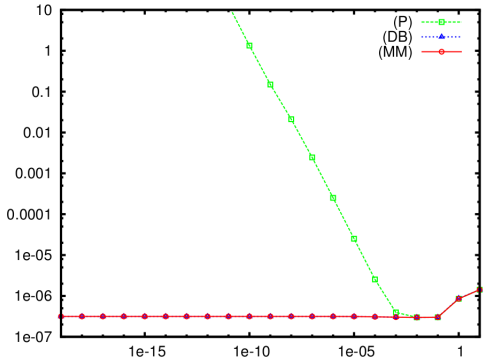

(c) L^2 error for a grid with 200×200 points.

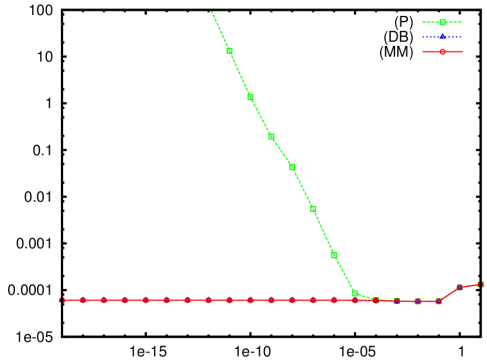

(d) H^1 error for a grid with 200×200 points.

FIGURE 4.2: Relative L^2- and H^1-errors between the exact solution ϕ^ε and the computed ones ϕ_M (MM), ϕ_D (DB), ϕ_P (P), as a function of ε and for different meshes.

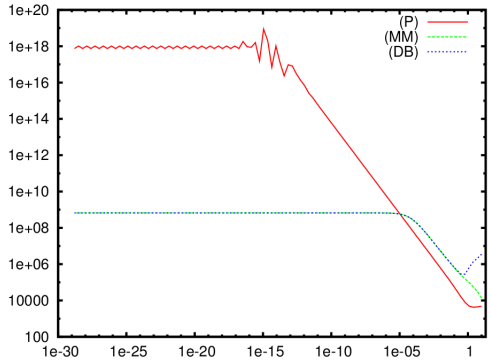

(a) mesh size : 100×100 points

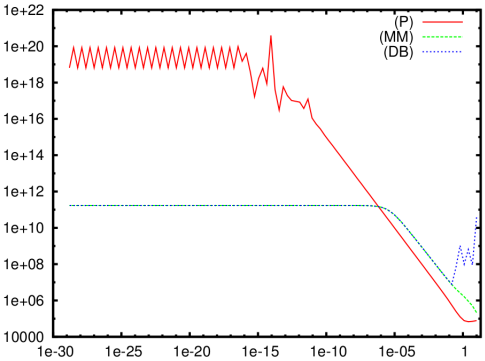

(b) mesh size : 400×400 points

FIGURE 4.3: Condition number estimate provided by the MUMPS solver .

Chapitre 5

Highly anisotropic parabolic equations

Chapter based on the articles of :
A. Mentrelli, C. Negulescu [1]
A. Lozinski, J. Narski, C. Negulescu [2]

This last chapter deals with the numerical study of a nonlinear, strongly anisotropic heat equation. As explained in the previous chapter, magnetically confined plasmas are characterized by highly anisotropic properties induced by the strong magnetic field B. The charged particles constituting the plasma move rapidly around the magnetic field lines, their transverse motion away from B is constrained by the Lorentz force, whereas their motion along B is relatively unrestricted. This results in an extremely large ratio of the parallel to the transverse thermal conductivities, as well as of other parameters characterizing the plasma evolution.

The objective of this part will be to treat the numerical problems arising (due to the anisotropy) in the energy conservation equation of the fluid model (3.18). Keeping only the problematic terms, we are thus interested in the particle (ions or electrons) temperature $u(t,x)$, solution of the evolution equation

$$(P)_\varepsilon \quad \begin{cases} \partial_t u - \frac{1}{\varepsilon}\nabla_{||}\cdot(A_{||}u^{5/2}\nabla_{||}u) - \nabla_\perp\cdot(A_\perp\nabla_\perp u) = 0\,, \quad \text{in} \quad [0,T]\times\Omega\,, \\ \frac{1}{\varepsilon}n_{||}\cdot(A_{||}u^{5/2}(t,\cdot)\nabla_{||}u(t,\cdot)) + n_\perp\cdot(A_\perp\nabla_\perp u(t,\cdot)) = -\gamma\, u(t,\cdot)\,, \quad \text{on} \quad [0,T]\times\Gamma_\perp\,, \\ \nabla_\perp u(t,\cdot) = 0\,, \quad \text{on} \quad [0,T]\times\Gamma_{||}\,, \\ u(0,\cdot) = u^0(\cdot)\,, \quad \text{in} \quad \Omega\,. \end{cases} \tag{5.1}$$

1. "Asymptotic-Preserving scheme for highly anisotropic non-linear diffusion equations", Journal of Comp. Phys.

2. "Highly anisotropic temperature balance equation and its asymptotic-preserving resolution", M2AN.

The coefficient γ is zero for electrons and $\gamma > 0$ for ions. The boundary Γ is decomposed into three components following the sign of the intersection with b :

$$\Gamma_{||} := \{x \in \Gamma \ / \ b(x) \cdot n(x) = 0\}\,,$$

$$\Gamma_{in} := \{x \in \Gamma \ / \ b(x) \cdot n(x) < 0\}\,, \quad \Gamma_{out} := \{x \in \Gamma \ / \ b(x) \cdot n(x) > 0\}\,,$$

and $\Gamma_\perp = \Gamma_{in} \cup \Gamma_{out}$. The vector n is here the unit outward normal to Γ. Most of the other notations are adopted from the previous chapter.

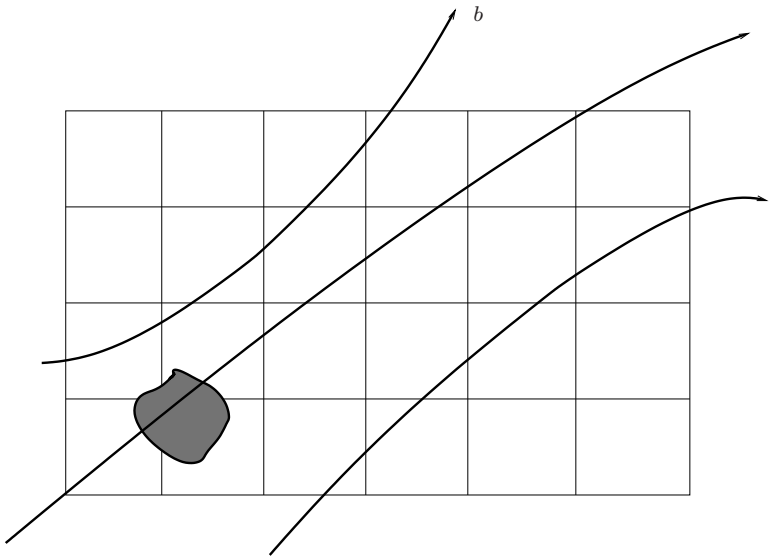

FIGURE 5.1: Diffusion of a hot temperature spot along the magnetic field lines.

The problem (5.1) describes the diffusion of an initial temperature u^0 during the time interval $[0, T]$, and its outflow through the boundary $\Gamma_\perp$ (see Fig. 5.1). A detailed mathematical study of this problem (existence/uniqueness/positivity of a weak solution) is provided in [39]. Some other classical works [1, 45] deal (from a mathematical point of view) with similar nonlinear parabolic problems. Indeed, this kind of highly anisotropic diffusive problem arises in several other important applications, as for example in magnetic resonance imaging (MRI), which is a powerful technique for studying the anatomy of the brain. Moreover highly anisotropic PDE's appear also in image processing and other computer vision problems.

Putting now formally $\varepsilon = 0$ in (5.1) leads to the following ill-posed problem, admitting infinitely many solutions

$$(R) \quad \begin{cases} -\nabla_{||} \cdot (A_{||} u^{5/2} \nabla_{||} u) = 0\,, \quad \text{in} \quad [0,T] \times \Omega\,, \\ n_{||} \cdot (A_{||} u^{5/2}(t,\cdot) \nabla_{||} u(t,\cdot)) = 0\,, \quad \text{on} \quad [0,T] \times \Gamma_\perp\,, \\ \nabla_\perp u(t,\cdot) = 0\,, \quad \text{on} \quad [0,T] \times \Gamma_{||}\,, \\ u(0,\cdot) = u^0(\cdot)\,, \quad \text{in} \quad \Omega\,. \end{cases} \tag{5.2}$$

Undoubtedly, all functions which are constant along the field lines, meaning $\nabla_{||}u \equiv 0$, and satisfying moreover the boundary condition on $\Gamma_{||}$, are solutions of this problem. From a numerical point of view, this ill-posedness in the limit $\varepsilon \to 0$ can be detected by the fact, that trying to solve (5.1) with standard schemes leads to a linear system, which is ill-conditioned for $0 < \varepsilon \ll 1$, in particular with a condition number of the order of $1/\varepsilon$. Refining the mesh (in the temporal variable) would help (up to a certain limit) to avoid this constraint, is however computationally too expensive.

The aim of this chapter will thus be to introduce an efficient numerical method, permitting to solve (5.1) accurately on a coarse Cartesian grid, which has not to be adapted to the field lines of b and whose mesh size is independent of the value of ε.

5.1 Numerical method

The construction of an AP-scheme, which shall be able to capture the various scales present in the problem with no additional numerical costs, in particular, which shall allow for a smooth transition between the singularly perturbed problem $(P)_\varepsilon$ and the Limit problem (L) as $\varepsilon \to 0$, passes through some preliminary mathematical steps. Firstly the Limit model has to be identified. It is defined as the problem whose solution is the limit of the singularly-perturbed problem solutions $\{u_\varepsilon\}_{\varepsilon>0}$ as ε tends to zero. Then, after this identification, the key idea of the AP-methodology is to reformulate the singularly perturbed problem into an equivalent problem, which is better suited for the limit as $\varepsilon \to 0$, in particular which captures the Limit problem as ε tends to zero.

The reformulation of the here proposed method is based on a "Hilbert-type" Ansatz, similar to the one introduced in the previous elliptic framework. Let us first discretize in space and then in time.

5.1.1 Semi-discretization in space

The variational formulation of the singular perturbation problem (5.1) reads : Find $u(t,\cdot) \in \mathcal{V} := H^1(\Omega)$ such that

$$(P)_\varepsilon \qquad \langle \partial_t u(t,\cdot),\, v\rangle_{\mathcal{V}^*,\mathcal{V}} + \frac{1}{\varepsilon}\int_\Omega A_{||}|u|^{5/2}\nabla_{||}u(t,\cdot)\cdot\nabla_{||}v\,dx \tag{5.3}$$
$$+ \int_\Omega A_\perp \nabla_\perp u(t,\cdot)\cdot\nabla_\perp v\,dx + \gamma\int_{\Gamma_\perp} u(t,\cdot)v\,d\sigma = 0, \quad \forall v \in \mathcal{V}$$

for almost every $t \in (0,T)$. As mentioned earlier, this problem becomes ill-posed if we take formally the limit $\varepsilon \to 0$. Only the leading term survives in this limit, so that any function from the kernel-space

$$\mathcal{G} := \{p \in \mathcal{V} \;/\; \nabla_{||}p = 0 \text{ in } \Omega\}$$

would be a solution. The well-posed Limit problem is however easy to establish, similarly to the elliptic methodology. One can restrain the test functions in $(P)_\varepsilon$ to be in the space

$\mathcal{G}$ so that the ε-dependent term disappears and the correct problem in the limit $\varepsilon \to 0$ reads : Find $u(t,\cdot) \in \mathcal{G}$ such that

$$(L)\ \ \langle \partial_t u(t,\cdot),\, v\rangle_{\mathcal{V}^*,\mathcal{V}} + \int_\Omega A_\perp \nabla_\perp u(t,\cdot)\cdot\nabla_\perp v\, dx + \gamma \int_{\Gamma_\perp} u(t,\cdot) v\, d\sigma = 0, \quad \forall v \in \mathcal{G}$$

for almost every $t \in (0,T)$.

The target is now to find a way in order to get a smooth transition between the singularly perturbed problem $(P)_\varepsilon$ and the limit problem (L) as $\varepsilon \to 0$. In order to do this, we introduce an auxiliary unknown q by the relation $\varepsilon \nabla_{||} q = u^{5/2}\nabla_{||} u$ in Ω, satisfying moreover $q_{|\Gamma_{in}} = 0$. This procedure rescales the nasty part of the equation permitting to get rid of the terms of order $O(1/\varepsilon)$. The reformulated problem, called in the sequel the Asymptotic-Preserving reformulation (AP-model) reads : Find $(u(t,\cdot), q(t,\cdot)) \in \mathcal{V}\times\mathcal{L}$, solution of

$$(AP)\ \ \begin{cases} \langle \dfrac{\partial u}{\partial t},\, v\rangle_{\mathcal{V}^*,\mathcal{V}} + \displaystyle\int_\Omega (A_\perp \nabla_\perp u)\cdot\nabla_\perp v\, dx + \int_\Omega A_\parallel \nabla_\parallel q\cdot\nabla_\parallel v\, dx + \gamma\int_{\Gamma_\perp} uv\, ds = 0, \\ \qquad\qquad\qquad\qquad\qquad\qquad\qquad\qquad\qquad\qquad \forall v \in \mathcal{V} \\ \displaystyle\int_\Omega A_\parallel u^{5/2}\nabla_\parallel u\cdot\nabla_\parallel w\, dx - \varepsilon\int_\Omega A_\parallel \nabla_\parallel q\cdot\nabla_\parallel w\, dx = 0, \quad \forall w \in \mathcal{L}\,, \end{cases} \tag{5.4}$$

where the Lagrange multiplier space is given by

$$\mathcal{L} := \{q \in L^2(\Omega)\ /\ \nabla_\parallel q \in L^2(\Omega) \text{ and } q|_{\Gamma_{in}} = 0\}. \tag{5.5}$$

System (5.4) is an equivalent reformulation (for fixed $\varepsilon > 0$) of the original $(P)_\varepsilon$-problem (5.3). Putting now formally $\varepsilon = 0$ in (AP) leads to the well-posed limit problem

$$(L')\ \ \begin{cases} \langle \dfrac{\partial u}{\partial t},\, v\rangle_{\mathcal{V}^*,\mathcal{V}} + \displaystyle\int_\Omega (A_\perp \nabla_\perp u)\cdot\nabla_\perp v\, dx + \int_\Omega A_\parallel \nabla_\parallel q\cdot\nabla_\parallel v\, dx + \gamma\int_{\Gamma_\perp} uv\, ds = 0, \\ \qquad\qquad\qquad\qquad\qquad\qquad\qquad\qquad\qquad\qquad \forall v \in \mathcal{V} \\ \displaystyle\int_\Omega A_\parallel u^{5/2}\nabla_\parallel u\cdot\nabla_\parallel w\, dx = 0, \quad \forall w \in \mathcal{L}\,, \end{cases} \tag{5.6}$$

which is equivalent to problem (L). Note that q acts here as a Lagrange multiplier for the constraint $u \in \mathcal{G}$, which provides the uniqueness of the solution. Hence the AP-reformulation permits a continuous transition from the $(P)_\varepsilon$-model to the L-model, which enables the uniform accuracy of the scheme with respect to ε.

To discretize the (AP)-system in space, let us choose a triangularisation of the domain Ω and introduce the finite dimensional spaces $\mathcal{V}_h \subset \mathcal{V}$ and $\mathcal{L}_h \subset \mathcal{L}$ of type $\mathbb{P}_k$ or $\mathbb{Q}_k$ on this mesh. The finite element discretization of (5.4) writes then : Find

$(u_h, q_h) \in \mathcal{V}_h \times \mathcal{L}_h$ such that

$$(AP)_h \quad \begin{cases} \displaystyle\int_\Omega \frac{\partial u_h}{\partial t} v_h \, dx + \int_\Omega (A_\perp \nabla_\perp u_h) \cdot \nabla_\perp v_h \, dx + \int_\Omega A_\parallel \nabla_\parallel q_h \cdot \nabla_\parallel v_h \, dx + \gamma \int_{\Gamma_\perp} u_h v_h \, ds = 0, \\ \qquad\qquad\qquad\qquad\qquad\qquad\qquad\qquad\qquad\qquad \forall v_h \in \mathcal{V}_h \\ \displaystyle\int_\Omega A_\parallel u_h^{5/2} \nabla_\parallel u_h \cdot \nabla_\parallel w_h \, dx - \varepsilon \int_\Omega A_\parallel \nabla_\parallel q_h \cdot \nabla_\parallel w_h \, dx = 0, \quad \forall w \in \mathcal{L}_h \, . \end{cases} \tag{5.7}$$

Remark that this system is continuous in time and also nonlinear, such that one has to develop now a procedure for the linearization and the discretization in time. This procedure has to be chosen carefully, such that the AP-property developed so far, will not be destroyed.

5.1.2 Semi-discretization in time

In order to approach numerically the time derivative in (5.7), we use three different schemes : a standard first order, implicit Euler scheme, the Crank-Nicolson scheme and a second order, L-stable Runge-Kutta method. These three methods will be exposed to numerical tests and compared.

Denoting by $\tau > 0$ the time-discretization step and introducing the forms

$$(\Theta, \chi) := \int_\Omega \Theta \chi \, dx \, , \tag{5.8}$$

$$a_{\parallel nl}(\Psi, \Theta, \chi) := \int_\Omega A_\parallel \Psi^{5/2} \nabla_\parallel \Theta \cdot \nabla_\parallel \chi \, dx \, , \tag{5.9}$$

$$a_\parallel(\Theta, \chi) := \int_\Omega A_\parallel \nabla_\parallel \Theta \cdot \nabla_\parallel \chi \, dx \, , \qquad a_\perp(\Theta, \chi) := \int_\Omega A_\perp \nabla_\perp \Theta \cdot \nabla_\perp \chi \, dx \, , \tag{5.10}$$

allows to present the three methods.

Implicit Euler scheme : Find $(u_h^{n+1}, q_h^{n+1}) \in \mathcal{V}_h \times \mathcal{L}_h$, solution of

$$(E_{AP}) \quad \begin{cases} (u_h^{n+1}, v_h) + \tau \left(a_\perp(u_h^{n+1}, v_h) + a_\parallel(q_h^{n+1}, v_h) + \gamma \int_{\Gamma_\perp} u_h^{n+1} v_h \, ds \right) = (u_h^n, v_h) \\ a_{\parallel nl}(u_h^n, u_h^{n+1}, w_h) - \varepsilon a_\parallel(q_h^{n+1}, w_h) = 0 \, , \end{cases} , \tag{5.11}$$

where the nonlinear term $(u_h^{n+1})^{5/2}$ was replaced by a first order approximation in τ :

$$(u_h^{n+1})^{5/2} = (u_h^n + O(\tau))^{5/2} = (u_h^n)^{5/2} + O(\tau). \tag{5.12}$$

This scheme is first order in time, unconditionally stable and asymptotic-preserving.

Crank-Nicolson scheme : Unfortunately, this method is not Asymptotic-Preserving. It gives reliable results and second order convergence under certain assumptions, as for example under the restrictive choice of a time step $\tau \sim \varepsilon / (u_h^n)^{5/2}$, which makes the

method inapplicable. If this condition is not verified, the numerical solution starts to oscillate and gives even negative temperatures. In other words, the Crank-Nicolson scheme is unable to model diffusion processes for large Δt, due to the inadequate approximation of the damping processes. It is an A-stable scheme, but not L-stable and the AP-property of a scheme is strongly related to the L-stability of the scheme.

Diagonally Implicit Runge-Kutta scheme : As we are interested in an AP-scheme, which is second order accurate in time, we propose now a two stage Diagonally Implicit Runge-Kutta (DIRK) scheme, which does not suffer from the limitations of the Crank-Nicolson discretization. The scheme is developed according to the following Butcher's diagram :

$$\begin{array}{c|cc} \lambda & \lambda & 0 \\ 1 & 1-\lambda & \lambda \\ \hline & 1-\lambda & \lambda \end{array} \tag{5.13}$$

with $\lambda = 1 - \frac{1}{\sqrt{2}}$.

Remarque 5.1.1 *(Butcher's diagram) The coefficients of the s-stage Runge-Kutta method are usually displayed in a Butcher's diagram :*

$$\begin{array}{c|ccc} c_1 & a_{11} & \cdots & a_{1s} \\ \vdots & \vdots & & \vdots \\ c_s & a_{s1} & \cdots & a_{ss} \\ \hline & b_1 & \cdots & b_s \end{array} . \tag{5.14}$$

Applying this method to approximate the following problem

$$\frac{\partial u}{\partial t} = Lu + f(t)\,, \tag{5.15}$$

reads : For given u^n, being an approximation of $u(t_n)$, the u^{n+1} is determined via :

$$u_i = u^n + \tau \sum_{j=1}^{s} a_{ij}(Lu_j + f(t + c_j\tau)), \tag{5.16}$$

$$u^{n+1} = u^n + \sum_{j=1}^{s} b_j u_j. \tag{5.17}$$

If $b_j = a_{sj}$ for $j = 1, \ldots, s$ than $u^{n+1} = u_s$.

The scheme (5.13) is known to be L-stable, thus providing the desired Asymptotic

Preserving property. It writes : Find $(u_h^{n+1}, q_h^{n+1}) \in \mathcal{V}_h \times \mathcal{L}_h$, solution of

$$
(RK_{AP}) \quad \left\{ \begin{array}{l} (u_{1,h}^{n+1}, v_h) + \tau\lambda \left(a_\perp(u_{1,h}^{n+1}, v_h) + \gamma \int_{\Gamma_\perp} u_{1,h}^{n+1} v_h \, ds + a_\parallel(q_{1,h}^{n+1}, v_h) \right) \\ \qquad\qquad = (u_h^n, v_h) \\ a_{\parallel nl}\left(u_h^n + \lambda(u_h^n - u_h^{n-1}), u_{1,h}^{n+1}, w_h\right) - \varepsilon a_\parallel(q_{1,h}^{n+1}, w_h) = 0 \end{array} \right. \tag{5.18}
$$

$$
\left\{ \begin{array}{l} (u_{2,h}^{n+1}, v_h) + \tau\lambda \left(a_\perp(u_{2,h}^{n+1}, v_h) + \gamma \int_{\Gamma_\perp} u_{2,h}^{n+1} v_h \, ds + a_\parallel(q_{2,h}^{n+1}, v_h) \right) \\ \qquad\qquad = (u_h^n, v_h) + \frac{1-\lambda}{\lambda}\left(u_{1,h}^{n+1} - u_h^n, v_h\right) \\ a_{\parallel nl}\left(u_h^n + (u_h^n - u_h^{n-1}), u_{2,h}^{n+1}, w_h\right) - \varepsilon a_\parallel(q_{2,h}^{n+1}, w_h) = 0 \end{array} \right.
$$

$$
u_h^{n+1} = u_{2,h}^{n+1}\,, \qquad q_h^{n+1} = q_{2,h}^{n+1}\,,
$$

with $u_{1,h}^{n+1}$ (respectively $u_{2,h}^{n+1}$) being the solution of the first (respectively second) stage of the Runge-Kutta method. The terms $u_h^n + \lambda(u_h^n - u_h^{n-1})$ and $u_h^n + (u_h^n - u_h^{n-1})$ are respectively the second order time-approximations of $u_h(t + \lambda\tau)$ and $u_h(t + \tau)$, used to linearize the problem.

For each time step we have therefore to assemble and solve two linearized problems. This method is two times slower than the Crank-Nicolson scheme, with the advantage however of maintaining the AP-property of the scheme, advantage which is crucial for $0 < \varepsilon \ll 1$.

5.2 Numerical results

In this last section we compare (for validation) the proposed implicit Euler-AP and DIRK-AP schemes with a standard linearized implicit Euler discretization of the original singularly perturbed problem (5.1). The test case is similar to the one introduced in the elliptic framework, *i.e.* the magnetic field is given by

$$
b = \frac{B}{|B|}\,, \quad B = \begin{pmatrix} (2y-1)\cos(\pi x) + \pi \\ \pi(y^2 - y)\sin(\pi x) \end{pmatrix}. \tag{5.19}
$$

and an exact solution is constructed in order to validate the AP-scheme

$$
p = \left(\cos\left(\pi y + (y^2 - y)\cos(\pi x)\right) + 4\right) T_m e^{-t} \tag{5.20}
$$

$$
q = p^{-3/2}\sin(3\pi x)/3\pi \tag{5.21}
$$

$$
u = p + \varepsilon q. \tag{5.22}
$$

The problem is supplied with a force term computed accordingly.

The space and time convergence of the methods is tested, with focus on the ε-dependence of the errors. To do this we choose first a small time step such that the time discretization error is much smaller than the space discretization error. We then vary the mesh size and perform simulations for 100 time steps. The L^2 relative errors between

the exact solution and the three schemes are plotted in Figure 5.2, as a function of the perturbation parameter ε. All three methods give as expected the third order space convergence in the L_2-norm for large values of ε. Moreover, due to the extremely small time step, the numerical precision is the same, no matter if one uses first or second order methods. As expected, for small values of ε only the Asymptotic Preserving schemes give good numerical solutions.

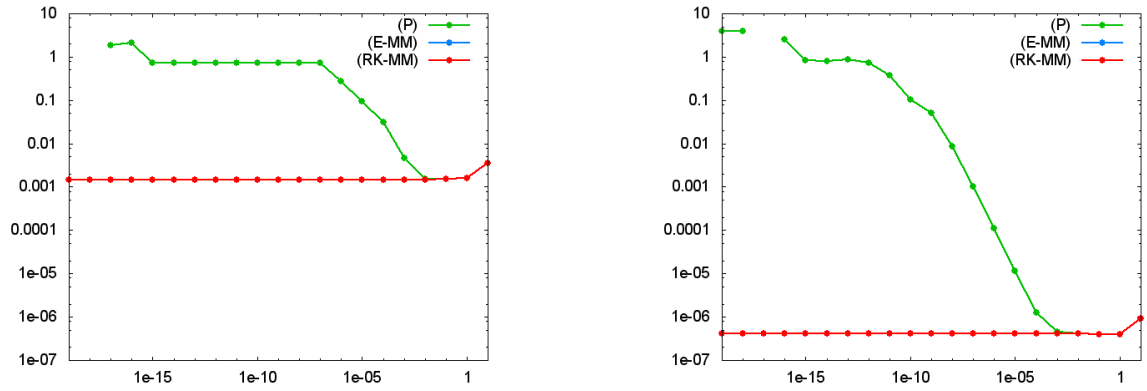

(a) $h = 0.1$ (b) $h = 0.00625$

FIGURE 5.2: Relative L^2-errors between the exact solution u^ε and the computed solution for the standard scheme (P_ε), Euler-AP method (E_{AP}) and DIRK-AP scheme (RK_{AP}) as a function of ε and for $h = 0.1$ resp. $h = 0.00625$. The time step is $\tau = 10^{-6}$.

Secondly we test the time convergence of the methods. To do this we choose a small mesh size such that the space discretization error is smaller than the time discretization error. We then vary the time step and perform simulations on a fixed grid. The results are summarized in Figure 5.3. Note that the (RK_{AP}) scheme is of second order in time as long as the error due to the time discretization dominates the error induced by the space discretization. The standard (P_ε)-scheme works well and is of first order, as long as ε is close to one. The (E_{AP}) scheme is of first order for all values of the anisotropic parameter. One has to observe here, that while the (RK_{AP}) scheme demands twice more computational time than the (E_{AP}) scheme, it gives much better precision.

To conclude, one can remark that the asymptotic-preserving schemes, (E_{AP}) and (RK_{AP}), are uniformly accurate with respect to the perturbation parameter ε. This essential feature can be very useful in situations where the anisotropy is variable in space, *i.e.* the parameter $\varepsilon(x)$ is x-dependent. No mesh-adaptation is any more needed in these cases, a simple Cartesian grid enables accurate results, with no regard to the ε-values. Hence, the AP-scheme we proposed here is very powerful, as it allows the use of the same scheme to discretize (P_ε) as well as the Limit model (L), in other words it is able to capture automatically the different scales in the problem, while the numerical discretization parameters (Δx and Δt) remain independent on the stiffness parameter ε. These parameters have only to be adapted to the scale of interest.

As a last numerical test, we investigate the evolution of the following initial Gaussian

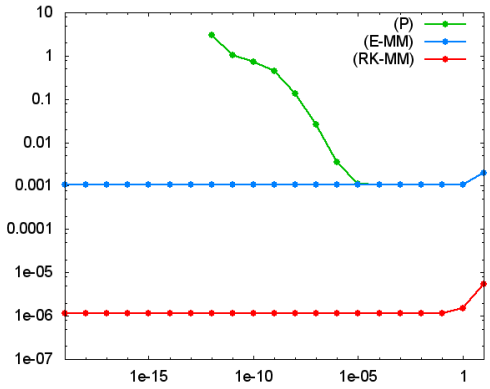

FIGURE 5.3: Relative L^2-errors between the exact solution u^ε and the computed solution with the standard scheme (P), the Euler-AP method (E_{AP}) and the DIRK-AP scheme (RK_{AP}) as a function of ε and for $\tau = 0.00625$. The spacial grid is 200×200.

peak, located in the middle of the computational domain :

$$u^0(x,y) = \frac{T_m}{2}\left(1 + e^{-50(x-0.5)^2 - 50(y-0.5)^2}\right), \tag{5.23}$$

where $T_m = 10^5\, K$ is the maximal temperature in the domain and the anisotropy direction is given as in the previous tests. We perform numerical experiments with the choice of $\varepsilon = 1$ and a coarse Cartesian grid. What can be observed is the nice rapid diffusion of the temperature along the magnetic field lines.

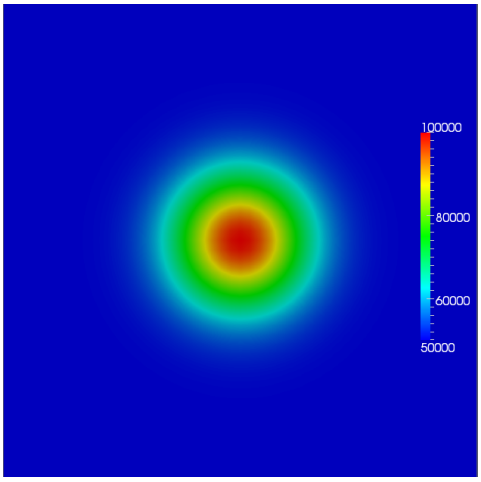

(a) $t = 0$

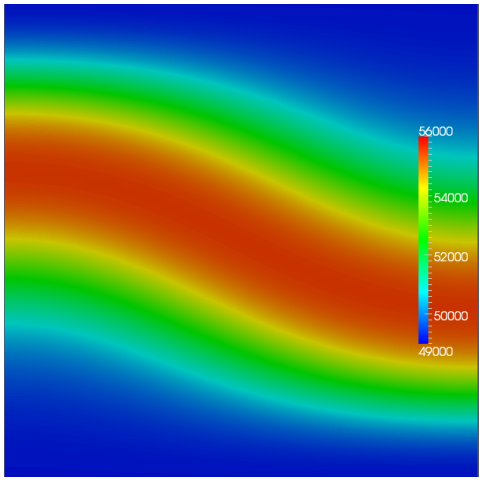

(b) $t = 0.01$

FIGURE 5.4: Numerical solution at different time steps for the Gaussian peak experiment, for $T_m = 10^5$ and $\varepsilon = 1$. Time step is $\tau = 0.01s$ and the mesh size is 50×50.

5.3 Magnetic islands

The Asymptotic-Preserving schemes introduced so far in the elliptic and parabolic framework (chapter 4 and 5) can no longer be used (in the here presented form) if the anisotropy field lines are closed in the study domain, in other words if the anisotropy field lines do not cross the boundary. Indeed, in both formulations we made use of the Lagrange multiplier space

$$\mathcal{L} = \{q \in L^2(\Omega) \ / \ \nabla_{||} q \in L^2(\Omega)\,, \ \ q_{|\Gamma_{in}} = 0\}\,,$$

where the condition $q_{|\Gamma_{in}} = 0$ was essential to be able to get a unique solution to the problem $\nabla_{||} q = \frac{1}{\varepsilon}\nabla_{||} u$ or equivalently to be able to decompose in a unique way $u = p + \varepsilon q$ with $\nabla_{||} p = 0$ and $\nabla_{||} u = \varepsilon \nabla_{||} q$. For all this, it is crucial that each field line enters the domain, such that one can fix q.
Closed anisotropy field lines are often encountered in tokamak plasma simulations, where the magnetic field is evolving in time and so-called *magnetic islands* are appearing.
In these cases stabilization techniques will help to circumvent the non-uniqueness problems. In particular, instead of (5.7) one has to solve the slightly modified system (modification of order $\mathcal{O}(h^2)$)

$$(AP)_h \quad \begin{cases} \displaystyle\int_\Omega \frac{\partial u_h}{\partial t} v_h \, dx + \int_\Omega (A_\perp \nabla_\perp u_h) \cdot \nabla_\perp v_h \, dx + \int_\Omega A_\parallel \nabla_\parallel q_h \cdot \nabla_\parallel v_h \, dx + \gamma \int_{\Gamma_\perp} u_h v_h \, ds = 0, \\ \qquad\qquad\qquad\qquad\qquad\qquad\qquad\qquad\qquad\qquad \forall v_h \in \mathcal{V}_h \\ \displaystyle\int_\Omega A_\parallel u_h^{5/2} \nabla_\parallel u_h \cdot \nabla_\parallel w_h \, dx - \varepsilon \int_\Omega A_\parallel \nabla_\parallel q_h \cdot \nabla_\parallel w_h \, dx = h^3 \int_\Omega q_h w_h \, dx, \quad \forall w \in \tilde{\mathcal{L}}_h\,, \end{cases} \tag{5.24}$$

where this time the Lagrangian multiplier space is given by $\tilde{\mathcal{L}} := \{q \in L^2(\Omega) \ / \ \nabla_{||} q \in L^2(\Omega)\}$. The stabilization term acts on the Lagrange multiplier space and is an artificial manner to render the problem $\nabla_{||} q = \frac{1}{\varepsilon}\nabla_{||} u$ coercive and hence uniquely solvable on the new space $\tilde{\mathcal{L}}$. This idea comes from the approximation of saddle-point problems, as for example the Stokes problem, where the stability helps to satisfy the inf − sup condition (which ensures the existence, uniqueness and convergence of the discrete mixed system) on a larger range of finite dimensional discrete spaces.

This work is at the moment in progress. The first results are shown in the next Figures, simulated by Jacek Narski [41]. These Figures illustrate the diffusion (at two different instants) of the temperature in a varying magnetic field, revealing islands.

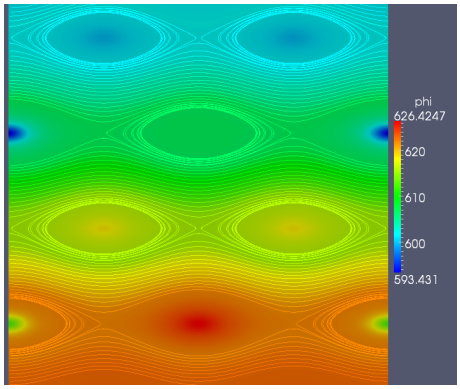

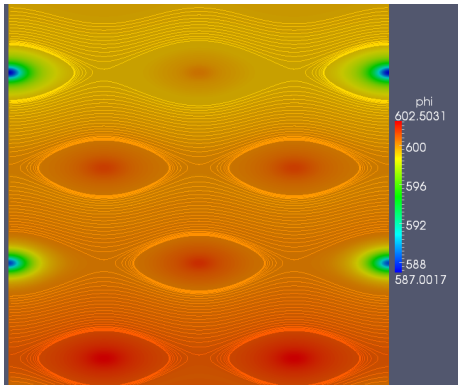

Summary

We presented in this review some efficient numerical schemes developed to treat singularly perturbed problems. The main difficulty of singularly perturbed problems is the occurrence of stiff terms, induced by some small perturbation parameter $0 < \varepsilon \ll 1$. Hence, the solutions exhibit a multiscale character, which is difficult to capture numerically.

The strategies introduced in this review for the construction of schemes preserving the asymptotic behaviour of the solutions in the limit $\varepsilon \to 0$ (called Asymptotic-Preserving schemes) are based on a detailed mathematical study of the dominant operator, the identification of the Limit model as $\varepsilon \to 0$ and the decomposition of the unknown in a macroscopic part (belonging to the kernel of the dominant operator) and a microscopic part. These two parts satisfy a coupled system of equations, equivalent to the initial singularly perturbed system. The advantage of the Micro-Macro system is that it leads automatically to the Limit model, when the perturbation parameter ε tends to zero. We would like to underline here that the construction of AP-schemes is not unique, and several other AP-strategies are presented in literature, for example based on a combination of splitting, penalization, exponential methods. We preferred the Micro-Macro approach in this review, as it is a rather elegant and systematic strategy, allowing also for a rigorous mathematical study.

After the obtention of the Micro-Macro coupled system, one has to take care when discretizing this system in order not to destroy the AP-properties with a non-adapted discretization. Several numerical tests have been also presented in this review to illustrate the efficiency of the developed AP-schemes. In particular these schemes are shown to be uniformly stable (in ε) along the transition from the initial problem (microscopic level) to the Limit problem (macroscopic level). This property is very important in practical applications, where the perturbation parameter can vary considerably within the study domain. In other words, the AP-schemes are able to approximate uniformly precise the solutions in both regimes, microscopic as well as macroscopic, and this on ε-independent grids, which have not to be adapted to the anisotropy direction.

The Asymptotic-Preserving techniques presented in this review can be applied to other singularly perturbed problems, coming from physics, biology, chemistry, economy *etc.* But each time, one has to study apart/independently the occurring dominant operator and construct an adapted AP-scheme for the special problem. No general AP-methodology can be proposed, valid for all problems.

Bibliographie

[1] D. Aronson, *The porous medium equation*, A. Fasano, M. Primicerio (Eds.), Nonlinear Diffusion Problems, Lecture Notes in Mathematics **1224** (1986), 1-46.

[2] A. Arseneev, *Global existence of a weak solution of the Vlasov system of equations*, U.R.S.S. Comp. Math. Phys. **15** (1975), 131–143.

[3] C. Bardos, P. Degond, *Global existence for the Vlasov-Poisson equation in three space variables with small initial data*, Ann. Inst. H. Poincaré, Anal. non linéaire **2** (1985), 101–118.

[4] R. Belaouar, N. Crouseilles, P. Degond, E. Sonnendrücker, *An asymptotically stable semi-lagrangian scheme in the quasi-neutral limit*, Journal of Scientific Computing **41** (2009), 341–365.

[5] N. Ben Abdallah, P. Degond, *On a hierarchy of macroscopic models for semiconductors*, J. Math. Phys. **37** (1996), 3306–3333.

[6] M. Bostan, *The Vlasov-Maxwell system with strong initial magnetic field. Guiding-center approximation*, SIAM J. Multiscale Model. Simul. **6** (2007), no. 3, 1026-1058.

[7] M. Bostan, The Vlasov-Poisson system with strong external magnetic field. Finite Larmor radius regime, Asymptot. Anal. **61** (2009), 91-123.

[8] M. Bostan, Transport equations with singular coefficients. Application to the gyrokinetic models in plasma physics, research report INRIA, hal :inria-00232800, submitted 2009.

[9] M. Bostan, Gyrokinetic Vlasov equation in three dimensional setting. Second order approximation, IAM J. Multiscale Model. Simul., **8** (2010), no. 5, 1923-1957.

[10] Y. Brenier, *Convergence of the Vlasov-Poisson system to the incompressible Euler equations*, Comm. Partial Differential Equations **25** (2000), 737–754.

[11] S. Brull, P. Degond, F. Deluzet, A. Mouton, *Asymptotic-Preserving scheme for a bi-fluid Euler-Lorentz model*, Kinetic and Related Models **4** (2011), 991 - 1023.

[12] F. Cordier, P. Degond, A. Kumbaro, *An Asymptotic-Preserving all-speed scheme for the Euler and Navier-Stokes equations*, Journal of Computational Physics.

[13] P. Crispel, P. Degond, M-H. Vignal, *An asymptotic preserving scheme for the two-fluid Euler-Poisson model in the quasineutral limit*, J. Comp. Phys. **223** (2007), 208-234.

[14] N. Crouseilles, M. Lemou, *An asymptotic preserving scheme based on a micro-macro decomposition for collisional Vlasov equations : diffusion and high-field scaling limits* , KRM **4** (2011), 441–477.

[15] F. Coron, B. Perthame, *Numerical passage from kinetic to fluid equations*, SIAM J. Numer. Anal. **28** (1991), 26–42.

[16] P. Degond, F. Deluzet, L. Navoret, A-B. Sun, M-H.Vignal *Asymptotic-Preserving Particle-In-Cell method for the Vlasov-Poisson system near quasineutrality*, J. Comput. Phys. **229** (2010), 5630–5652.

[17] P. Degond, F. Deluzet, A. Sangam, M-H. Vignal, *An asymptotic preserving scheme for the Euler equations in a strong magnetic field*, J. Comput. Phys. **228** (2009), 3540-3558.

[18] P. Degond, J-G. Liu, M-H. Vignal, *Analysis of an asymptotic preserving scheme for the Euler-Poison system in the quasineutral limit*, SIAM J. Numer. Anal. **46** (2008), 1298-1322.

[19] P. Degond, M. Tang, *All speed scheme for the low mach number limit of the Isentropic Euler equation*, Communications in Computational Physics, **10** (2011), 1-31.

[20] G. Dimarco, L. Pareschi, "Exponential methods for kinetic equations", SIAM J. Num. Anal. **49** (2011), 2057-2077.

[21] G. Dimarco, L. Pareschi, "High order asymptotic-preserving schemes for the Boltzmann equation", Comptes Rendus Mathematique **350** (2012), 481-486.

[22] R. J. DiPerna, P.-L. Lions, *Global weak solutions of the Vlasov-Maxwell system*, Comm. Pure Appl. Math. XVII (1989), 729–757.

[23] F. Filbet, S. Jin, "A class of asymptotic preserving schemes for kinetic equations and related problems with stiff sources", J. Comp. Physics **229** (2010), no. 20, .

[24] F. Filbet, S. Jin, "An Asymptotic Preserving Scheme for the ES-BGK model pof the Boltzmann equation", J. Sci. Computing **46** (2011), no. 2, 204-224.

Homogenization of the Vlasov equation and of the Vlasov-Poisson system with strong external magnetic field, Asymptotic Anal. **18** (1998), 193-213.

[25] F. Golse, L. Saint-Raymond, *The Vlasov-Poisson system with strong magnetic field in quasineutral regime*, Math. Models and Meth. in Appl. Sci. **13** (2003), 661-714).

[26] F. Golse, L. Saint-Raymond, *The Vlasov-Poisson system with strong magnetic field*, J. Math. Pures et Appl. **78** (1999), 791-817.

[27] E. Grenier, *Limite quasi-neutre en dimension 1*, Journées Équations aux dérivées partielles (1999), 1-8.

[28] M. H. Holmes, *Introduction to perturbation methods*, Springer-Verlag, New York, 1995.

[29] E. Horst, R. Hunze, *Weak solutions of the initial value problem for the unmodied nonlinear Vlasov equation*, Math. Meth. Appl. Sci. **6** (1984), 262–279.

[30] S. Jin *Efficient Asymptotic-Preserving (AP) schemes for some multiscale kinetic equations*, SIAM J. Sci. Comp. **21** (1999), 441–454.

[31] S.Jin, L.Pareschi, G.Toscani, *Diffusive relaxation schemes for multiscale discrete-velocity kinetic equations*, SIAM J. Numerical Analysis **35** (1998), no. 6, 2405–2439.

[32] A. Klar, *An Asymptotic Induced Scheme for Nonstationary Transport Equations in the Diffusive Limit*, SIAM J. Num. Anal. **35** (1998), no. 3, 1073–1094.

[33] A. Klar, *Asymptotic Induced Domain Decomposition Methods for Kinetic and Drift Diffusion Semiconductor Equations*, SIAM J. Sci. Comp. **19** (1998), no. 6, 2032–2050.

[34] C. Le Bris, *Systèmes multi-échelles. Modélisation et simulation*, Springer-Verlag, Berlin Heidelberg, 2005.

[35] M. Lemou, F. Méhats, *Micro-macro schemes for kinetic equations including boundary layers.*

[36] M. Lemou, L. Mieussens, "A new asymptotic preserving scheme based on micro-macro formulation for linear kinetic equations in the diffusion limit", SIAM J. Sci. Comput. **31** (2008), no. 1, 334–368.

[37] P.-L. Lions, B. Perthame, *Propagation of moments and regularity for the 3- dimensional Vlasov-Poisson system*, Invent. Math. **105** (1991), 415–430.

[38] J.-G. Liu, L. Mieussens, *Analysis of an asymptotic preserving scheme for linear kinetic equations in the diffusion limit*, SIAM J. Numer. Anal. **48** (2010), no. 4, 14741491.

[39] A. Lozinski, J. Narski, C. Negulescu, *Highly anisotropic temperature balance equation and its asymptotic-preserving resolution*, M2AN.

[40] A. Mentrelli, C. Negulescu, *Asymptotic-Preserving scheme for highly anisotropic non-linear diffusion equations*, Journal of Comp. Phys.

[41] J. Narski, M. Ottaviani, *Asymptotic-Preserving scheme in a magnetic island context*, in preparation.

[42] K. Pfaffelmoser, *Global classical solutions of the Vlasov-Poisson system in three dimensions for general initial data*, J. Differential Equations **95** (1992), 281–303.

[43] F. Poupaud, *Diffusion approximation of the linear semiconductor Boltzmann equation : analysis of boundary layers*, Asymptotic Analysis **4** (1991), 293–317.

[44] J. Schaeffer, *Global existence of smooth solutions to the Vlasov-Poisson system in three dimensions*, Comm. Partial Differential Equations **16** (1991), 1313–1335.

[45] J. Vázquez, *The porous medium equation : mathematical theory*, Oxford University Press, USA, 2007.